

Supramolecular Nanotube Architectures Based on Amphiphilic Molecules

Toshimi Shimizu,* Mitsutoshi Masuda, and Hiroyuki Minamikawa

Nanoarchitectonics Research Center (NARC), National Institute of Advanced Industrial Science and Technology (AIST),
Tsukuba Central 5, 1-1-1 Higashi, Tsukuba, Ibaraki 305-8565, Japan

Received June 22, 2004

Contents

1. Introduction	1401
2. Theoretical Background of Chiral Self-Assembly	1404
3. Methods for Nanotube Formation	1407
3.1. Chiral Self-Assembly	1407
3.2. Packing-Directed Self-Assembly	1408
3.3. Amphiphilic Polymer Assembly	1408
3.4. Molecular Sculpting	1408
3.5. Template Processes	1409
3.6. Other Methods	1409
4. Molecular Structure and Nanotube Morphology	1409
4.1. Low-Molecular-Weight Amphiphiles	1409
4.2. Amphiphilic Polymers	1420
4.3. Polymerization and Cross-Linking	1421
5. Control of Dimensions	1423
5.1. Outer Diameter	1423
5.2. Inner Diameter	1424
5.3. Length	1425
5.4. Wall Thickness	1426
6. Synthesis of Hybrid Tubular Structures	1427
6.1. Classification of Template-Directed Syntheses	1427
6.2. <i>exo</i> -Templating	1427
6.3. <i>endo</i> -Templating	1432
7. Applications and Properties	1434
7.1. Technological Applications	1434
7.2. Mechanical Properties	1435
7.3. Nanotube–Vesicle Networks	1436
7.4. Properties of Water Confined in a Hollow Cylinder	1438
8. Concluding Remarks	1438
9. Acknowledgment	1439
10. References	1439

1. Introduction

Amphiphilic molecules, of which soap is a typical example, possess antagonistic hydrophilic and hydrophobic moieties in the same molecule. Carbohydrate amphiphiles, commonly referred as glycolipids, greatly contribute to the structural stability and the function of biomembranes in living systems.^{1,2} In aqueous media, lipid molecules self-assemble into diverse aggregate morphologies, depending on the molecular shape and solution conditions such as lipid concentration, electrolyte concentration, pH, and temperature.³ On the basis of many systematic experiments, Kunitake et al. detailed the relation-



Toshimi Shimizu (center) was born in Osaka, Japan, in 1952. He received his B.S. (1975) and M.S. (1977) degrees in polymer chemistry from Kyoto University, Japan, and in 1983 he received his Ph.D. degree, also from Kyoto University. In 1977, he joined the Research Institute of Polymers and Textiles, part of what was then the Agency of Industrial Science and Technology (now the National Institute of Advanced Industrial Science and Technology, AIST), Japan. After postdoctoral research at the Free University Berlin with Professor J.-H. Fuhrhop, he joined the National Institute of Materials and Chemical Research (NIMC), AIST, in 1993. Since 2001, he has been the director of the Nanoarchitectonics Research Center (NARC), AIST. He is also now directing a Core Research for Evolutional Science and Technology (CREST) project entitled “Functional High-Axial-Ratio Nanostructure Assembly for Nano-Space Engineering” funded by the Japan Science and Technology Agency (JST). His research focuses on noncovalent synthesis and structural analysis of high-axial-ratio nanostructures generated by the self-assembly of amphiphilic molecules.

Mitsutoshi Masuda (left) was born in Kagawa, Japan, in 1966. He received his Ph.D. in organic chemistry from Tokyo University of Agriculture and Technology, Japan, in 2000. He joined the Research Institute of Polymers and Textiles in 1992. He joined NIMC in 1993 and started working with Dr. Toshimi Shimizu in 1994. After a period of postdoctoral work with Prof. E. W. Meijer at the Eindhoven University of Technology in 2001 on the polymerization of columnar assemblies, he began working at NARC. His key research interests are the self-assembly of glycolipids and covalent fixation of the assemblies for the construction of well-defined nano-objects.

Hiroyuki Minamikawa (right) received his B.Sc. (1986) and M.Sc. (1988) degrees in chemistry from the University of Tokyo. He worked at the Research Institute of Polymers and Textiles from 1988 to 1992 and at NIMC from 1993 to 2001. He has studied the physicochemical properties of synthetic glycolipid assemblies and their applications for membrane proteins. Since 2001, he has been working with Dr. Toshimi Shimizu at NARC. His research interests include the molecular design of synthetic glycolipids, and structural and thermodynamic aspects of glycolipid assemblies.

ships between the structures of synthetic bilayer-forming compounds and the resulting self-assembled morphologies:^{4–6} the molecular conformation, a variety of functionalities necessary for aggregation, and the location and orientation of those functionalities

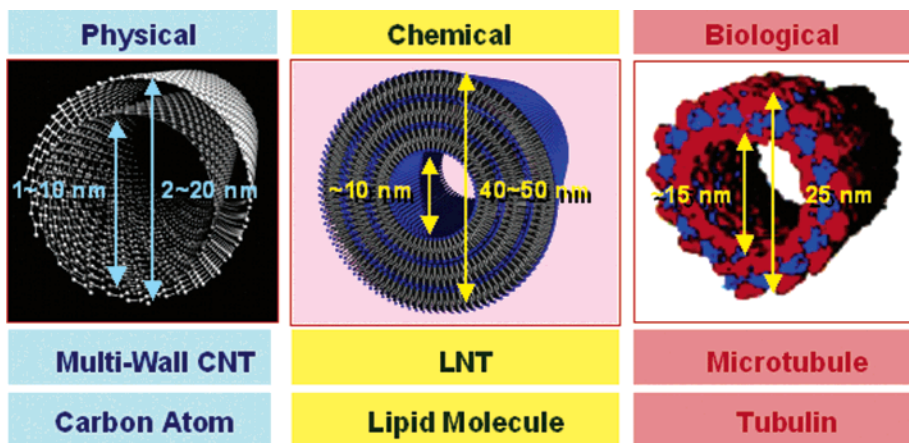


Figure 1. Representative nanotube structures with a hollow cylinder ca. 10 nm wide, the profiles of which are classified on the basis of physical, chemical, and biological viewpoints. The bottom column indicates the building block that makes up the tubular assemblies. The images of the carbon nanotube and the microtubule are provided by NEC Corporation and National Partnership for Advanced Computational Infrastructure (NPACI), respectively.

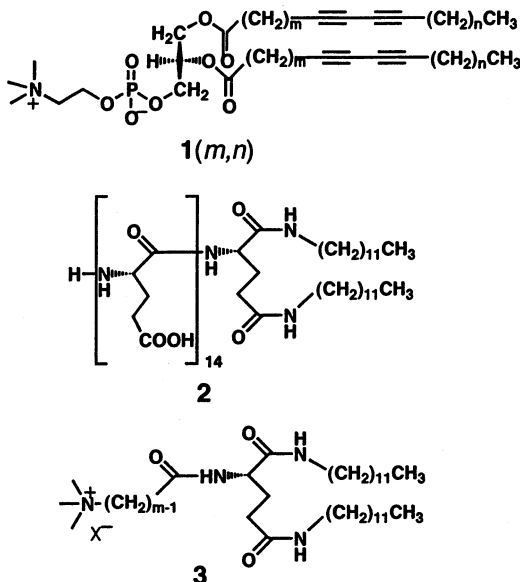
play a crucial role in determining the self-assembling behavior.^{7,8} Thus, rational design of molecular structures and self-assembly conditions permits the regulation of the self-assembled morphologies with 1–100 nm dimensions with single-nanometer precision.

Carbon nanotubes, which were first discovered by Iijima in the early 1990s,^{9,10} have recently demonstrated the reality of the world of nanotechnology. In a chemical field, there are hollow cylindrical supramolecular objects consisting of many identical lipid molecules as building blocks. The dimensions of the smallest lipid nanotubes (LNTs) are similar to those of both multiwall carbon nanotubes (CNTs) and microtubules consisting of tubulin proteins (Figure 1). These three tubular objects share a common feature: the hollow cylindrical structures are stabilized by helical arrangements of constituent units (carbon atoms, lipid molecules, or tubulin dimers).

Although studies of carbon nanotubes in a physical field and biologically generated microtubules are numerous, there have been only a few systematic studies of lipid or polymer nanotubes.^{11,12} No definite guidelines for the design of molecular structures of nanotube-forming amphiphiles have been laid out. The relationship between the combination of hydrophilic and hydrophobic moieties in the amphiphiles and the size of the resulting nanotube structures has not been determined.

Hollow cylindrical structures of lipid molecules appeared in a series of aggregate morphologies with high axial ratios. The first reports of the formation of LNTs from bilayer-forming amphiphiles **1**(8,9),^{13–16} **2**,¹⁷ and **3**^{18,19} came independently and almost simultaneously from three research groups in the United States and Japan. It should be noted that these nanotubes were reported about seven years before Iijima discovered the existence of multiwall carbon nanotubes.⁹

Many amphiphilic polymers can self-assemble to generate various morphologies, including micelles, rods, and vesicular aggregates.^{20,21} Nanotube formation is, however, limited to several block copolymer systems.^{22–27} The reason for this limitation is that nanotube formation generally requires highly ordered



molecular packing and anisotropic intermolecular interactions, and most coil-coil block copolymers show higher chain flexibility and fewer anisotropic intermolecular interactions than low-molecular-weight lipids. Furthermore, many of the polymer nanotubes are generated under kinetic conditions and then become trapped, for example, by the glassy nature of the insoluble core of the nanotube. Thus, among the several types of diblock copolymers, rod-coil block copolymers have a tendency to form polymer nanotubes.

The diameters of lipid- and copolymer-based nanotubes characteristically span the region between 10 and 1000 nm. Neither top-down-type microfabrication procedures nor any fabrication methods for carbon nanotubes can generate tubular structures with these dimensions. Therefore, lipid- and copolymer-based nanotubes with well-defined hollow cylinders, whose diameters are 10–100 times those of the smallest molecular nanotubes,^{28–30} are expected to act as novel host substances in mesoscale host-guest chemistry. These cylinders should be able to accommodate guest substances 10–100 times as large as

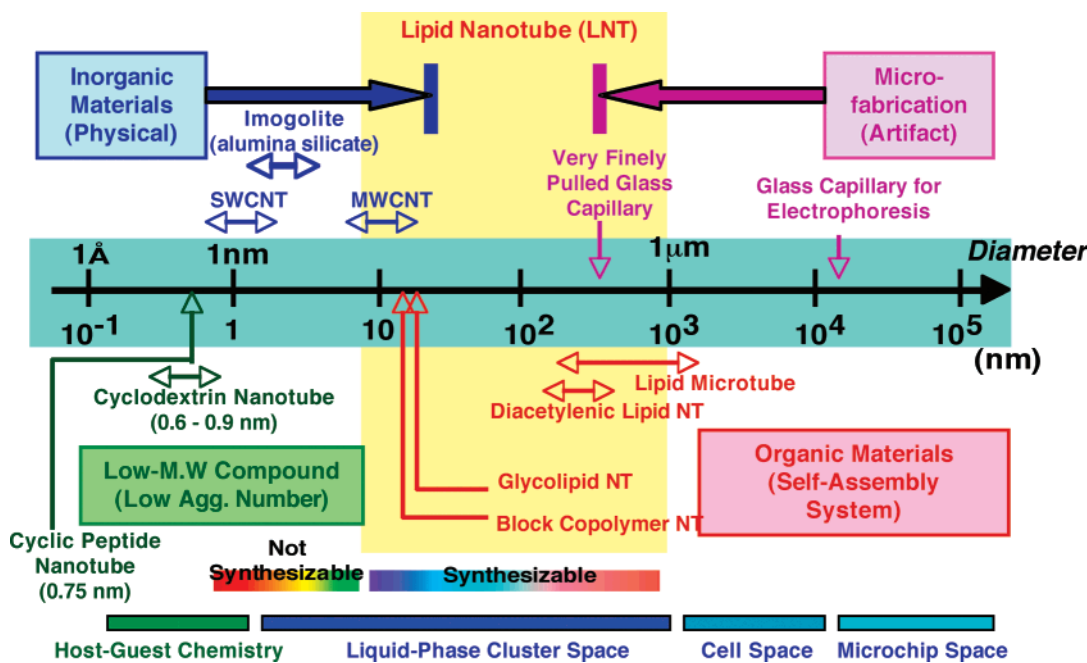


Figure 2. Diameter distribution of tubular structures that exist in the real world. Lipid nanotubes with less than 10 nm diameters are generally unavailable. Abbreviations: LNT, lipid nanotube; NT, nanotube; SWCNT, single-wall carbon nanotube; MWCNT, multiwall carbon nanotube; M.W, molecular weight; Agg., aggregation.

conventional guest molecules such as metal cations, aromatic compounds, or a single polymer chain. The diameter distribution of a variety of known tubular objects is summarized in Figure 2. Molecular nanotubes such as cyclodextrin and cyclic peptide nanotubes have inner diameters less than 1 nm.^{28–35} The cyclodextrin nanotubes can encapsulate a variety of single polymer chains in the inner cavity, whereas cyclic peptide nanotubes can translate alkali or alkali metal cations through to the inner volume. Carbon nanotubes, metal sulfides such as molybdenum disulfide,^{36,37} and clay layer structures such as imogolite³⁸ span generally the diameter region from 1 to 10 nm, which is larger than the diameters of molecular nanotubes. On the other end of the size spectrum are hollow polymer fibers with diameters of ca. 100 μm . The smallest tubular materials commercially available may be finely pulled glass capillaries for micro-injection use, which have a 500 nm inner diameter at the tip (Femtotip, Eppendorf Co. Ltd.). Lipid- and copolymer-based nanotubes are the main nanotubes in the 10–1000 nm size region (see Figure 2).

The need to improve miniaturization and device performance in the microchip and microelectronics industry has recently inspired many investigations into supramolecular chemistry. In particular, the ability to precisely control the inner and outer diameters of self-assembled LNTs directly determines their suitability for technological applications. Understanding how structural variation affects nanotube dimensions at the molecular level would facilitate a more efficient and systematic approach to generating rationalized tubular libraries. The purpose of this review is to summarize recent advances and to address several approaches to controlling the dimensions of lipid and polymer nanotubes, focusing on the outer and inner diameters, lengths, and membrane wall thickness.

Synthetic inorganic nanomaterials, although diverse in composition, generally lack the structural variety characteristic of supramolecular structures and other organic structures.³⁹ In addition, the structural hierarchy and macroscopic shape of inorganic nanostructures, such as spheres,^{40–42} tubes,^{43,44} fibers,^{45,46} and hollow shells,^{44,47–49} depend on the subtle interplay of extrinsic factors associated with the growth mechanism.

Recently, self-assembled tubular structures made of glycolipids or phospholipids have been used as templates to yield metal oxide nanotubes, as well as organic–metallic and organic–inorganic nanohybrids with high axial ratios.^{11,50–52} Figure 3 illustrates the variety of nanotubes derived from the self-assembly of lipids and amphiphilic copolymers. Lipid head-groups can function as templates for the nucleation, growth, and deposition of inorganic substances on the external surface of preformed organic templates (Figure 3c, d, and h). The well-known 1(8,9) nanotubes have been successfully mineralized with nickel,¹¹ copper,¹¹ alumina,⁵¹ and silica.⁵² Metal nanowires less than 50 nm wide can also be produced by templating a hollow cylinder of tobacco mosaic virus (TMV)⁵³ or LNTs (Figure 3e and g).⁵⁴ Furthermore, silica nanotubes obtained using a self-assembled rod as a template for the sol–gel reaction of silica precursors can provide a novel confined nanospace for the self-assembly of lipids, leading to the fabrication of a variety of hybrid nanotubes with concentric organic and inorganic layers (Figure 3j, k, and m).⁵⁵ Such hollow cylindrical nano- and microstructures made of organic, inorganic, or organic–inorganic hybrid materials have potential technological applications as sensor/actuator arrays,^{56,57} nanowires,⁵⁸ and optoelectronic devices.^{59,60}

The variety of self-assembled tubular morphologies with well-defined diameters, lengths, and wall thick-

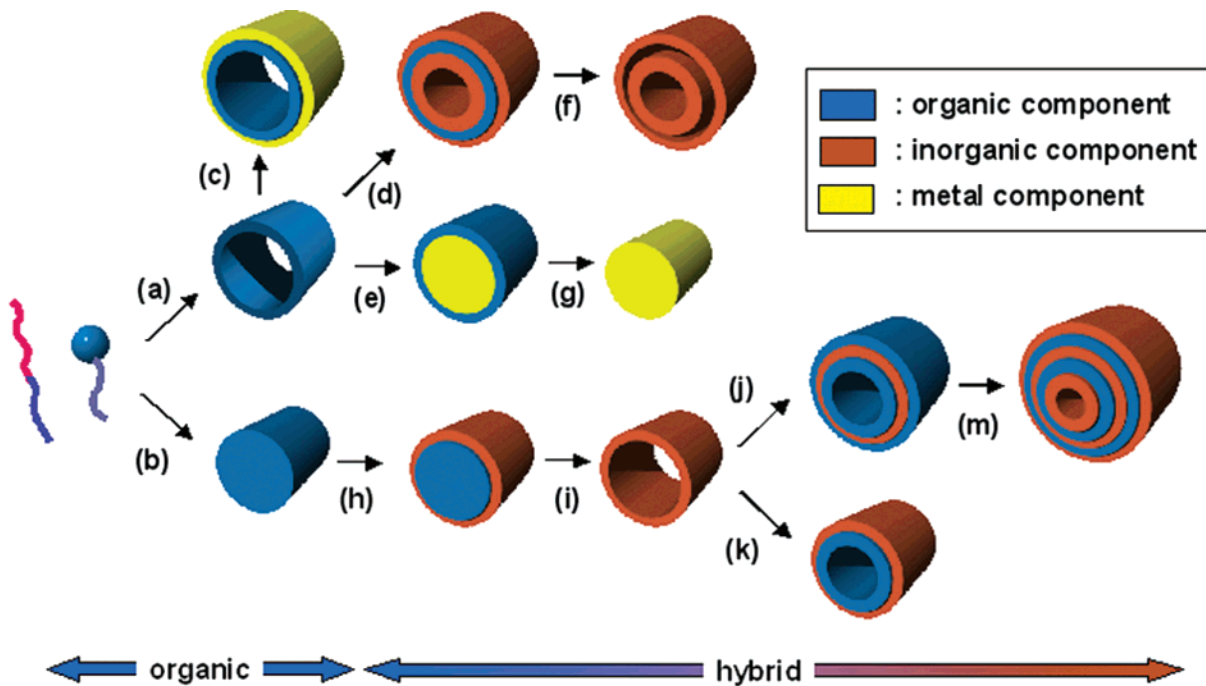


Figure 3. Variety of nanotube structures whose syntheses start with molecular self-assembly of low-molecular-weight or polymer amphiphiles. (a and b) Molecular self-assembly into a nanotube or rod. (c) Coating of metals. (d and f) Deposition of metal alkoxides on the surfaces of the nanotubes and the subsequent calcination into a double-layered metal oxide nanotube. (e and g) Filling of metals and the subsequent removal of the organic shell that will result in the formation of a metal nanowire. (h and i) Deposition of metal alkoxides on the surface of the rod and the subsequent calcination into a single-layered metal oxide nanotube. (j and k) Molecular self-assembly by using a silica nanotube as a template. (m) Deposition of metal alkoxides on the surface of a hybrid nanotube.

nesses possess fascinating characteristics for creating novel hybrid tubular nanostructures. Note that the generation of a variety of tubular structures consisting of inorganic, organic–inorganic, and organic–metal hybrids starts with molecular self-assembly. Therefore, in this review, the term *supramolecular nanotube architectures* is defined broadly to include hybrid nanotubes as well. We begin this review with a description of the theoretical background for the chiral self-assembly of LNTs (section 2) and then present an overview of methods for nanotube formation (section 3). Next, we focus on progress in research on molecular structure and supramolecular nanotube architectures made in the past decade (sections 4 and 5, respectively). We next describe the template-directed production of inorganic tubular structures (section 6), which are promising applications of LNTs. Finally, we also touch on the novel properties of single LNTs (section 7).

First, however, we must define the terminology of tubular structures. The tubes that have emerged recently can be grouped into two principal classifications, depending on tube diameter: (1) nanoscale tubes (*nanotubes*) and (2) microscale tubes (*microtubules* or *tubules*) (Figure 4). Depending on the tube constituents, a species name is added as a prefix: for example, *carbon nanotube*, *lipid nanotube*, or *gold nanotube*. The term *tubule* generally refers to a small tube or canal: *uriniferous tubule* and *seminiferous tubule* are examples that can be found in medical dictionaries. *Microtubule* is a well-known term for a cytoskeletal element of eukaryotic cells that is a long, generally straight, hollow tube. Although the term

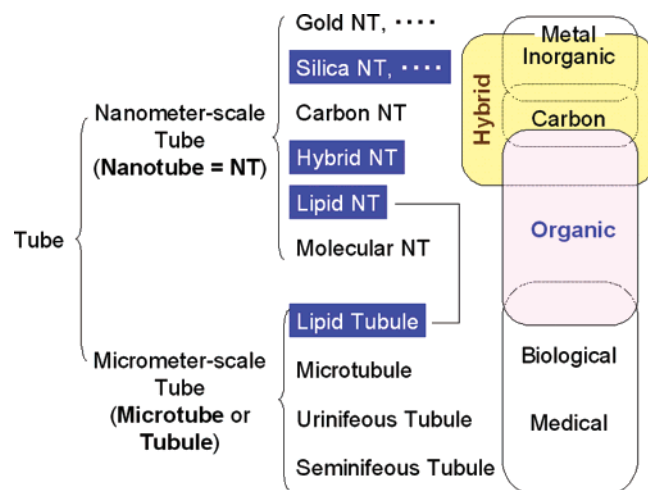


Figure 4. Classification of tubes that involve nanotubes and microtubes (or tubules). The term *lipid tubule* is treated here as a synonym of the term *lipid nanotube*.

lipid tubule is also commonly used, it seems to be synonymous with the term *lipid nanotube*. To confer generality on the terminology of nanotubes and to avoid confusion, we use the terms *lipid nanotube* and *polymer nanotube* in place of *lipid tubule*, together with *silica nanotube*, *gold nanotube*, and *hybrid nanotubes*.

2. Theoretical Background of Chiral Self-Assembly

Theories based on molecular chirality have been used to explain the molecular packing of LNTs.

According to these theories, chiral interactions cause constituent molecules to pack at a nonzero angle with respect to their nearest neighbors (Figure 5),⁶¹ and

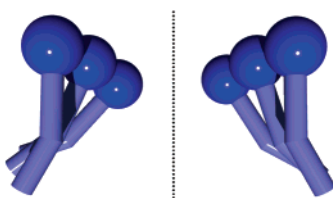


Figure 5. Schematic illustration that shows chiral molecular assembly, in which molecules packed at a nonzero angle with respect to the nearest neighbors.

the chirality of the molecule induces one particular orientation to be energetically preferable in a solid bilayer membrane. This situation causes twisting of the bilayer membrane, which will, in some cases, result in the formation of a cylindrical hollow. This section focuses on elastic theories of tilted chiral bilayer structures. The distinct geometries adopted by lipids are typically described within a consistent framework of continuum elastic models of membranes.^{62–64} The theories partly explain LNT structures in which the lipid molecules pack in a chiral manner. Although nanotubes formed from nontilted bilayer structures are known, we will mention them only briefly, at the end of this section.

An elastic theory of LNT structures based on elastic theories of liquid crystals has been discussed.⁶⁵ To describe molecular packing in a liquid crystal, the elastic theory assumes three phenomenological terms: splay, twist, and bend (Figure 6). For a nematic phase, the total elastic energy is written as

$$F_{\text{nematic}} = \frac{1}{2}K_1(\nabla \vec{d})^2 + \frac{1}{2}K_2(\vec{d} \cdot \nabla \times \vec{d})^2 + \frac{1}{2}K_3(\vec{d} \times \nabla \times \vec{d})^2 \quad (1)$$

Here K_1 , K_2 , and K_3 are the elastic constants of splay, twist, and bend deformations, and the vector \vec{d} is a unit vector parallel to the long axis of a molecule (the director in Figure 7). In nematic and nonchiral smectic phases, the total energy is at a minimum when all the terms equal zero, in which case the molecules pack parallel to one another (a flat membrane if the phase is a layered structure).

To describe helical ribbons and nanotubes composed of tilted chiral bilayer structures, two types of

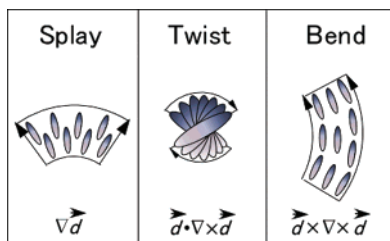


Figure 6. Spray, twist, and bend deformations in elastic theory. The mathematical symbol d means the director that denotes the long axis of a molecule. ∇d and $\nabla \times d$ are the divergence and the rotation of the director, respectively.

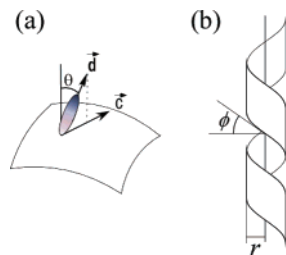


Figure 7. Geometrical definitions: (a) the director \vec{d} , the c -director \vec{c} , and the tilt angle θ ; (b) the radius r and the pitch angle ϕ of the helical ribbon.

elastic energy equations for a chiral liquid crystalline phase have been employed. For a chiral nematic phase or cholesteric phase, the elastic energy includes a linear term in addition to the quadratic terms:

$$\begin{aligned} F_{\text{cholesteric}} = & \frac{1}{2}K_1(\nabla \vec{d})^2 + \frac{1}{2}K_2(\vec{d} \cdot \nabla \times \vec{d} - q)^2 + \\ & \frac{1}{2}K_3(\vec{d} \times \nabla \times \vec{d})^2 = \frac{1}{2}K_1(\nabla \vec{d})^2 + \frac{1}{2}K_2(\vec{d} \cdot \nabla \times \vec{d})^2 + \\ & \frac{1}{2}K_3(\vec{d} \times \nabla \times \vec{d})^2 - K_2q(\vec{d} \cdot \nabla \times \vec{d}) + \text{constant} \quad (2) \end{aligned}$$

The constant q is a phenomenological parameter that denotes spontaneous twist of the molecular alignment in the chiral phase. The cholesteric liquid crystalline phase is not layered, but this type of energy equation has been successfully applied to the tilted layered structure.

Chiral smectic C phases (SmC* phases) are composed of tilted layers with chiral symmetry which spontaneously curves the layer. The elastic energy can be derived from consideration of the symmetry.⁶⁶ Because the full expression is complex, we will not describe the details in this review. In this elastic energy expression, there is a linear term (D_2) that is related to twisting and bending of the layers in the SmC* phases.

To describe the geometry of helical ribbons and nanotubes, cylindrical coordinates are introduced. Figure 7 illustrates a director \vec{d} , a c -director \vec{c} , and the tilt angle θ of a lipid molecule in a membrane, and the pitch angle ϕ of a helical ribbon. The c -director \vec{c} is a unit vector that indicates the molecular tilt direction on the membrane surface. Among the elastic theories, two models have been proposed for the c -director alignment. In the “uniform tilt” model, the tilt direction is aligned in a uniform helical manner (Figure 8a and b). In the “tilt modulation” model, the tilt direction varies across a membrane sheet (Figure 8c and d). Some of the theories discussed below implicitly assume the tilted structure, and others explicitly discuss the effects of the tilt angle θ and the tilt direction in the equations.

In 1988, Helfrich and Prost proposed an elastic theory that describes the intrinsic bending of chiral membranes.⁶⁷ In addition to quadratic elastic terms for the membrane, the theory includes a linear K^* term for the chirality. The constant K^* is essentially identical to the D_2 term in the elastic theory for SmC* phases.⁶⁶ Minimization of the total elastic energy

gives a helical ribbon instead of a flat one. The sign of K^* determines the helical sense of the ribbons (right- or left-handed). Furthermore, a larger K^* value leads to a larger curvature and, consequently, to a smaller radius r of the helical ribbon. This feature implies that the chirality is directly related to the curved morphology in this theoretical approach. To evaluate the pitch angle ϕ , Helfrich and Prost assumed a one-constant approximation and obtained an angle of 45° . With a similar elastic energy, the temperature effect on the structures was examined, and the curvature radius r was found to decrease as the temperature increased.^{68,69}

In two papers, Ou-Yang and Liu discuss the effect of the molecular tilt on the radius r and the pitch angle ϕ of helical ribbons and nanotubes.^{70,71} They applied the elastic theory of cholesteric liquid crystals to tilted chiral bilayer membranes. For helical ribbon and nanotube structures, they assumed uniform tilt (Figure 8a and b). In their discussion of tube struc-

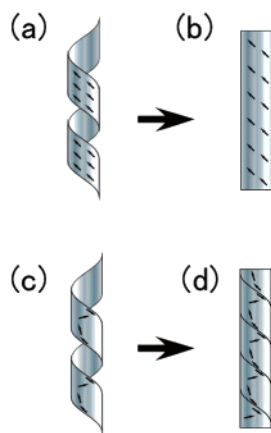


Figure 8. Models of uniform tilt and tilt modulation in the formation of helical ribbons and nanotubes. The arrows indicate the molecular tilt directions (the c -directors) on the nanostructure surfaces. (a) A helical ribbon with uniform tilt. (b) A nanotube with uniform tilt. (c) A helical ribbon with tilt modulation can grow into (d) a nanotube with helical markings.

tures, only the twist term was minimized, and the result was a pitch angle ϕ of 45° . They were able to determine how the nanotube curvature radius r depends on the molecular tilt. When the molecules align normal to the membrane ($\theta = 0$), the membrane is flat in mechanical equilibrium. When the molecules tilt, the membrane tends to bend. As θ increases, r decreases monotonically. Note that a slight change in θ causes a drastic change in r . This prediction suggests the possibility of controlling r by adjusting θ .

Since the first theory was published by Helfrich and Prost,⁶⁷ subsequent theories have been evaluated on the basis of whether they can reproduce a pitch angle ϕ of 45° for helical ribbon structures. A model bile mixture forms helical ribbons in water.⁷² Instead of 45° , the helical ribbons showed high and low pitch angles ϕ of 54 and 11° . The elastic theory of SmC* phases was applied to the helical ribbon structure with uniform tilt in order to explain these distinctive pitch angles. The energy minimization showed that the helical pitch angle ϕ is determined by a ratio of

two elastic constants. Hence, the two distinctive pitch angles were attributable to the different elastic constants of the helical ribbons, whose compositions can be different in this mixture system. For the pitch angles of 54 and 11° , the ratios of the constants were estimated as 3.4 and 0.0015 , respectively. However, Selinger et al. pointed out that the ratio of 0.0015 is surprisingly small.⁷³

Diacetylenic phospholipid **1**(8,9) self-assembled in ethanol into LNTs, which indicate helical markings as a striped pattern on the outer surfaces.⁷⁴ Circular dichroism (CD) measurements facilitated discussion of nanotube formation from a wound ribbon. Selinger et al.⁷³ developed an elastic explanation that is completely consistent with Schnur's results;⁷⁴ their elastic theory permits variations of the molecular tilt direction in the stripe on the membrane surface (Figure 8c). This "tilt modulation" model is clearly different from the "uniform tilt" model, if we recognize that the tilt direction discontinuously changes at the boundary of the neighboring stripes in this tilt modulation model. By adding some terms to the Helfrich-type energy equation, the minimization reproduced the tilt modulation in helical ribbons and nanotubes. Selinger et al. also discussed how the tilt modulation is relevant to the low-pitch helical ribbons reported by Chung et al.⁷² They also examined a term to induce ripple patterns on the tube surface.

Komura and Ou-Yang discussed the high and low pitch angles in relation to the tilt models and successfully obtained solutions for uniform tilt and tilt modulation.⁷⁵ They employed the elastic energy equation for cholesteric liquid crystals without any additional terms and then derived the Euler–Lagrange equation from the elastic energy. In the energy minimization of these solutions, the uniform tilt model gives high pitch angles, $>45^\circ$, and the tilt modulation model gives the optimal low pitch angle, $<30^\circ$. Further energy consideration allowed for evaluation of the optimal high pitch angle, which was 52° . This value agrees well with the experimentally observed value of 54° .⁷²

Over the last two decades, several elastic theories have been developed to model chiral tilted bilayer structures involved in the formation of helical ribbons and nanotubes. The earlier models successfully describe morphologies of LNTs and helical ribbon structures. Additional work has extended the theories and led to interesting proposals for the mechanism of formation; conversion between ribbons, nanotubes, and vesicles; and a possible tilt modulation on the membrane surface. In particular, the models suggest the interesting possibility that nanotube diameters could be drastically changed by slight changes in the lipid tilt angle. For experimentalists, these mathematical models are attractive in terms of suggesting molecular designs for nanotube technology.

Will it ever be possible to use the various models to calculate all the parameters for a given molecular structure and predict nanotube dimensions? Unfortunately, such parameters are hard to evaluate because the elastic theory is purely phenomenological and the coefficients are not derived directly from the

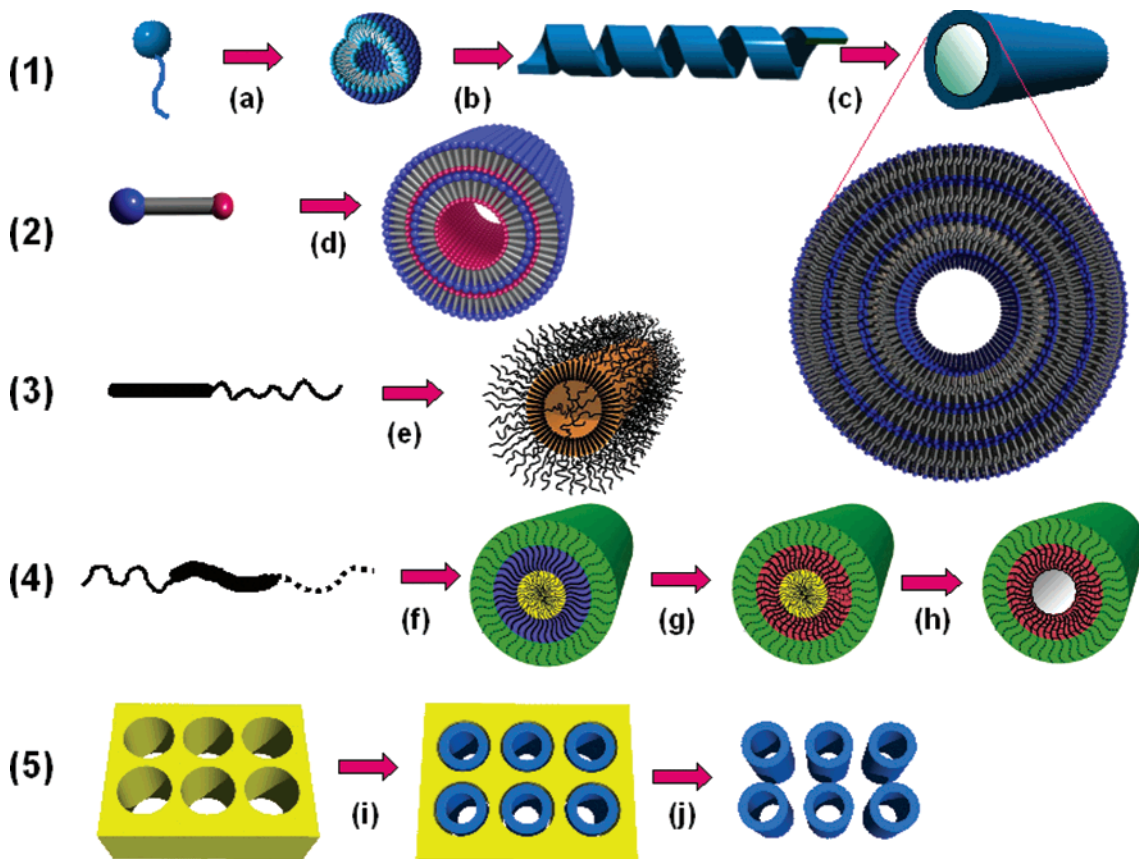


Figure 9. Variety of methods to yield nanotube structures: (1) chiral molecular self-assembly; (2) packing-directed self-assembly based on an unsymmetrical bolaamphiphile; (3) self-assembly of a rod–coil copolymer into a nanotube; (4) nanotube formation from a triblock copolymer via a molecular sculpting process, which involves (f) self-assembly, (g) cross-linking of the shell, and (h) decomposition of the core by ozonolysis; (5) self-assembly or deposition of molecules inside the pore as a substrate.

molecular structures. Some chiral pair potentials have been proposed for cholesteric liquid crystalline phases,⁷⁶ but these potentials are also phenomenological and the coefficients are unknown. Reliable molecular design on the basis of elastic theories may require additional systematic experimental surveys of nanotube structures.

Elastic theories assume uniform tilt or tilt modulation for the LNT structures. Experimentalists may decide to determine the molecular tilt direction in actual systems. A fluorescence method was proposed to test the tilt modulation model proposed by Selinger.⁷³ However, individual nanotubes are too tiny to determine the tilt direction experimentally using conventional measurement techniques. Combining scanning probe microscopy with nanoscale spectroscopy may enable us to examine the tilt direction at the scale of tens of nanometers, or diffractometry or spectroscopy may be applicable, if we can align nanotubes parallel to one another. For experimentalists in nanoscience, these are interesting challenges.

We can expect further development in theories of nanotube formation. The elastic theories have almost completely neglected crystalline-like molecular packing, since these theories were derived from the theories of liquid crystalline phases. However, for efficient formation of actual nanotubes, rational consideration of directional intermolecular interactions, such as hydrogen bonding and $\pi-\pi$ stacking,

seems critical. To evaluate the effects of these interactions, we may need to introduce some in-plane directional or positional orders in the theories.^{77–80} The orders will be similar to hexatic or positional orders observed in hexatic smectic or “crystalline” smectic phases. Note also that several LNT systems are composed of nontilted bilayer structures (see section 3.2).^{81,82} These structures have been discussed on the basis of a “wedge-shaped” molecular structure. A mathematical model has been suggested for the molecular design of such systems.⁸² Also in the model, the role played by directional intermolecular interactions should be considered. In addition to the mathematical elastic theories, molecular dynamics calculations could be a promising approach. Such calculations would permit estimation of the chiral packing of neighboring molecules in membranes.

3. Methods for Nanotube Formation

Figure 9 summarizes representative practical methods for generating nanotubes, including chiral molecular self-assembly, packing-directed self-assembly, polymer assembly, molecular sculpting, and templated synthesis using a pore.

3.1. Chiral Self-Assembly

Chiral self-assembly involves a helically coiled ribbon structure as an intermediate (Figure 9(1)).

After hot aqueous dispersions of nanotube-forming amphiphiles are cooled, there are two routes for nanotube formation. One route proceeds with shortening of the helical pitch of the ribbon and maintaining a constant tape width (Figure 10a),^{72,83} whereas

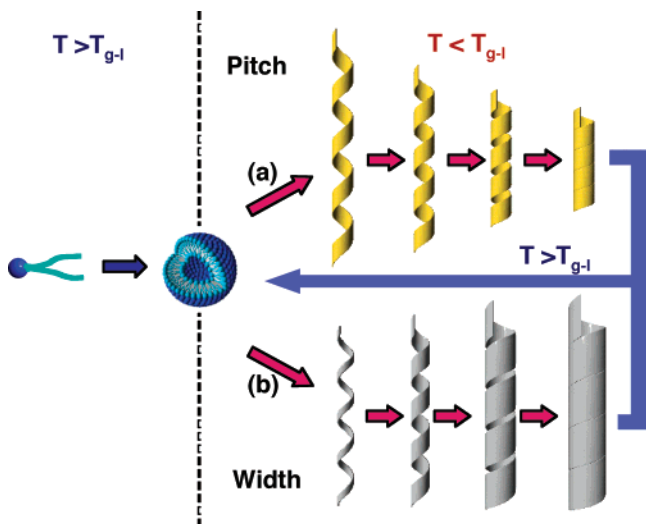


Figure 10. Possible formation mechanism of lipid nanotubes based on chiral molecular self-assembly. The illustration of the spherical vesicle was provided courtesy of Dr. Yoko Takiguchi of Nagoya University.

the second involves widening of the tape width and maintaining a constant helical pitch (Figure 10b).¹⁹ The latter route is more common in the literature than the former one. Both the ribbons and the nanotubes are stable only at temperatures below the gel-to-liquid crystalline phase transition temperature (T_{g-I}) of the amphiphiles ($T < T_{g-I}$). Heating the nanotube dispersion to temperatures above T_{g-I} ($T > T_{g-I}$) induces instant morphological conversion from nanotubes into spheres.

3.2. Packing-Directed Self-Assembly

In addition to the chiral self-assembly scheme described above, there is a route based on packing-directed self-assembly (Figure 9(2)). In this route, no chiral morphologies such as helically twisted or coiled ribbons appear during the course of the reaction. Wedge-shaped amphiphiles have a tendency to assemble into hollow cylindrical structures, as detailed in section 5.2. However, prediction of self-assembled morphologies from a designed amphiphile structure becomes complicated if the packing of hydrophobic chains is crystalline. Only when the amphiphile possesses hydrophobic chains in a fluid state is the following structural guideline for self-assembly applicable for predicting an aggregate morphology. Israelachvili proposed an optimal surface area per polar headgroup, which depends on the packing parameter, $P = v/(a_0 l_c)$, where v is the volume of the hydrophobic chain, a_0 is the polar head surface area at the critical micellar concentration (cmc), and l_c is the chain length (Figure 11).³ If $P < \frac{1}{3}$, the amphiphile has a tendency to form spherical micelles; if $\frac{1}{3} < P < \frac{1}{2}$, cylindrical micelles will be favored; if $\frac{1}{2} < P < 1$, bilayers with a spontaneous curvature (vesicles) are produced; if $P > 1$,

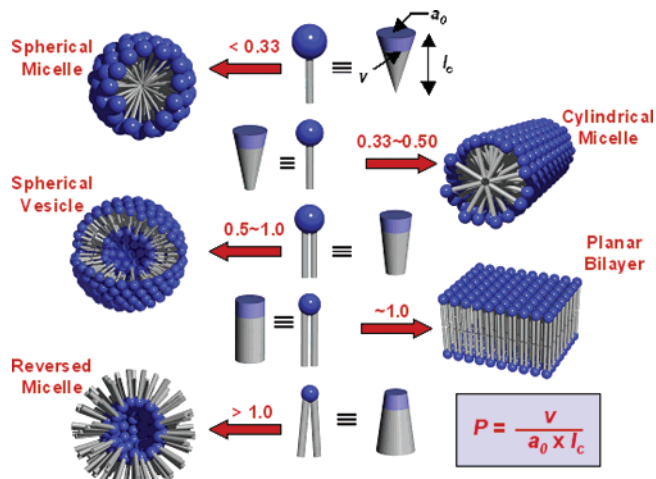


Figure 11. Various self-assembled morphologies depending on the critical packing parameter (P) of each lipid.

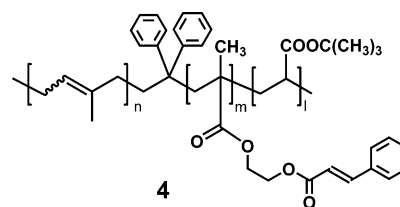
= 1, planar bilayers will be favored; and if $P > 1$, micellar aggregates with a reverse curvature will be formed.

3.3. Amphiphilic Polymer Assembly

In the hope of generating nanotubes, various researchers have examined the self-assembly of amphiphilic polymers in solution mainly by using linear chain diblock copolymers, owing to their synthetic accessibility. For self-assembly, organic solvents play an important role in increasing the solvent affinity of a block copolymer, behaving as a selective solvent for a block. Then, a block miscible with the solvent is exposed on the outer surface of aggregates, and the nonmiscible block is located inside the aggregates (Figure 9(3)). The self-assembled morphologies depend on a number of structural factors and experimental conditions: block chain lengths, ratios of blocks, molecular weights and their distribution, chain composition, the stereochemistry of the polymer chain, solvent composition, temperature, incubation time, concentration, and preparation order.

3.4. Molecular Sculpting

An alternative method has been proposed to construct polymer nanotubes by making use of so-called molecular sculpting of cross-linked nanofibers (Figure 9(4)).^{84,85} The advantage is that this procedure makes the best use of the amphiphilic properties of polymers. For example, a triblock copolymer [polyisoprene-block-poly(2-cinnamoyloxyethyl methacrylate)-block-poly(tert-butyl acrylate), PI-*b*-PCEMA-*b*-PtBA] 4 initially self-assembled into coaxial cylindrical



micelles. Then photo-cross-linking of the PCEMA shell and subsequent removal of the PI internal core

by ozonolysis resulted in nanotube formation. The PtBA corona chain rendered solvent dispersibility to the nanotubes.⁸⁴ Transmission electron microscopy (TEM) observation of a light stripe in the center of each cylinder and uptake of rhodamine B into the nanotube provided evidence for the presence of hollow cylindrical structures. A similar procedure was used to construct robust hollow spheres from shell cross-linked micelles.⁸⁶ It might be possible to control the inner and outer diameters of the obtained nanotubes by changing the length of each block. Furthermore, the aldehyde group that was generated can be modified easily by ozonolysis of double bonds at the inner tubular surface and eventually form the covalent bond with other functional groups. This advantage will lead to encapsulating nanomaterials selectively, and fixing through a covalent linkage. On the basis of a similar strategy, nanotube structures have been constructed by the formation of a linear assembly of porphyrin dendritic building blocks, covalent linkage of dendritic wedges of the molecules, and subsequent removal of the constituent porphyrin core.⁸⁷

3.5. Template Processes

Template methods to prepare polymer nanotubes involve two approaches, *endo*-templating and *exo*-templating, the choice of which depends on the shape and role of the template. Figure 9(5) shows a template consisting of a microporous alumina or polycarbonate membrane (*endo*-templating; see section 6.3). The *exo*-templating approach is based on a one-dimensional nanomaterial like a nanorod or nanofiber (see section 6.2).^{88–91} These template methods are applicable not only to the self-assembly of amphiphilic molecules⁹² but also to nanotube formation from polymers,^{93,94} metals,^{95–97} and polymerizable monomers.^{98,99} The typical process involves selective removal of the template after nanotube formation. Therefore, the resulting nanotubes must exhibit high chemical and physical stability and be resistant to harsh conditions such as basic 6 M NaOH or dichloromethane, which are used to remove the alumina or polycarbonate membrane, respectively.

The pore diameters of the template films used as *endo*-templates typically lie between 15 and 400 nm, with low dispersity ($\pm 10\%$) and depths of 0.1–100 μm .⁸⁹ Ordered, porous membrane-like honeycomb fabricated using silicon lithography is also available. Therefore, discrete nanotubes can be obtained with good control of all the dimensions. After removal of the honeycomb template, the resultant nanotubes hold together to form a free-standing nanotube film, in which the nanotubes are arranged perpendicularly to the surface plane. The inner- and outermost surfaces of the nanotubes can be modified by layer-by-layer deposition of cationic and anionic polymers into the porous template.⁹⁴ A peptidic bolaamphiphile, for example, was found to self-assemble in a honeycomb template to give nanotubes with controlled, narrowly dispersed diameters, whereas nanotubes formed without the membrane template had a wide diameter distribution (20–1100 nm).⁹² Nanotubes with extremely high axial ratios are also obtainable in large quantities by coating divergent nanofiber templates

with a monomer.^{91,100} Chemical vapor deposition, polymerization, and subsequent selective removal of the nanofiber template result in nanotube formation.

3.6. Other Methods

Template-free polymerization of aniline and pyrrole in the presence of acid as a dopant also results in nanotube formation.^{101,102} Polyaniline and polypyrrole nanostructures can be grown by a self-assembly process using ammonium persulfate as an oxidant in the presence of a protonic acid as a dopant. Micelles formed from anilinium cations, dopant, and surfactant act as templates in the nanotube-formation process. The average diameters can be tuned from 140 to 340 nm by varying the ratio of the monomer and the protonic acid and by changing the acid dopant.

4. Molecular Structure and Nanotube Morphology

4.1. Low-Molecular-Weight Amphiphiles

Phospholipids. The most extensively studied building block for LNTs is the diacetylenic phospholipid, 1,2-bis(tricos-10,12-diynoyl)-*sn*-glycero-3-phosphocholine 1(8,9), which has eight methylenes between the ester and the diacetylene group and nine methylenes between the diacetylene group and the terminal methyl group.^{12,13,61,79,103–105} This polymerizable phospholipid was designed not for the purpose of preparing nanotube aggregates but for increasing the durability of lipid aggregates based on bilayer membranes.^{106–110} When aqueous or ethanolic aqueous dispersions of 1(8,9) are cooled below the gel-to-liquid crystalline phase transition temperature, LNTs with diameters of approximately 500 nm and lengths between 50 and 200 μm spontaneously assemble. Several research groups have synthesized a number of polymerizable phospholipids and extensively studied the relationship between the molecular structures and consequent self-assembled nanostructures in terms of chiral molecular architecture.^{74,111–121}

Table 1 summarizes what is known about the relationship between the structure of the amphiphiles and the resultant morphologies based on chiral or packing-directed self-assembly. Schnur et al. detailed a number of achievements regarding LNTs in a review of work from 1984 to 1993.^{11,12} Basically, the *R*-enantiomer of 1(8,9) produces nanotubes with a right-handed exterior helical marking, whereas the *S*-enantiomer always results in nanotubes with a mirror-image, left-handed exterior helical marking. This opposite expression of enantiomeric molecular chirality at the supramolecular level is well-known for a number of amphiphiles that can form chiral nanostructures with high axial ratios.^{19,122–124}

Outer layers of multilamellar nanotubes often exhibit a helical marking of single handedness related to the molecular chirality.^{103,122} An interesting result has been reported on the relationship between the intrinsic molecular chirality and the initial helical ribbon formation process.⁸⁰ Differential phase-contrast microscopy of a pure enantiomer of 1(8,9) under conditions of very slow cooling (0.25 °C/h) revealed

Table 1. Molecular Structures of Low-Molecular-Weight and Polymer Amphiphiles and the Dimensions of the Resultant Self-Assembled Tubular Structures

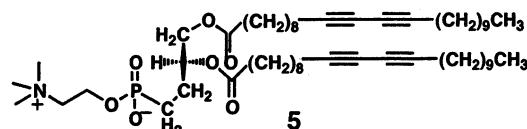
amphiphile	dimension					solvent ^a	ref
	length (L) (μm)	inner diameter (i.d.) (nm)	outer diameter (o.d.) (nm)	thickness (th) (nm)			
phospholipid	1(8,9)	50–200	~500			wat	12, 13, 61, 79
	5	23.5 \pm 11.1	1182 \pm 135			et/wat	125
	80(8) + 1(8,9)		50–60			wat	252, 263, 264
	82(n)		80 \pm 20 to 960 \pm 120	8		met/wat	259, 261
glycolipid	83	16.6 \pm 8.6	1076 \pm 90			et/wat	265
	6, 8	>500	8–10			wat	132
	12	1–10	50–70			wat	133, 134, 136
	25	>50	91–310	3.5	10–15	wat	144
	27		40–50			wat	148
	37		110–130			wat	154
	38		25–30			wat	154
	42b		35–40			wat	154
	60(n)	300–500	14–27	5.25		wat	165
peptidic amphiphile	37 + 90	~5	27			wat	82
	46		1000–2000	100		wat	277
others	49		80–130			tol	166, 167
	50		52	4		wat	131
	59	50–70	58–78	4		wat	173
	63	49		1.5		wat	81
	64, 65		170–390	45–75		chx	205
	67	14		3		thf	206
polymer amphiphile	69	3–5	~300			wat	210
	70	1200	2000			wat	215
	88		16			wat	216
	73	5–25	27			wat	276
	74	0.6–100	1000–3000	~200		tfa/dcm	221
	76	200–300	21–23	7		hx, ddc	26
	77		100	20		wat/dmf	22
			25–30	22		wat	250

^a Abbreviations of solvents: wat, water; et, ethanol; met, methanol; tol, toluene; chx, cyclohexane; thf, tetrahydrofuran; tfa, trifluoroacetic acid; dcm, dichloromethane; hx, hexane; ddc, dodecane; dmf, dimethylformamide.

that, in the first seconds of the initial self-assembly process, the probability of forming a left-handed helical ribbon is roughly equal to the probability of forming a right-handed one. This means that the molecular chirality is expressed in the subsequent, slower ensheathment process of layer addition. Enantiomerically pure phosphonate **5** also produces left-

modynamics of the melting behavior of **1(8,9)** nanotubes is attributable to a crossover from two-dimensional to three-dimensional melting as a function of wall thickness.¹²⁹ The solvent also has an important effect on the thermodynamics of LNTs. Whether the nanotubes melt continuously or discontinuously depends on the type of alcohol, the alcohol/water ratio, and the lipid concentration.¹²⁸ Thus, CD and specific heat measurements can be explained in terms of two distinct thermodynamic processes; the discontinuous melting is a first-order transition of the lipid bilayers from the ordered L_β phase to the disordered L_α phase, and the continuous melting reflects an increase in the lipid solubility with temperature.

Glycolipids. A large variety of self-assembled morphologies generated from synthetic amphiphiles have been extensively studied from the viewpoint of how the introduction of various hydrophilic moieties, such as glucose, galactose, other aldopyranose-type sugars, and noncyclic sugars, affects self-assembled morphologies.^{122,130,131} The presence and local environment of diyne units in the hydrophobic chain of *N*-gluconamides has been shown to affect self-assembled morphologies;¹³² for example, among polymerizable gluconamides **6–9**, amphiphiles **6** and **8**, in which 1,3-nonadiynyl units are combined with *N*-methyl- and *N*-pentylgluconamides, formed nano-



and right-handed helices.¹²⁵ These results are compatible with the theory of the collective tilt of bilayer membranes in chiral symmetry-breaking models of nanotube formation.¹²⁶ However, the formation of homochiral helices from enantiomerically pure **1(8,9)** is consistent with molecular dimensions based on chiral-packing theories.⁷³

The melting feature of the **1(8,9)** nanotubes in alcohol/water solutions is governed by changes in the lipid solubility in relation to the L_β to L_α transition temperature, as indicated by CD and specific heat measurements (Figure 12).^{127,128} Single-bilayer nanotubes melt continuously, whereas multiple-bilayer nanotubes melt discontinuously. The change in the ther-

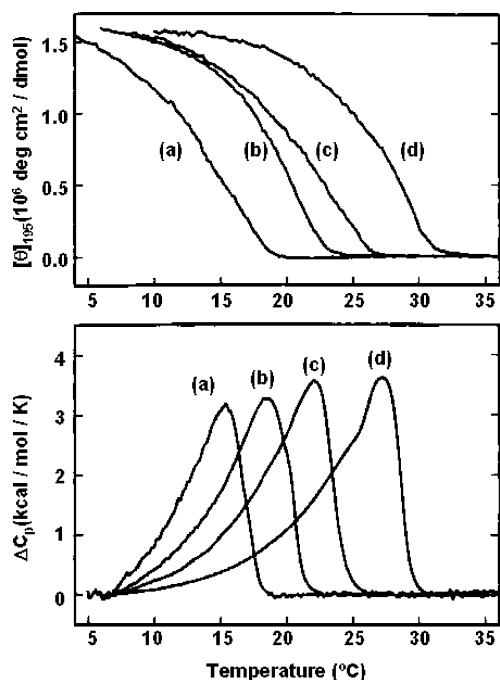
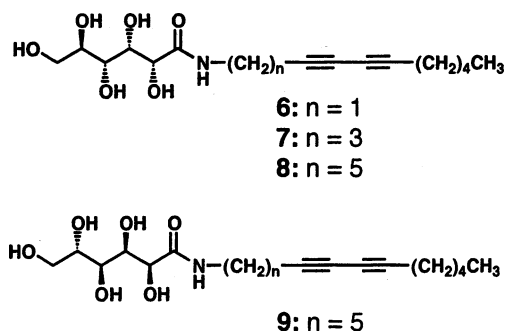
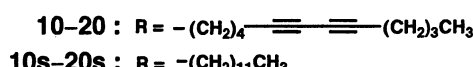
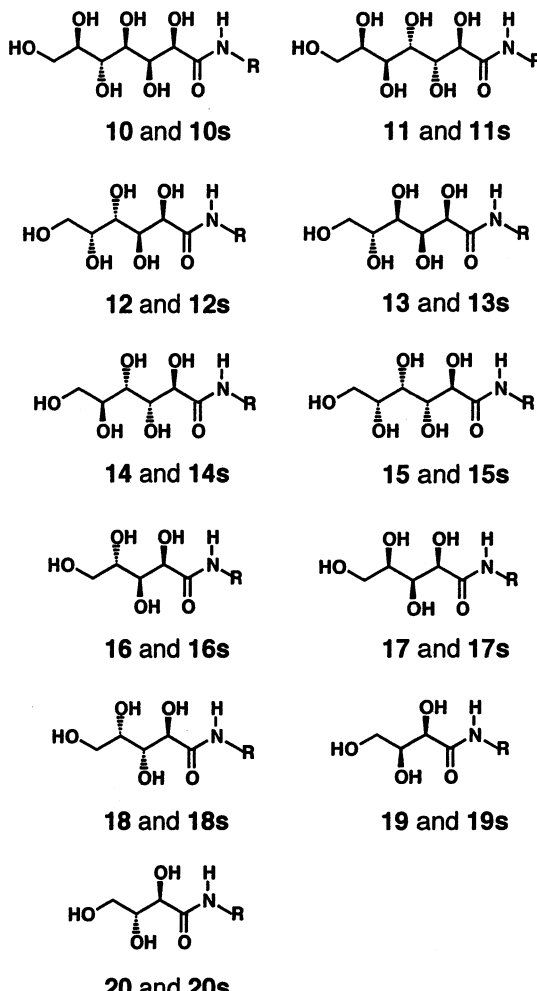


Figure 12. Concentration dependence of the CD spectra at 195 nm (top) and specific heat (bottom) of the **1(8,9)** nanotubes prepared in methanol/water (90:10) at lipid concentrations of (a) 0.5, (b) 1.0, (c) 2.0, and (d) 5.0 mg/mL. (Reproduced with permission from ref 128. Copyright 1997 American Chemical Society.)

tube structures (Table 1).¹³² The amphiphiles **7** and **9** self-assembled to form micellar rods.



A series of diacetylenic aldonamides (**10–20**) has also been prepared to increase the stability of self-assembled objects; these compounds differ in the structure of the open-chain sugar headgroup.^{133–135} The aldonamides possess headgroups derived from two aldoheptoses, D-glycero-D-glucuronamide **10** and D-glycero-L-mannose **11**; four aldohexoses, D-galactonamide **12**, D-glucuronamide **13**, L-mannose **14**, and D-gulonamide **15**; three aldopentoses, L-arabonamide **16**, L-xylonamide **17**, and L-lyxonamide **18**; and two aldotetroses, L-threonamide **19** and D-erythrionamide **20**. Table 2 summarizes the effect of the headgroup on the supramolecular morphologies of the diacetylenic aldonamides when the headgroup was varied systematically from heptose to hexose, to pentose, to tetrose.^{133,134,136} Among the aldonamides described above, diacetylenic glycero-mannose **11**, galactonamide **12**, mannose **14**, gulonamide **15**, and lyxonamide **18**, and the N-dodecyl derivatives (**12s**, **14s**, **16s**, and **18s**) of the galactonamide, mannose, arabonamide,

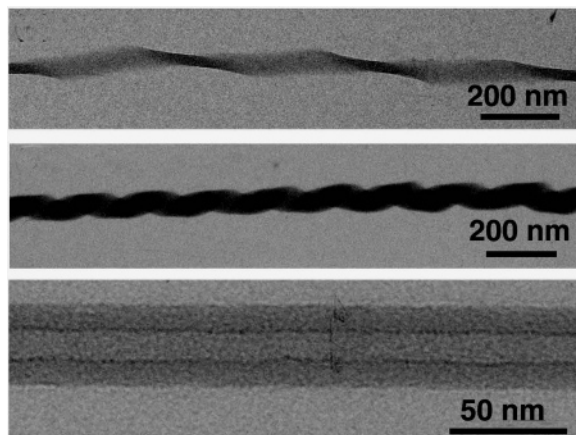


and lyxonamide, respectively, were found to produce nanotubes in aqueous dispersions. Head-to-head bilayer packing is associated with nanotube formation, whereas head-to-tail packing arrangement and “dromic” hydrogen-bonding patterns are critical for the fiber-like assemblies.^{133,134,136}

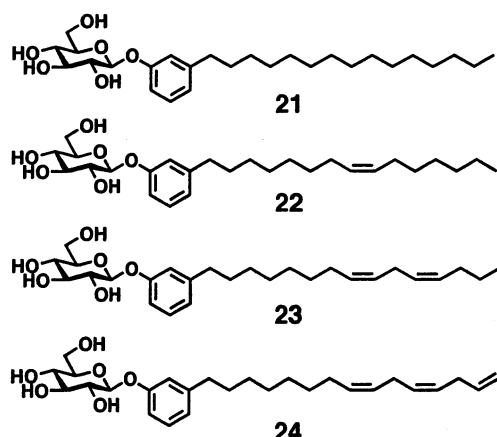
Synthetic amphiphiles with cyclic sugars as hydrophilic moieties are also known to produce chiral supramolecular fibers and ribbons by self-assembly in aqueous media.^{122,123,137–143} The self-assembly of synthetic glycolipids **25** produces smaller LNTs relative to those so far obtained from tube-forming compounds, which can be characterized by 10–15 nm inner diameters, 40–50 nm outer diameters, and axial ratios of more than 1000 (Table 1 and Figure 13, bottom).¹⁴⁴ The starting material for **25** is cardanol, a mixture of long-chain phenols obtained from *Anacardium occidentale* L.¹⁴⁵ Glycolipids **25** are obtainable as a mixture of 1-O-3'-n-(pentadecyl)phenyl-β-D-glucopyranoside (**21**), 1-O-3'-n-(8'(Z)-pentadecenyl)phenyl-β-D-glucopyranoside (**22**), 1-O-3'-n-(8'(Z),-11'(Z)-pentadecadienyl)phenyl-β-D-glucopyranoside (**23**), and 1-O-3'-n-(8'(Z),11'(Z),14'-pentadecatrienyl)phenyl-β-D-glucopyranoside (**24**) (**21:22:23:24**, 5:50:16:29 wt %). The type of fibrous self-assembled morphology obtained from **25** or **21** depends on

Table 2. Supramolecular Morphology of Hydrated *N*-Dodeca-5,7-diynyl aldonamides and *N*-Dodecylaldonamides¹³⁶

headgroup	<i>N</i> -dodeca-5,7-diynyl		<i>N</i> -dodecyl	
	morphology		morphology	
D-glycero-D-glucose	10	sheets	10s	
D-glycero-L-mannose	11	helices and nanotubes	11s	
D-galactose	12	helices and nanotubes	12s	helices and nanotubes
D-glucose	13	sheets	13s	braided fibers
L-mannose	14	nanotubes	14s	helices and nanotubes
D-gulose	15	nanotubes	15s	sheets
L-arabinose	16	braided fibers	16s	helices and nanotubes
L-lyxose	18	open and closed nanotubes	18s	open and closed nanotubes
L-threose	19	sheets	19s	sheets

**Figure 13.** TEM images of one-dimensional, twisted (top), coiled (middle), and tubular morphologies (bottom) self-assembled from glycolipids **21** (top) and **25** (middle and bottom).

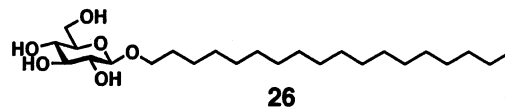
whether the hydrophobic chains include unsaturated units. To our knowledge, this finding represents the first example of morphological control of helical architectures by unsaturation of the hydrophobic chains. Unsaturation of the alkyl chain also strongly influences the diversity in gelation and aggregation behavior of the glycolipids **21–25**.¹⁴⁶



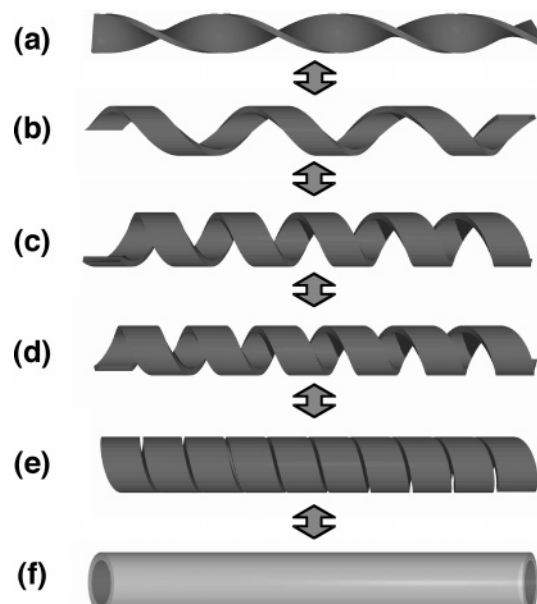
21(~5%) / 22(~50%) / 23(~16%) / 24(~29%) : 25

Interestingly, coiled nanofibers (Figure 13, middle) self-assembled from **25** gradually converted to a tubular morphology. Saturated homologue **21** produced no tubular structures even after 1 year. In the present phenolic glycoside **25**, π – π interaction between the aromatic rings is indispensable for stabilizing nanotubes. In comparison, octadecyl β -D-

glucopyranoside **26**, which lacks aromatic rings, forms no fiber structures.¹⁴⁴



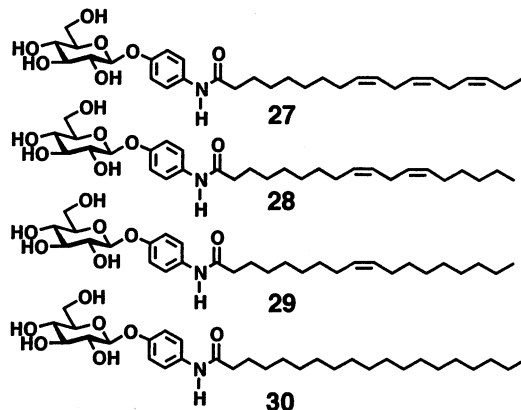
Rational control of self-assembled morphologies has been achieved by binary self-assembly of saturated homologue **21** and monoene derivative **22**, which proved to give a twisted ribbon (Figure 13, top) and tubular morphology on self-assembly (not shown), respectively.¹⁴⁷ This new method can generate a diversity of self-assembled high-axial-ratio nanostructures, ranging from twisted ribbons and helical ribbons to nanotubes (Figure 14). In particular, this

**Figure 14.** Schematic illustrations of the self-assembled morphologies of helical solid bilayers in high-axial-ratio nanostructures: (a) twisted ribbon; (b and c) loosely coiled ribbon; (d) tightly coiled ribbon; (e) nanotube with helical marking; (f) nanotube without helical marking.

method is promising in that it can not only provide nanotube structures individually with or without helical marking but also tune the helical pitch of the ribbon. These morphologies should be optimally matched to the requirements of a specific nanostructure application for miniaturization.

There have been no systematic studies of the influence of unsaturation, that is, the influence of the

number and position of the double bond units on the self-assembly behavior of synthetic amphiphiles into high-axial-ratio nanostructures including tubular architectures. Our own research group has reported the self-assembly of a series of long-chain phenyl glucosides **27–30** that differ in the number of cis double bonds (0–3) in the hydrocarbon chain.¹⁴⁸ In



an aqueous dispersion, **27–29** self-assembled into twisted nanofibers (**29**), helical ribbons (**28**), and nanotubular structures (**27**), as the number of cis double bonds increased (Table 1 and Figure 15).

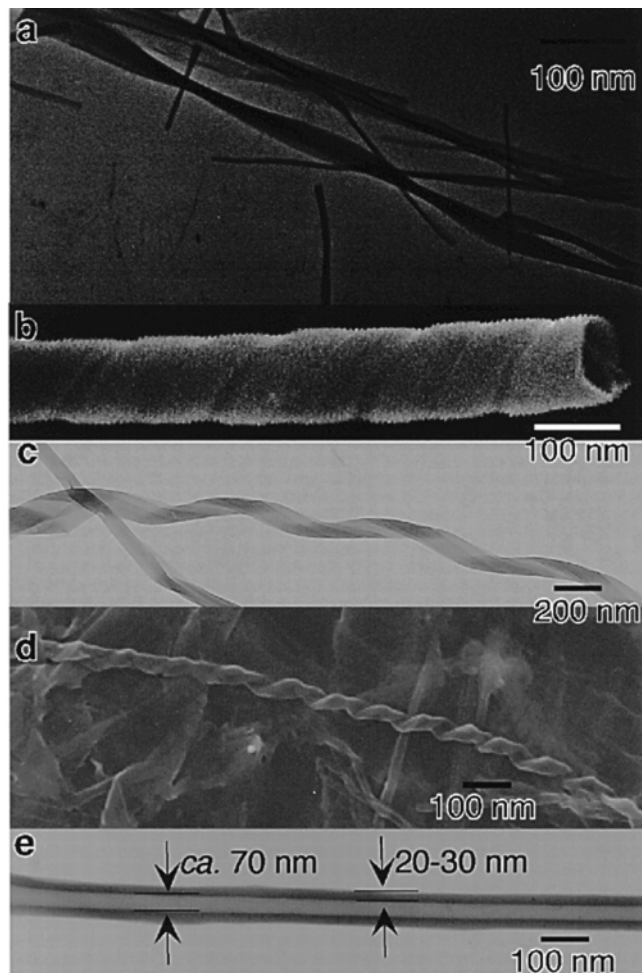
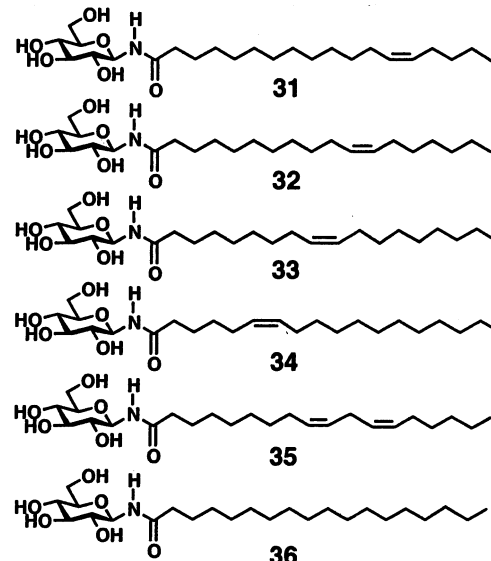


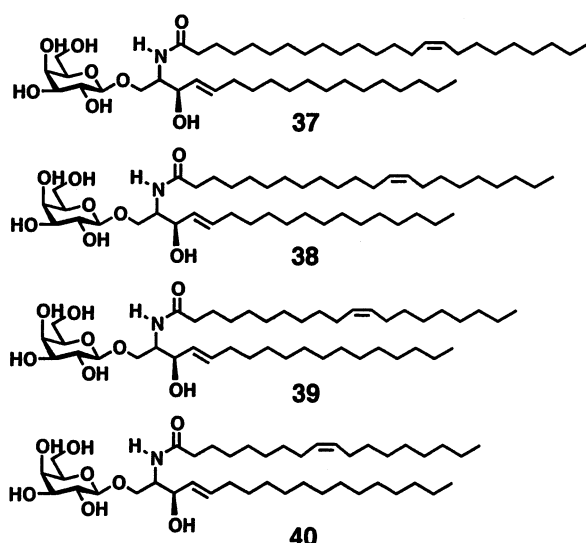
Figure 15. EF-TEM and SEM images of the self-assembled morphologies from (a) **29**, (b and c) **28**, and (d and e) **27**. (Reproduced with permission from ref 148. Copyright 2002 American Chemical Society.)

Evidence for nanotube formation from **27** and **28** was obtained from careful CD spectroscopy. The CD spectra of self-assembled **27** and **28** show strong negative bands at 225 and 237 nm, respectively, indicating nanotube formation by chiral assembly. Similarly, the position of the cis double bond significantly influenced the homogeneity of the outer diameters of the self-assembled nanotubes from *N*-gluconamide derivatives **31–36**.¹⁴⁹

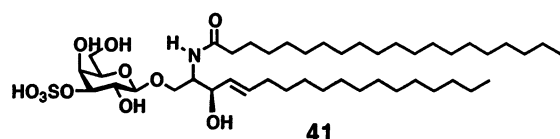


Tubular assemblies made of naturally occurring glycolipids have also received increasing attention because of their potential advantages as drug delivery vehicles.¹⁵⁰ Among naturally occurring lipids, sphingolipids such as galactosylceramides and related derivatives have been extensively studied in terms of their assembly into cochleate cylinders, nanotubes, and nanofibers.^{50,151,152} Kulkarni et al. reported that galactosylceramide (GalCer) **37** containing nervonoyl ($24:1^{\Delta 15(\text{cis})}$) acyl chains self-assembles into nanotubular structures in excess water.¹⁵³ To define the structural parameters that modulate nanotube formation, the same research group examined the self-assembly behavior of a synthetic galactosylceramide homologue containing a single cis double bond by varying the total acyl carbon number from C18 to C24: the self-assembly of $24:1^{\Delta 15}\text{GalCer}$ **37**, $22:1^{\Delta 13}\text{GalCer}$ **38**, $20:1^{\Delta 11}\text{GalCer}$ **39**, and $18:1^{\Delta 9}\text{GalCer}$ **40** produced nanotubes (25–30 nm diameters), smooth nanotubes (35–40 nm diameters), right-handed helical ribbons, and a variety of other morphologies including multilamellar cylinders and liposome-like structures, respectively (Table 1).¹⁵⁴ Replacement of the galactose headgroup with a glucose moiety resulted in needle- and fiber-like microstructures.¹⁵⁵ The same replacement of the sugar headgroup in cardanyl glycolipids **25** causes the opposite transformation, that is, from a needle-like crystal to nanotube structures.¹⁴⁴

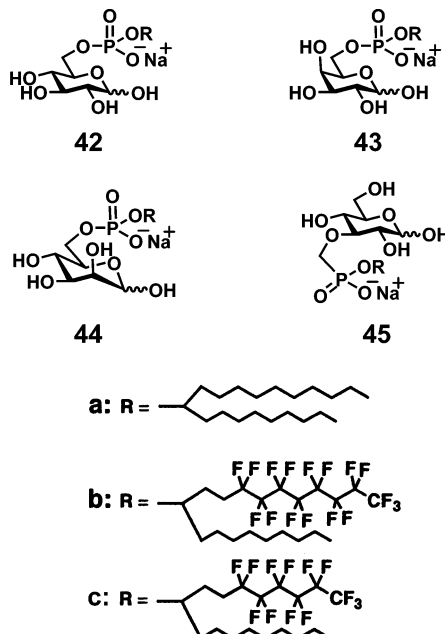
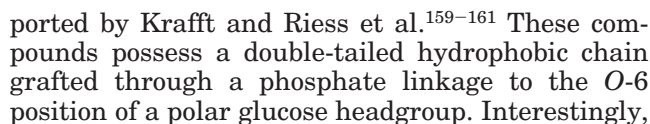
Galactosylceramides **37–40** and sulfatide **41** are generally found in enriched quantities in myelin sheath and in intestinal and kidney branch border membranes. These compounds provide structural stability to impart and maintain the curvature and



cylindrical shape of certain membranes.^{156,157} It is surprising that naturally occurring galactosylceramides tend to form helical ribbon-like structures within the cells of patients afflicted with globoid cell leukodystrophy.¹⁵⁸



A new family of nanotube-forming amphiphiles, anionic glucophospholipids **42–45**, have been re-



no LNTs were formed from the galactose or mannose derivatives. The formation of nanotubes is pH dependent and is favored at higher pH, since the amphiphiles are negatively charged. Small-angle X-ray scattering (SAXS) and small-angle neutron

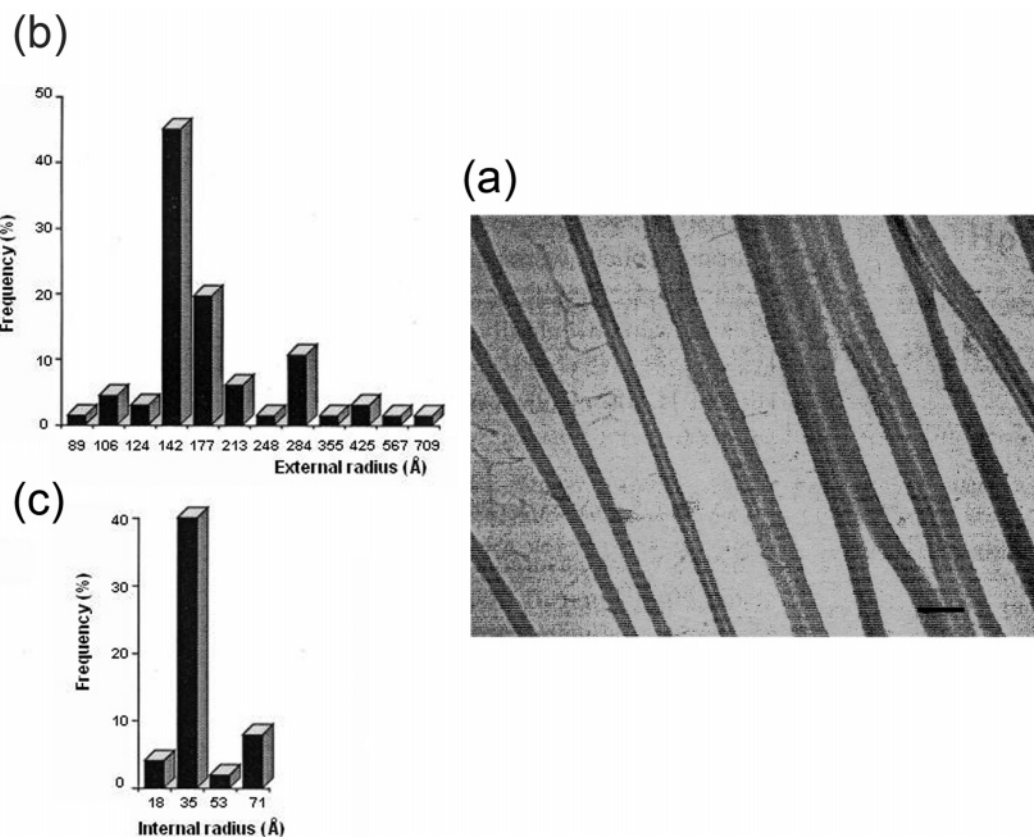


Figure 16. (a) Cryo-TEM photograph of an aqueous dispersion of **42b** (3%, w/v) at room temperature and the distribution of cross-sectional radii of the nanotubes (scale bar = 100 nm). (b) External radius and (c) internal radius. (Reproduced with permission from ref 165. Copyright 1999 Academic Press.)

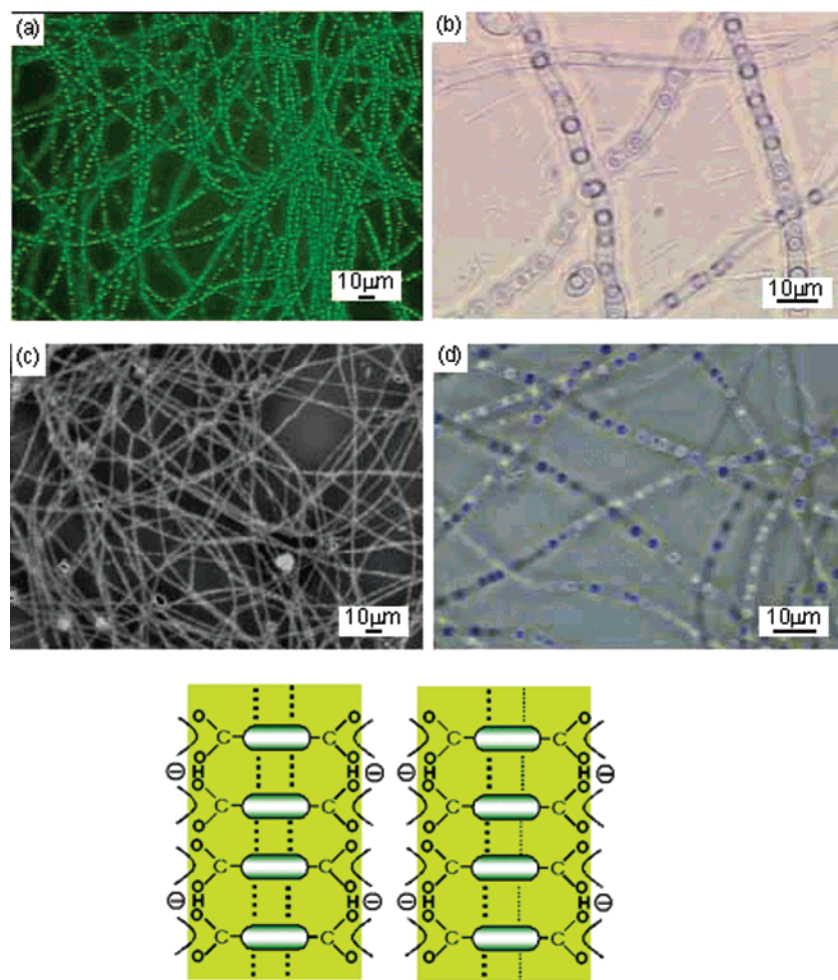
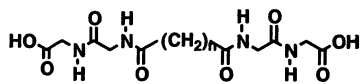


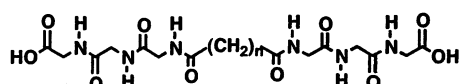
Figure 17. (a, b) Phase-contrast and (c, d) dark-field optical micrographs for the vesicle-encapsulated microtubes formed from 46e. (bottom) Schematic representation of the intralayer acid/anion interaction that is responsible for the microtube formation.

scattering (SANS), which have been applied for gels formed by a steroid derivative in various organic solvents,^{162–164} revealed the details of the tubular dimension from **42b**.¹⁶⁵ The hollow cylindrical nanotubes have an external diameter of 14 nm and an internal diameter of 3.5 nm, for a wall thickness of 5.25 nm; the wall consists of three interdigitated and/or tilted bilayer structures (Table 1 and Figure 16). To the best of our knowledge, the obtained inner diameter seems to be the smallest among the nanotubes formed from synthetic lipid molecules.

Peptidic Amphiphiles. A new family of dicarboxylic oligopeptide bolaamphiphiles with oligoglycine headgroups, **46a**, **46c**, **46e**, and **47b**, self-assembles into vesicle-encapsulated microtubes.



46a: $n = 6$, **46b:** $n = 7$, **46c:** $n = 8$, **46d:** $n = 9$,
46e: $n = 10$, **46f:** $n = 11$, **46g:** $n = 12$, **46h:** $n = 14$



47a: n = 6, 47b: n = 10

Optical microscopy, including phase-contrast and laser scanning microscopy, revealed well-defined microtube structures with closed ends and a uniform diameter (about 1–2 μm) (Table 1 and Figure 17).¹⁶⁶

All the microtubes encapsulated a number of vesicular assemblies in the confined aqueous compartment. Microtube formation occurred only when the oligomethylene chain had an even number of carbons (C6, C8, and C10) and the constituent amino acid residues were Gly-Gly and Gly-Gly-Gly.¹⁶⁷ Both vectorial formation of acid-anion dimers and loose interpeptide hydrogen-bond networks are responsible for the microtube self-assembly (Figure 17, bottom). Careful atomic force microscopy of the microtubes from **46e** revealed a distorted hexagonal arrangement of the peptide headgroups on the surface and hierarchical formation of structures (bent molecule-distorted layer-columnar domain-membrane wall) in a profile of the microtube membrane.¹⁶⁸

Interestingly, single-head, single-tail-type peptide amphiphile **48** with a glycylglycine moiety proved to coordinate to divalent or trivalent transition-metal cations such as Fe^{3+} , La^{3+} , Mn^{2+} , Co^{2+} , Cu^{2+} , and Zn^{2+} , producing tubular structures upon self-assembly.¹⁶⁹ The nanotubes precipitated immediately after the addition of metal salts to a weakly alkaline

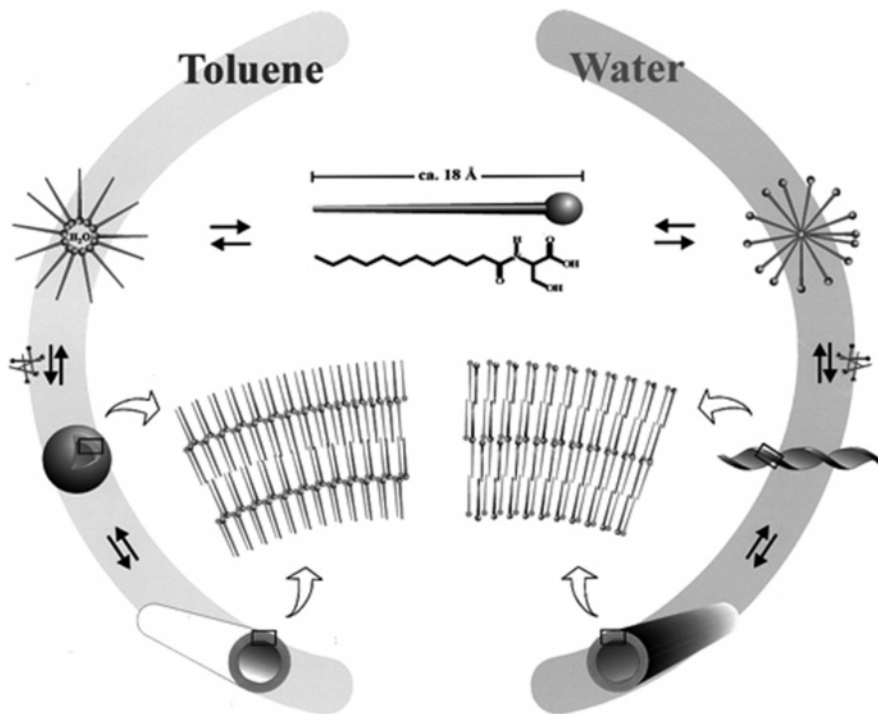
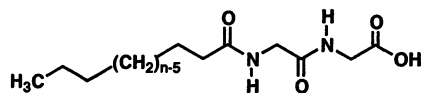


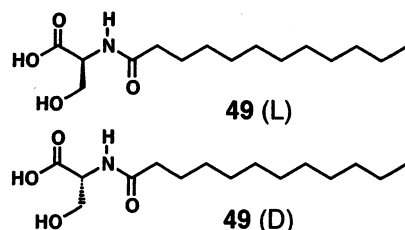
Figure 18. Schematic illustration of the different pathways of aggregated **49** from micellar bilayers in water (micelles, helical ribbons, nanotubes) as well as from inverse bilayers in toluene (micelles, multilayered vesicles, nanotubes) toward smooth tubular rods. (Reproduced with permission from ref 131. Copyright 2001 American Chemical Society.)

aqueous solution of **48**. This finding indicates that organic–inorganic hybrid nanotubes can also be formed in a similar way as nanofibers.^{170–172}



48: ($n = 10, 11, 12, 13, 14$, and 15)

By using cryo-electron microscopy, Boettcher et al. detailed the molecular packing features and aggregation pathways of tubular structures in organic solvents.¹³¹ Hot solutions ($>80\text{ }^{\circ}\text{C}$) of *N*-dodecanoyl (D- or L-) serine (**49**) in toluene were cooled to room



temperature to produce gels consisting of LNTs and vesicles. Comparative cryo-transmission electron microscopy permitted the first direct comparison of the molecular tubular structures (diameters, 80 – 130 nm) obtained from the amino acid amphiphile **49** under normal and reversed polarity conditions (Table 1 and Figure 18). All supramolecular assemblies had similar multilayers with a measured periodicity of 3.30 ± 0.01 nm both in water and in toluene, giving normal bilayers with the hydrophilic headgroups oriented toward the aqueous environment and “inverse” bilayers with the alkyl

chains oriented toward the hydrophobic toluene phase, respectively.

Lu et al. have observed that severely truncated variants of the disease-associated β -amyloid peptide—for example, the seven-residue (16–22) peptide amphiphile $\text{CH}_3\text{CO}-\text{KLVFFAE}-\text{NH}_2$ (**50**)—form nanotube structures by means of fusion of the edges of the coiled ribbons in an aqueous environment.¹⁷³ SANS and SAXS results revealed a hollow cylinder structure with an outer diameter of 52 nm and a wall thickness of 4 nm, suggesting the presence of a peptide bilayer (Table 1). Indeed, branched nanotubes composed of a bilayer structure, having an average diameter of 30–50 nm, were observed to self-assemble from surfactant-like peptides.¹⁷⁴ The peptide monomer contains a hydrophilic headgroup composed of charged aspartic acids and a hydrophobic tail made of alanine, valine, or leucine. Peptides having a propensity to form β -sheet structures self-assemble into fibers (not nanotubes) from twisted ribbons or helical tapes with increasing concentration.^{175,176} Molecular dynamics (MD) simulations proved to be useful to gain an insight into how the peptide tapes and ribbons are governed by the microscopic molecular interactions.^{177,178}

In biology, proteins that interact with lipids play an important role in shaping stable vesicular structures in cellular membrane systems.¹⁷⁹ A number of membrane tubules have been observed to form the Golgi complex, the trans Golgi network, and the connections between the Golgi stacks of eukaryotic cells.^{180–184} What is the minimal machinery required to form such membrane tubules? A de novo-designed 18-mer amphiphilic α -helical peptide, KLLKLLLKLL-WLKLLKLLL, was found to transform spherical liposomes from a Golgi-specific phospholipid mixture

into tubules resembling those from the Golgi apparatus in scale and shape.^{180,185}



50

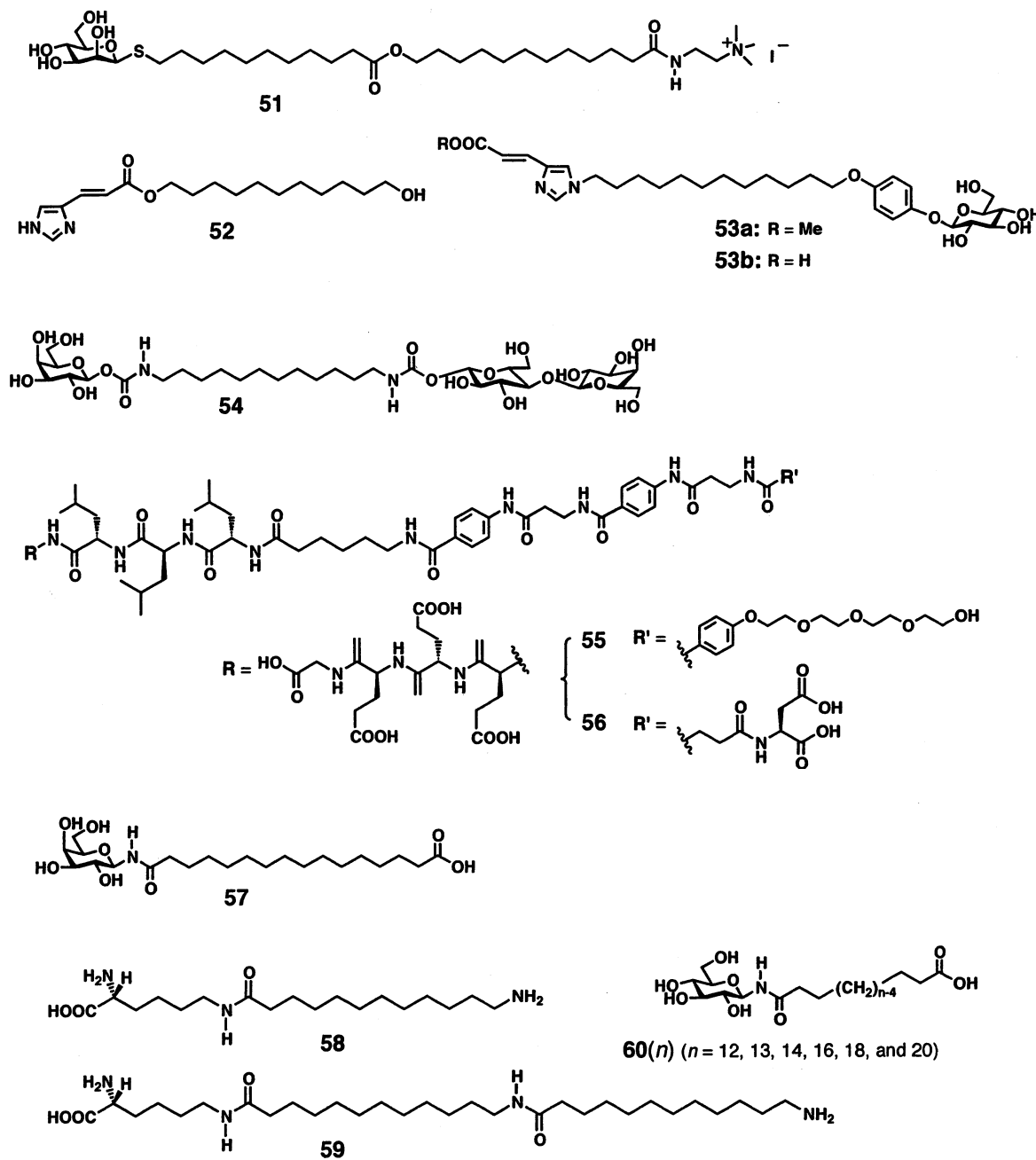
Unsymmetrical Bolaamphiphiles (Chart 1).

Heteroditopic 1, ω -amphiphiles, which have headgroups that differ in size or properties, tend to form nanotubular structures by self-assembly.^{138,186,187} Synthetic unsymmetrical bolaamphiphiles **51–56** have been found to assemble into tubular assemblies.^{81,188–191} Nanofibers,^{191–195} vesicles,^{196–198} and crystals^{199–201} are also formed from other bolaamphiphiles. Most of the bolaamphiphiles pack in antiparallel fashion to form symmetrical monolayer lipid membranes (MLMs), except for bolaamphiphile

57, which has one galactose headgroup and one carboxylic headgroup and orients in parallel fashion to form an unsymmetrical MLM (Figure 19).¹⁹⁹

Fuhrhop et al. have reported that rod micelles and nanotubes of unsymmetrical bolaamphiphiles **58** and **59**, which have one amino acid (D- and L-lysine or D- and L-ornithine) headgroup and one ammonium chloride headgroup, self-assemble to form membranes of monomolecular thickness (Table 1 and Figure 20).⁸¹ It is unknown whether the amino acid groups are arranged statistically or asymmetrically, with the smaller amino groups on the inner surface, as is observed for some vesicles.¹⁹⁶ Unsymmetrical bolaamphiphiles **60(n)**, which have D-glucose and carboxylic acid headgroups and were designed according to a similar molecular design to that of Fuhrhop, proved to produce nanotube structures

Chart 1



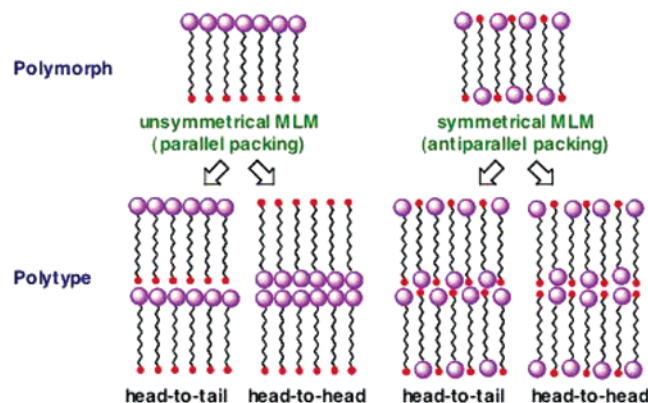


Figure 19. Formation of monolayer lipid membranes (MLMs) from unsymmetrical bolaamphiphiles and resultant structures formed by the stacking of the MLMs.

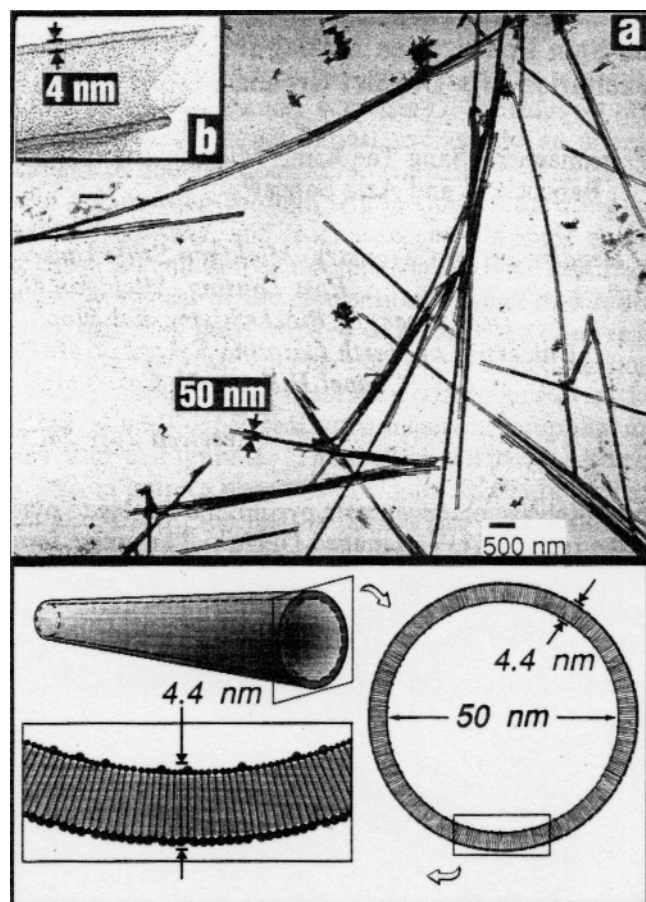


Figure 20. (a) TEM image of molecular monolayer nanotubes made of **59** (pH 10.5, negatively stained with 2% phosphotungstate). (b) Magnification of part (a) showing the 4 nm monolayer membrane. The model of the nanotube assumes a statistical arrangement of headgroups with some preference for the smaller amino headgroup on the smaller inner surface (bottom). (Reproduced with permission from ref 81. Copyright 1993 American Chemical Society.)

exclusively (Table 1).⁸² Clear TEM images of the nanotubes filled with a phosphotungstate staining reagent revealed 30–43 nm outer diameters, 14–29 nm inner diameters, and lengths of several hundred micrometers (Figure 21). By comparing the membrane stacking periodicity obtained from powder X-ray diffraction with the molecular packing within

single crystals, our own research group was able to give strong evidence that these nanotubes consist of an unsymmetrical MLM, in which the molecules pack in parallel. The evaluated inner diameters are compatible with calculated values for the bolaamphiphiles with different oligomethylene spacer lengths (see section 5.2).

Cholesterol Derivatives (Chart 2). The formation of cholesterol monohydrate crystals may be a trigger of cholesterol gallstone disease.^{123,202–204} Incubation of model bile-containing sodium taurocholate **61**, phosphatidylcholine **62**, and cholesterol with the molar ratio 97.5:0.8:1.7—for a few days in water resulted in self-assembly of helices, nanotubes, and plate-like crystals in that order over time.⁷² Furthermore, the cells of patients afflicted with globoid cell leukodystrophy were found to include helical ribbon-like structures leading to tubular morphology.¹⁵⁸ A simple aqueous solution of elementary bile steroid derivative **63** (lithocholic salt) can produce steroid nanotubes that show quite monodisperse cross sections with an inner cylindrical cavity of 49 nm diameter (Table 1 and Figure 22).²⁰⁵ The wall thickness estimated by TEM or SAXS, ca. 1.5 nm, corresponds closely to a monomolecular length of the steroid.

To our knowledge, tubular morphologies with hollow cylindrical structures have been detected in aqueous solutions or dispersions but have never been observed in organic solvent systems. Shinkai's research group is the first to report nanotube formation from synthetic amphiphiles in a nonaqueous solvent.²⁰⁶ Cholesterol-based organogelators **64** and **65**, which have monoaza-18-crown-6 and 1,10-diaza-18-crown-6 moieties, respectively, self-assemble in cyclohexane to form tubular structures with 45–75 nm wall thicknesses and 170–390 nm inner diameters (Table 1). Microscopic observation of a multilamellar structure for the wall indicated that these structures grew from curved lamellar sheets into paper-like rolls. In a related finding, helically coiled ribbon structures formed first in the organogel prepared with the new cholesterol-based organogelator **66**, which bears a dibenzo-30-crown-10 moiety.^{207,208} As is often the case with nanotube-forming amphiphiles in aqueous media, nanotube formation occurred via a linear ribbon and subsequent formation of a helical ribbon as a metastable intermediate structure.

Others (Chart 3). The work on amphiphilic hexaperi-hexabenzocoronene **67** followed the interesting work on "supramolecular peapods" composed of linear zinc porphyrin nanotubes and fullerenes.²⁰⁹ Compound **67** was observed to self-assemble in tetrahydrofuran into graphitic nanotubes.²¹⁰ These π -electric, discrete nanotubular objects have uniform 14 nm inner diameters, 3 nm wall thicknesses, and aspect ratios greater than 1000 (Table 1). Interestingly, upon oxidation, a single piece of this redox-active nanotube across 180-nm-gap electrodes showed an electrical conductivity of 2.5 M Ω at 285 K.

The self-assembly behavior of a new series of bis-(quaternary ammonium) gemini surfactants **68(n-2-m)** has been examined in aqueous solutions to determine how the molecules' dissymmetry affects their self-assembled morphologies.^{211–213} Clusters of

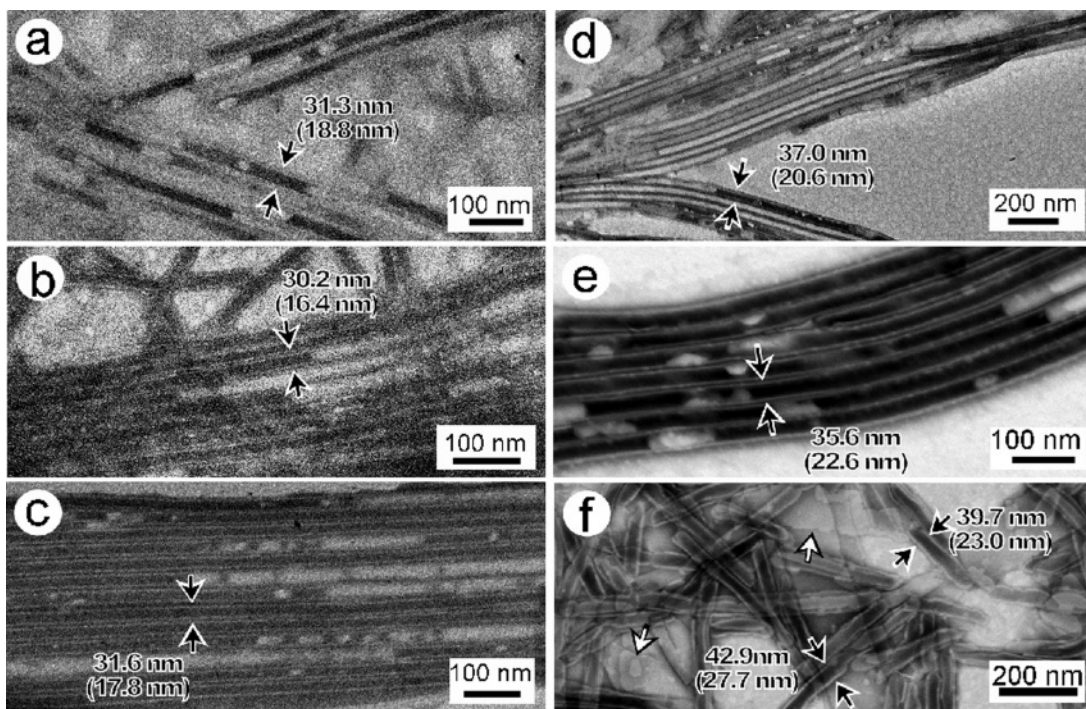
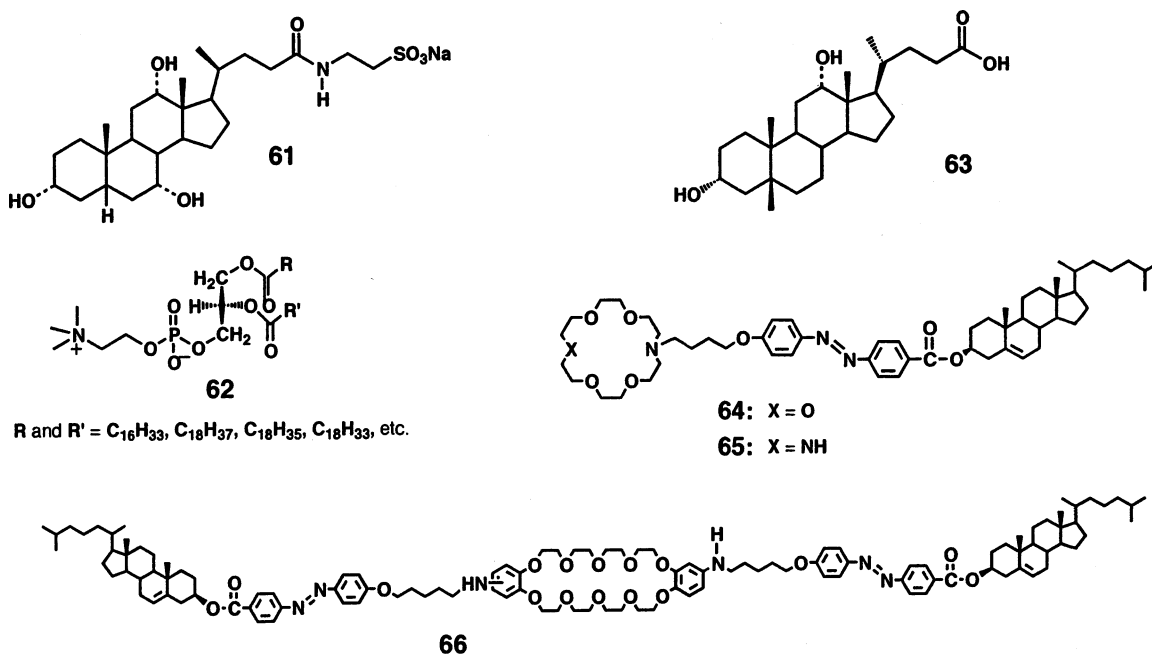


Figure 21. TEM pictures of the nanotubes formed from (a) **60(12)**, (b) **60(14)**, (c) **60(16)**, (d) **60(18)**, (e) **60(20)**, and (f) the sodium salt of **60(18)**. Each sample was centrifuged and negatively stained with phosphotungstate. The numerical values indicate the outer and inner diameters (in parentheses) of the nanotube indicated by arrows.

Chart 2



long and entangled tubule-like structures form from **68(14-2-14)**, **68(16-2-16)**, and **68(18-2-18)**, strongly depending on the chain length and the molecular dissymmetry. In particular, the chirality of the self-assembled microstructures can be varied by changing the counterion enantiomers.²¹⁴

Microtubes are also formed by the self-assembly of macrocyclic lipid **69**, which mimics an archaeal membrane lipid and contains a 1,2-bis(tricosano-10,12-dienoyl)-sn-glycero-3-phosphocholine moiety (Table 1).²¹⁵ Lipid analogue **70**, synthesized by acylation of 1-(N,N-1-dimethylamino)-ethyl-2,3-dihydroxybutyramide with two molecules of pentacosano-10,12-dienoic

acid, was found to produce long lipid tubules (>1000 μm) in the presence of acid (Table 1).²¹⁶ Also observed were interesting nested structures in which spirals reside inside the hollow. A single-chain bolaamphiphile containing two Schiff base rigid segments connected by an oxydiphenylene chromophore group, N,N-bis[4-trimethylammonium bromo-dodecyloxyacetylaldehyde]diamines **71a** and **71b**, can also form tubular assemblies and bundles of fibers, respectively, in dilute aqueous solutions.²¹⁷ Replacing the rigid oxydiphenylene moiety in the rigid segment center with a flexible methylene chain (**71c** and **71d**) converts the self-assembled morphologies from linear ag-



Figure 22. Cryo-TEM images of a vitrified aqueous dispersion containing 0.1% sodium salt of **63**. Thick arrows indicate twisted ribbons, double thin arrows refer to a nanotube end, and arrowheads show where a nanotube is disintegrating into (or formed from) a wide ribbon. (Reproduced with permission from ref 205. Copyright 2002 Wiley-VCH.)

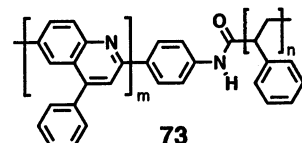
gregates to spherical vesicles. This finding emphasizes the importance of the connector structure for controlling the morphology of the bolaamphiphile monolayer.

Naturally occurring LNTs densely cover the surfaces of pine needle stomata. CO₂ and O₂ gases are exchanged through these LNTs, which filter dust particles from the air.^{218,219} The nanotubes are mainly composed of the secondary alcohol nonacosan-10-ol

(**72**).²²⁰ It is unknown whether the naturally occurring nonacosan is a pure enantiomer. Fuhrhop et al. actually reproduced the nanotube formation using synthesized pure enantiomer (*S*)-**72** through self-assembly.²¹⁹

4.2 Amphiphilic Polymers

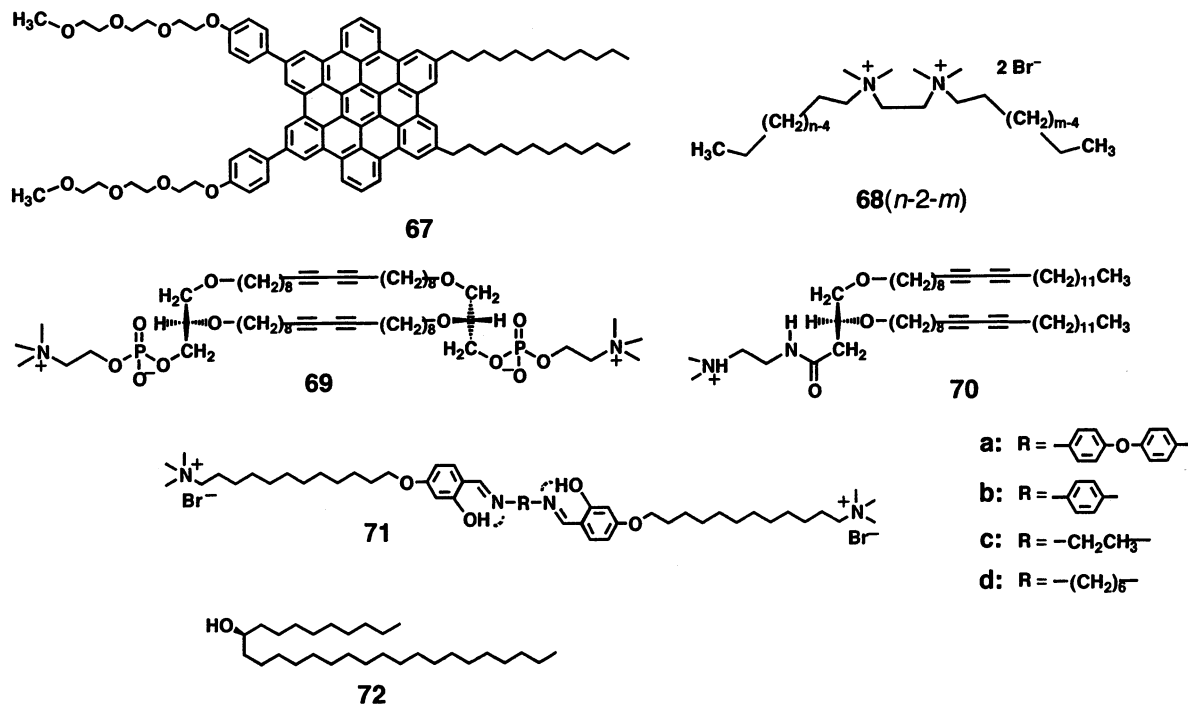
Rod–Coil Block Copolymers. Rod–coil block copolymers have a rigid rod block that tends to form a highly crystalline domain and provide anisotropic intermolecular interactions. Poly(phenylquinoline)-block-polystyrene (PPQ-*b*-PS) (**73**) self-assembles to



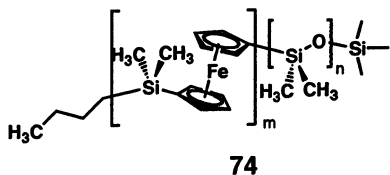
form spheres, lamellae, microtubes, or vesicles in mixtures of trifluoroacetic acid (TFA) and dichloromethane.²²¹ The main determinants of the morphologies are the initial solvent composition and the evaporation rate of the solvent. Microtubes with 1–3 μm outer diameters become the major morphology when the TFA composition is high (>90%) (Table 1). The rod block PPQ, which is more miscible with TFA than PS is, distributes on the outside of the microtube. The shorter rigid block results in smaller assemblies. The self-assemblies are extremely robust at 200 °C (*T*_g of the PS block = 100 °C). The PS block can capture fullerene, but the presence of spherical molecules inhibits the formation of nonspherical aggregates.

Redox-active organometallic nanotubes with widths of 29–40 nm can be obtained from the self-assembly of the rod–coil block copolymer poly(ferrocenyldimethylsilane)-block-poly(dimethylsiloxane) (PFS-*b*-

Chart 3



PDMS) (**74**) (Table 1).^{25,26} The relatively rigid ferro-

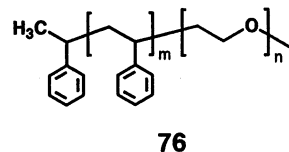
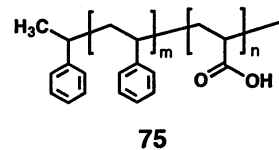


cenyl group provides self-assembled redox-active materials with its semiconducting properties, and it can also serve as a ceramic precursor that can catalyze carbon nanotube formation. The PFS40-*b*-PDMS480 and PFS80-*b*-PDMS960 copolymers self-assemble to form nanotubes in *n*-hexane and *n*-dodecane, which are good solvents for the PDMS block (see Figure 9(3)). The PDMS/PFS block length ratio of the copolymer affects the final morphology. If the PDMS/PFS ratio is between 1:12 and 1:18, long hollow nanotubes form,^{25,26} whereas a block ratio of 1:6 results in the formation of cylindrical micelles.²²² Addition of water to the self-assembly solvent (hexane) induces the conversion of discrete nanotubes into bundles.

The molecular weight of **74** had no effect on the wall thickness and nanotube diameter when the rod-coil block ratio was constant. The wall thickness of the nanotube was almost constant (9–12 nm). If the PFS block undergoes chain folding, an average of four folds for PFS40-*b*-PDMS480 and eight folds for PFS80-*b*-PDMS960 are required to maintain this shell thickness.²⁶ Interestingly, this system showed reversible phase-transition behavior similar to that observed for lipid aggregates of low-molecular-weight amphiphiles.²²³ On cooling, spherical micelles in an aqueous dispersion transformed into rod micelles and finally nanotubes. Thus, these self-assembled morphologies are equilibrium structures similar to those formed from low-molecular-weight lipids.

The molecular design requirements for the construction of polymer nanotubes are not yet clear, since the theory of coil-crystalline block copolymer micelles primarily predicts a lamellar structure for the crystalline block.²²³ A fraction of the soluble PDMS chain may penetrate into the interior of long hollow tubes. This suggests that the space filling need of the PDMS coil may be balanced by the strongly disfavored interfacial energy of the PFS crystalline domain. In relation to the interfacial energy, it is interesting to note that the nanotube length can be controlled from a few micrometers to 100 μm by changing the solvent from *n*-hexane to *n*-dodecane.²⁶ The interfacial energy between the PFS block and lower linear alkanes is much smaller than that between the PFS and dodecane. As a result, exposure of the PFS domain at the nanotube end is more unfavorable in *n*-dodecane, and the high axial ratio of the nanotube in *n*-dodecane increases.

Coil-Coil Block Copolymers. Polystyrene-*b*-poly(acrylic acid) (PS-*b*-PAA) (**75**) and polystyrene-*b*-poly(ethylene oxide) (PS-*b*-PEO) (**76**) aggregate into various morphologies such as spheres, rods, vesicles, lamella, nanotubes, and large compound micelles (Table 1).^{22,23,27,224,225} In these so-called crew-cut aggregates, the corona-forming block is much



shorter than the core-forming block.²²⁶ The aggregate morphology of these kinetically trapped self-assemblies is affected by many factors. The ratio between the two blocks is especially important for controlling their morphologies, which is also the case for the rod-coil block copolymers described above. The assemblies are prepared by dropwise addition of water, a poor solvent for the hydrophobic block, into a polymer solution in DMF, followed by dialysis to remove the residual DMF completely.

For nonionizable PS-*b*-PEO block copolymers **76**, the PS/PEO block ratios are critical determinants of the morphologies. Copolymers with 240/15 to 240/45 ratios often produce tubular morphologies.²² As the PEO block is made longer and longer, the resulting morphology progresses from lamellar tape and lamellar rods to spherical micelles.^{224,227} The wall thicknesses of the nanotubes are typically ca. 20 nm, and their outer diameters are ca. 100 nm. The lengths can reach hundreds of micrometers. The formation mechanism of these nanotube is unclear, although adhesive contact and fusion of vesicles are involved. The intermediate structures in the transition from vesicles to tubes support this view (Figure 23).²² Although those nanotubes possess bilayer membrane structures, the chirality and helical nature of the polymer amphiphile are less important than those of tube-forming amphiphiles with low molecular weights for the construction of nanotubes. However, as compared with the self-assembly of the low-molecular-weight amphiphiles, a superhelix structure formed from a chiral block copolymer is of special interest, since such a coiled morphology is known as an intermediate of lipid nanotube architectures based on chiral self-assembly.²²⁸

4.3. Polymerization and Cross-Linking

Polymerization of self-assembled tubular architectures can fix and stabilize well-defined nanotubes^{229–231} and enable further processing, such as modification²³² and positioning to a solid substrate. Polymerization of tubular self-assemblies with minimal distortion of the well-ordered architecture requires that attention be paid to the compatibility of the repeat distance of a polymer chain. When polymerizable lipid molecules are used within a lamellar nanotube structure, polymerizable groups that can give a polymer chain with a molecular repeat distance of 0.44–0.50 nm should be employed. If the distance is shorter than that, the polymerization will terminate early, and the tubular architectures may even be destroyed. This topological requirement for the polymerization pre-

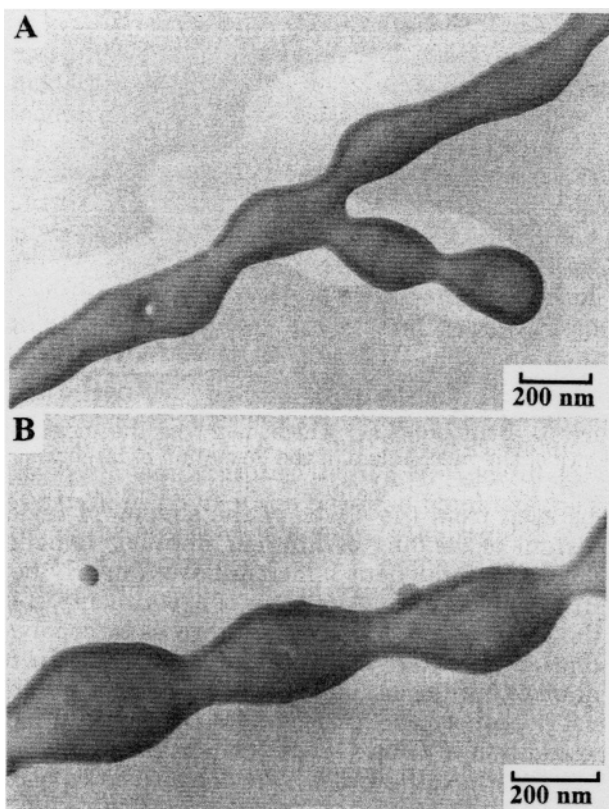
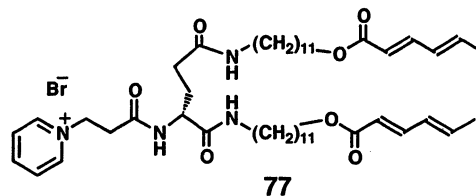


Figure 23. TEM micrograph of PS(240)-*b*-PEO(15) block copolymer **76**. Possible intermediates of the vesicle to nanotube transition: (A) a nanotube with attached vesicle; (B) a nanotube with an oscillatory perturbation in the diameter. (Reproduced with permission from ref 22. Copyright 1998 American Chemical Society.)

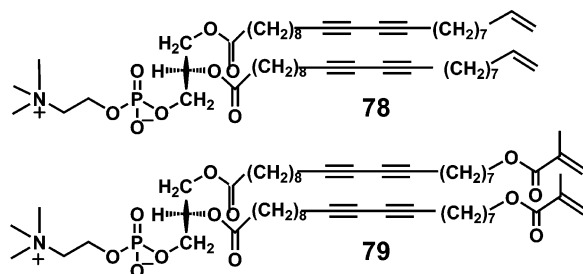
cludes the use of efficient 1,2-polymerization processes such as radical polymerization of methacrylates, which gives a repeat distance of ca. 0.25 nm. By contrast, 1,4-chain polymerization gives a repeat distance of ca. 0.48 nm.²³³ Thus, polymerization of diacetylene, diene, and dienoyl groups has been used extensively in topochemical reactions in the crystalline state,^{234–237} thermoplastic elastomers,²³⁸ bilayer membranes,^{239–241} monolayer membranes,²³⁷ hexagonal mesophases,^{242,243} columnar stacks,²⁴⁴ and nanofibers.^{245,246} The extensively studied diacetylenic lipid 1(8,9) was in fact developed for the purpose of stabilizing liposomes.^{106,107,110}

The conversion of nanotubes into helical ribbons upon polymerization takes place for many diacetylenic lipids, as mentioned above.^{132,247-249} This is probably because the resultant en-yne (alternate chain of double and triple bonds) polymer chain rigidifies the tubular membrane. Consequently, the polymerization process unrolls the nanotube membranes formed by a rolling-up mechanism and transforms them into twisted or helical ribbons with membranes that are less curved than those of the nanotubes. In this respect, the dienoyl or diene moieties are potential polymerizable groups for the nanotube formation, since the resultant polymer will have a more flexible ethylene-monoene polymer chain. In fact, the corresponding lipid **77** self-assembled to form a helical tape but transformed into a tubular morphology after polymerization, as men-

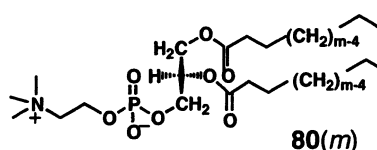
tioned above (Table 1).^{250,251} The diameters (25–30 nm) of the obtained nanotubes were nearly equal to those of the original helices, but the aspect ratio of the nanotubes was very low (<10).



The first attempt of polymerization for LNTs was carried out by UV (254 nm) irradiation of **1**(8,9)¹³ or **1**(8,6).²⁴⁸ The polymerization of **1**(8,9) was moderately successful, since the polymerized nanotube transformed into a flake-like morphology²⁴⁸ or into helical and twisted ribbons.²⁴⁹ However, some reports merely mention that polymerization failed to induce any morphological changes.¹³ They also describe that monomer conversion to a polymer reached 20%²⁵² or 40%.²⁴⁸ The difference between these two values is probably due to the difference in polymerization conditions. Relatively lower monomer conversion in the **1**(8,9) system is due to restricted movement of the monomer lipids during UV polymerization. Two approaches were attempted to overcome the inefficiency of polymerization using **1**(8,9) nanotubes as a matrix.¹²⁰ The first approach involved incorporation of additional polymerizable moieties in the diacetylenic lipid monomer. Vinyl (**78**) and methacrylate (**79**) groups were placed at the terminus of the acyl chains of **1**(8,9) to polymerize them by UV and γ -ray irradiation after confirmation of nanotube formation. Polymerization of both systems showed improved monomer conversion; no residual monomers were found after irradiation. However, in both cases, extensive polymerization also disrupted the tubular structures somewhat.



The second approach involved mixing of **78** or **79** with **1**(8,9). This attempt succeeded in increasing the monomer conversion with retention of the tubular morphology.¹²⁰ Similar enhanced conversion was also observed when **1**(8,9) was mixed with the nonpolymerizable shorter-chain analogue **80**(8).²⁵² The polym-



erization of LNTs enhances not only the stability of

Table 3. Experimental Conditions or Structural Factors That Affected the Regulation of Lipid Nanotube Dimensions

affected dimension	amphiphile	conditions and factors	ref
outer diameter (o.d.)	82(n)	headgroup structure and size, and incubation media (pH, ionic strength, etc)	259, 261
	80(m) + 1(m,n)	binary mixing	252, 263, 264
	5	replacement of the C—O—P linkage with the C—C—P linkage in 1(8,9)	125
	83	replacement of the C—C—P linkage with the C—P linkage in 5	265
inner diameter (i.d.) length (L)	60(n)	molecular length of unsymmetrical bolaamphiphile	82
	1(8,9)	solvent composition	266, 267
	1(8,9)	cooling rate	79
thickness (th)	32	time and rate of mechanical stirring	269
	1(8,9)	solvent composition of ethanol/water, methanol/water	267

the tubular morphology on dehydration but also robustness against thermal, mechanical, and chemical stimuli, and yet it reduces the solubility of LNTs in the solvent in which the monomer component dissolves.^{120,133,136,253} The polymerization of mixtures of **1(8,9)** and the vinyl-terminated analogue **78** also gave robust nanotubes that retained their morphologies upon brief sonication, freeze-drying, and redispersion in water and organic solvents. However, the polymerized pure **1(8,9)** nanotube was unstable under the same conditions.¹²⁰ Differential scanning calorimetry studies of the polymerized nanotubes showed no remarkable gel-to-liquid crystalline phase transition, although this clearly occurs for the self-assembled nanotubes.^{133,248}

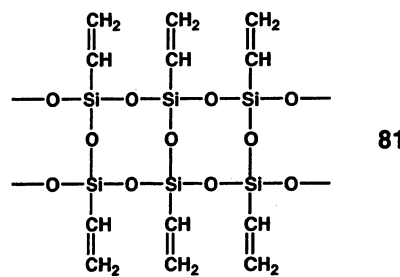
A variety of single-head, single-chain diacetylenic lipids, such as glycopeptide lipids,²⁴⁷ achiral phospholipids,²⁵³ and glycolipid,^{132,133,136} have been synthesized, and their self-assembly morphology and polymerizability within assemblies have been tested. Most of the diacetylenic aldonamides, including galactonamide **12**, gluconamide **13**, mannoamide **14**, and gulonamide **15**, form nanotubes, as well as helical ribbons as a minor morphology. The morphologies and dimensions of the nanotubes depend on the stereochemistry of the sugar headgroup, the length of the hydrophobic chain, and the position of the diacetylenic group. All the nanotubes maintained their shape during polymerization,^{133,136} whereas analogues of **13** that differed in the length of the diacetylenic chain and in the position of the diacetylene moiety transformed into helical rods or did not undergo polymerization.¹³² After polymerization, lipids **12** and **14** were purple in color ($\lambda_{\text{max}} = 600\text{--}610\text{ nm}$), while **13** and **15** were reddish orange ($\lambda_{\text{max}} = 500$ and 523 nm).

The observation that diacetylene polymerization proceeds efficiently within **1(8,9)** nanotubes or other LNTs suggests that the molecules pack in a highly ordered state, since this type of polymerization is known to require critical structural alignment.^{234,254} This is the reason that the diacetylene moieties of **1(8,9)** polymerize only at temperatures below the gel-to-liquid crystalline phase transition temperature (T_{g-1}), ca. $40\text{ }^{\circ}\text{C}$ for **1(8,9)**.²⁴⁸ In contrast, the dienoyl group can be polymerized either below or above the T_{g-1} .^{231,250}

The conversion, degree of polymerization, and connectivity of the polymer chain strongly affect the properties of polymerized nanotubes, including their

stability and elasticity and the impermeability of the membrane. There is no detailed information about those properties, owing to the poor solubility of polydiacetylene itself.²⁴⁹ Cross-linking of multiple polymerizable groups in the monomer assembly also prevents solubilization and analysis of the polymerized nanotubes. Furthermore, there are many factors that determine the polymerizability, such as the position of the polymerizable groups, the hydrophobic chain length, the degree of interdigitation of lipids, the dimensions of the nanotubes, and the details of the nanotube-to-ribbon transformation triggered by polymerization, as well as the mechanical properties of polymerized nanotubes.

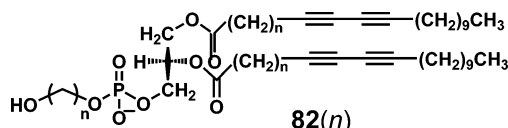
Interestingly, a ladder-like polymer made of polyvinylsilsesquioxane **81** plays an important role in the synthesis of organic tubular polymers. The ladder-like polymer with the syn-isotactic structure combines with different coupling agents to form nanotubes with various inner diameters.^{255,256}



5. Control of Dimensions

5.1. Outer Diameter

A short review focusing on advances that led to the ability to control the architecture of assemblies generated from lipid **1(8,9)** has already been published.²⁵⁷ Continuum theory^{67,68,71,258} predicts that diameters can be controlled by varying the molecular chirality and the molecular tilt with respect to the bilayer planes.¹² Table 3 summarizes the factors that determine LNT dimensions upon chiral or packing-directed self-assembly. In the LNT formation of **1(8,9)**, the kinetics control optimizing the cooling rate, the solvent composition (alcohol/water), lipid concentration, or cosurfactants proved to be insensitive to the nanotube diameter.¹⁰⁵ Negatively charged diacetylenic lipids **82(n)**, derivatives in which the headgroup structure of **1(8,9)** is modified, were



synthesized in an effort to control the nanotube diameter. Lipids **82(2)** underwent metal-ion-assisted self-assembly to form hollow cylinders. The diameters of the nanotubes ranged from 80 ± 20 to 960 ± 120 nm, depending sensitively on the lipid headgroup size, the pH, the ionic strength of the dispersion medium, and the nature of the anions (Table 3).^{259–261} However, these approaches have not yet proven practical for industrial application.

Changes in experimental conditions, such as the mixing ratio between alcohol and water in the dispersion media, the speed of mixing, the type of alcohol used, and the cooling rate, affect the shape and morphology of the resultant molecular assemblies. In this regard, addition of the short-chain saturated lipid 1,2-bis(dinonanoyl)-*sn*-glycero-3-phosphocholine [**80(8)**] to **1(8,9)** not only increased polymerization efficiency but also altered the dimensions and morphology of the aggregate.^{252,262} Extensive studies showed that the use of an equimolar mixture of short-chain lipid **80(8)** and **1(8,9)** markedly affected the outer diameter of the resultant nanotubes. The mixing procedure provided nanotubes having 50–60 nm diameters, which are an order of magnitude smaller than those of pure **1(8,9)** nanotubes (Figure 24).²⁶³ The nanotube phase remained stable for at

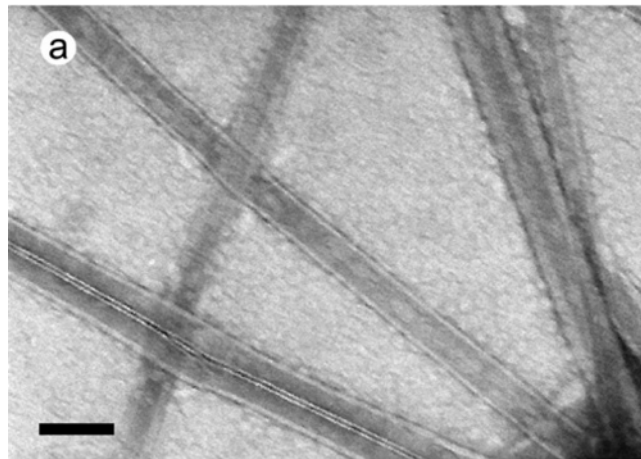


Figure 24. Negative stained TEM image of nanotubes formed from an equimolar mixture of **1(8,9)** and **80(8)** (2 mM total lipid concentration) (scale bar = 100 nm). (Reproduced with permission from ref 263. Copyright 2001 American Chemical Society.)

least 3 months at 4°C . Interestingly, continued incubation of the nanotube aqueous suspension caused a gradual transformation into a lipid gel phase consisting of interconnected helical ribbons, and this behavior was strongly dependent on the total lipid concentration. Further study suggested that, in the twisted ribbon phase, the nonanoyl chains of **80(8)** are disordered to allow the entire membrane to be fluid.²⁴⁹ Thus, polymerization of **1(8,9)** may trigger spontaneous nanotube-to-ribbon transformation in the mixture.²⁴⁹ Furthermore, binary lipid mixtures

composed of short-chain saturated phospholipids **80(m)** and diacetylenic phospholipids **1(m,n)** have been carefully examined to tune the nanotube diameters; increasing n from 9 to 13 results in an increase in the diameter of the nanotubes from 79 ± 8 to 127 ± 12 nm.²⁶⁴

Subtle modification of the molecular structure of **1(8,9)** markedly affects the outer diameters. An analogue (**5**) of **1(8,9)** in which the C–O–P phosphoryl linkage between the choline headgroup and the glycerol backbone is replaced by a C–C–P phosphonate functionality produces nanotubes with diameters twice the diameter of **1(8,9)** nanotubes.¹²⁵ Furthermore, structurally modified analogue **83**, in which the C–C–P linkage is replaced by a C–P linkage, produces new nanotubes having diameters 1.94 times the diameter of **1(8,9)**, significantly shorter lengths, and thinner membranes (Table 3).²⁶⁵ Despite the differences in nanotube diameters, **1(8,9)**, **5**, and **83** have similar interlamellar spacings d (Figure 25). Thus, small changes in bond lengths and bond angles associated with replacement of the C–C–P linkage are large enough to produce a noticeable change in self-assembled morphology.

5.2. Inner Diameter

A novel and practical approach for controlling inner diameters has been developed by designing the

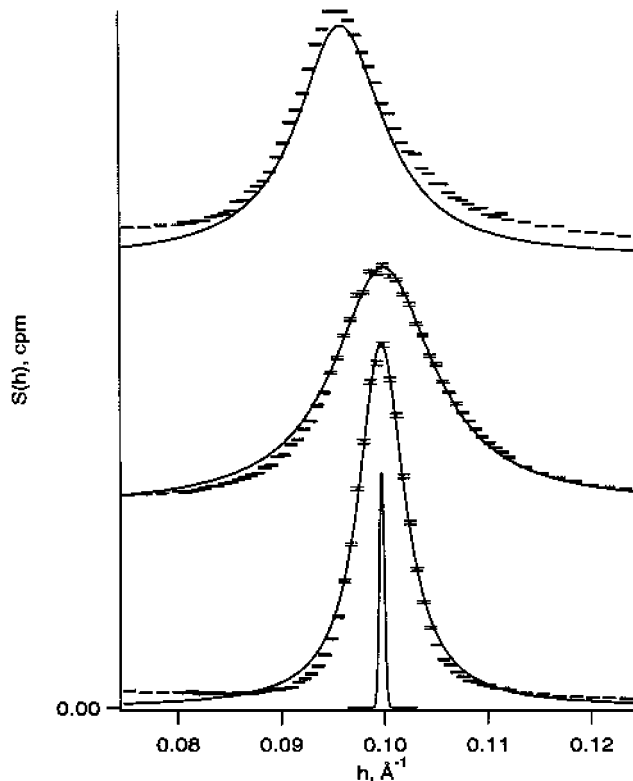
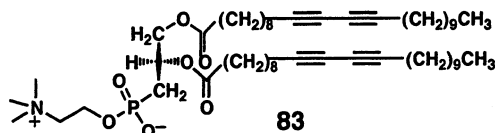


Figure 25. Small-angle X-ray scattering showing the interlamellar fundamental peaks from phosphonate nanotubes with **5** (top), **83** (middle), and **1(8,9)** nanotubes (bottom). The data are drawn to the same scale but offset vertically for clarity. The solid trace is the 0.0007 \AA^{-1} fwhm instrument resolution, drawn to a different vertical scale. (Reproduced with permission from ref 265. Copyright 2002. American Chemical Society.)



unsymmetrical bolaamphiphiles ω -[N - β -D-glucopyranosylcarbamoyl]alkanoic acids **60**(n). These molecules have a glucose moiety at one end and a carboxyl group, which is small relative to the glucose moiety, at the other, and the two groups are connected by oligomethylene chains with an even number of carbons (12, 14, 16, 18, and 20).⁸² Given that a nanotube consists of unsymmetrical MLMs of wedge-shaped molecules and that the relatively larger headgroups occupy the outer surfaces of the MLM (Figure 26),

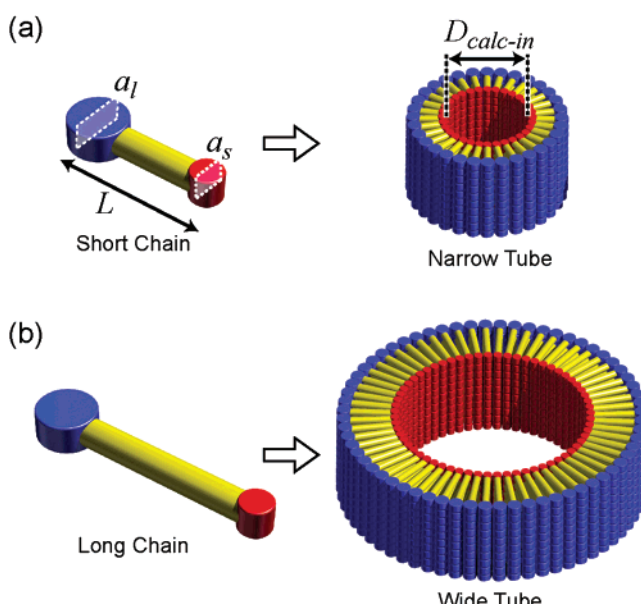


Figure 26. Schematic models of unsymmetrical bolaamphiphiles **60**(n) with (a) a short and (b) a long oligomethylene chain and the resultant tubular assemblies self-assembled from each model.

the innermost diameter ($D_{\text{calc-in}}$) can be defined by eq 3, where a_s , a_l , and L are the cross-sectional areas of the small headgroup and the large headgroup and the molecular length, respectively.

$$D_{\text{calc-in}} = 2a_s L / (a_l - a_s) \quad (3)$$

If a_s and a_l are held constant, then $D_{\text{calc-in}}$ is proportional to L , that is, proportional to the connecting oligomethylene chain length. Varying the carbon number of the oligomethylene spacer from $n = 14$ to $n = 20$ permits control of the inner diameters in the range of 17.7 to 22.2 nm in steps of approximately 1.5 nm/2-carbons (Figure 27 and Table 4).

5.3. Length

As mentioned above, optimization of nanotube morphology for a given application is critical if the full technological potential of the nanotube is to be realized. For example, intermediate-length (1 $\mu\text{m} < L < 10 \mu\text{m}$) and short LNTs (<1 μm) may serve as connectors and components for sensor devices, re-

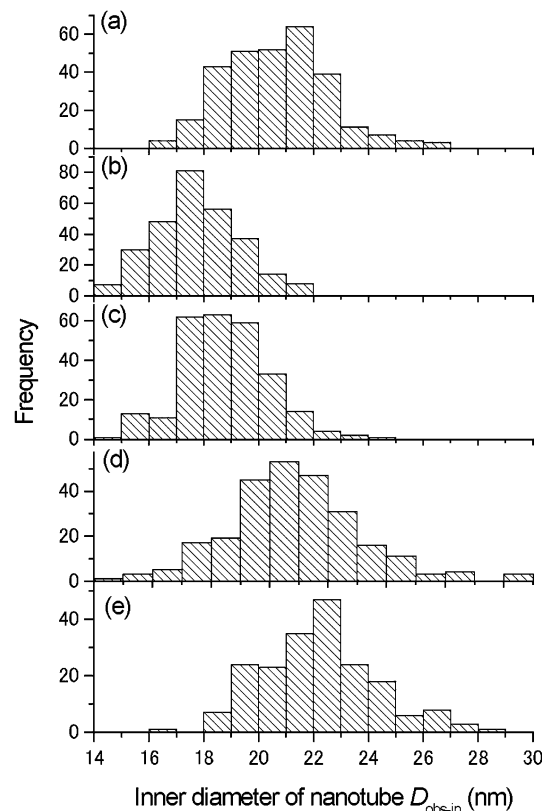


Figure 27. Observed inner diameters ($D_{\text{obs-in}}$) of the LNTs from (a) **60**(12), (b) **60**(14), (c) **60**(16), (d) **60**(18), and (e) **60**(20), evaluated from negatively stained TEM images.

Table 4. Calculated Inner Diameters Based on Eq 3 and Obtained Values from TEM Observations⁸²

chain length of 60 (n)	molecular length (L) (nm)	$D_{\text{calc-in}}^a$ (nm)	$D_{\text{obs-in}}^b$ (nm)
$n = 12$	2.62	15.6	20.6 ± 1.9
$n = 14$	2.87	17.1	17.7 ± 1.6
$n = 16$	3.12	18.6	18.7 ± 1.6
$n = 18$	3.38	20.2	20.8 ± 2.3
$n = 20$	3.64	21.7	22.2 ± 2.1

^a The $D_{\text{calc-in}}$ (calculated inner diameter) values were calculated by substituting each value of L , $a_l = 0.295 \text{ nm}^2$, and $a_s = 0.221 \text{ nm}^2$ into eq 3. ^b $D_{\text{obs-in}}$ (observed inner diameter) is the number average inner diameter estimated from more than 250 nanotubes randomly chosen on TEM images.

spectively. Nanotube length can be regulated for **1**(8,9) nanotubes over a range of a few micrometers to hundreds of micrometers by changing the solvent composition (Table 3).^{266,267} In methanol/water mixtures, nanotubes are made up of single-bilayer walls, and the length reaches a maximum in 85% methanol. In ethanol/water mixtures, the nanotubes obtained consist of more than five bilayers and are longest in 70% ethanol.

The dependence of LNT length on cooling rate was first noticed for the **1**(8,9) nanotubes in wide- and low-angle X-ray diffraction studies.^{79,268} In an ethanol/water mixture, a decrease in the cooling rate through the gel-to-liquid crystalline phase transition temperature (T_{g-1}) led to a remarkable increase in the average length of the resulting nanotubes, as well as a decrease in the wall thickness. Nanotube formation is driven by a reversible first-order phase transi-

tion from an intralamellar, chain-melted L_α phase to a chain-frozen L_β' phase. Therefore, these transition characteristics permit tuning of the nanotube length by regulation of the cooling rate. Nanotube morphologies were examined over a wide range of cooling rates, from $0.08\text{ }^\circ\text{C/h}$ to $10^5\text{ }^\circ\text{C/h}$, and nanotube lengths varied from 1 to $100\text{ }\mu\text{m}$ (Figure 28).⁷⁹

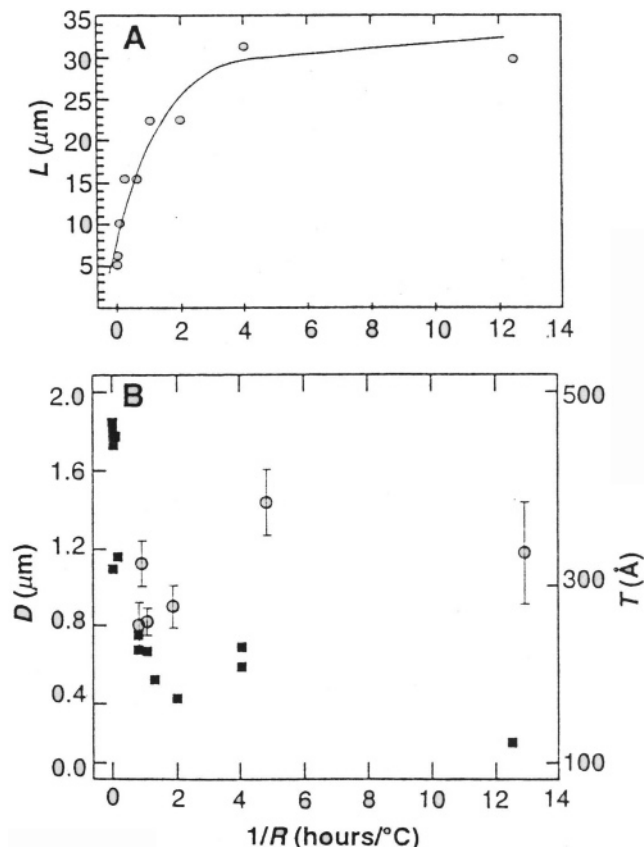


Figure 28. (A) Relation between mean nanotube length L and the inverse of the cooling rate, $1/R$, through the transition from spherical vesicle to nanotube phase. All points on this plot arise from the same lipid concentration, $\sim 100\text{ mg/mL}$. The line is merely a guide to the eye. (B) Plot of $1/R$ versus nanotube mean diameter D (open circles) (left scale) and versus nanotube wall thickness T (filled squares) (right scale). (Reproduced with permission from *Science* (<http://wwwaaas.org>), ref 79. Copyright 1995 American Association for the Advancement of Science.)

However, variation of the cooling rate had no remarkable effect on the LNT diameters.

So far, all the research on length control has focused on changing the conditions of the self-assembly process, such as the solvent composition, the cooling rate, and the addition of metal salts, as mentioned above. However, none of the approaches have succeeded in producing short nanotubular structures. A simple approach for obtaining intermediate-length and short LNTs using a mechanical stirring system has been reported.²⁶⁹ When a suspension of *N*-(11-*cis*-octadecenoyl)- β -D-glucopyranosylamine (**32**) was mechanically stirred at 500 rpm, the LNT lengths could be controlled by varying two factors: the stirring time (10 min or 6 h) and the stirring rate (Table 3 and Figure 29). In this regard, the lyophilized LNTs can be cut shorter and more quickly than the water-filled LNTs under the same stirring condi-

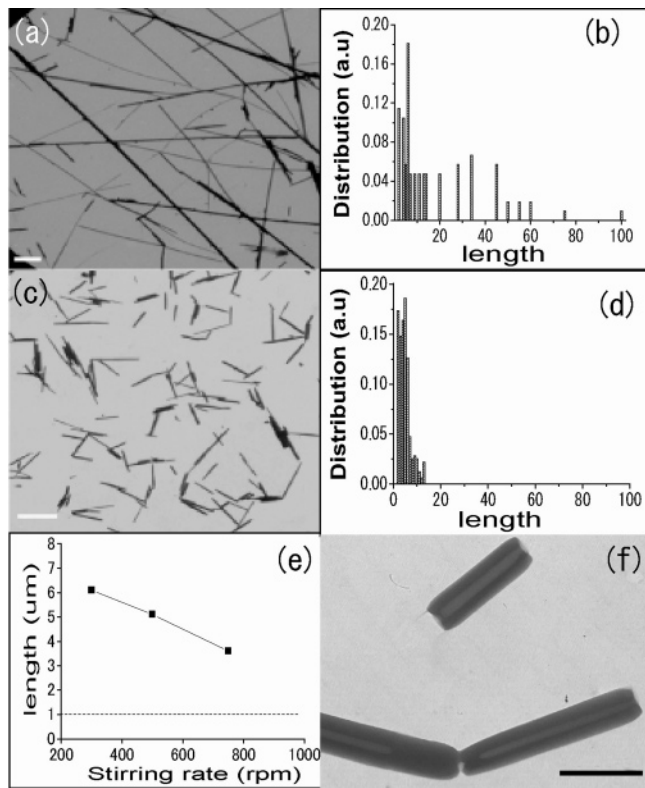


Figure 29. TEM images and the length distribution of shortened LNTs of **32** at different stirring times at 500 rpm: (a and b) after 10 min (scale bar = $10\text{ }\mu\text{m}$); (c and d) after 6 h (scale bar = $10\text{ }\mu\text{m}$). (e) Plot of the average length of the shortened LNTs versus stirring rate. (f) TEM image of lyophilized lipid nanotubes after stirring for 10 min at 500 rpm (scale bar = 500 nm). (Reproduced with permission from ref 269. Copyright 2003 The Chemical Society of Japan.)

tions, giving stable short LNTs with $600\text{--}800\text{ nm}$ lengths.

5.4. Wall Thickness

Solvents play an important role in determining nanotube fine structure, particularly the outer diameter and wall thickness. Careful studies have clearly demonstrated that nanotubes precipitated from a methanol/water solution of **1**(8,9) consist of single bilayers with a wall thickness of approximately 8 nm, whereas nanotubes obtained from ethanol/water or water consist of multiple bilayers (Table 3).²⁶⁷

The intensity of the CD signal is highly dependent on whether lipid molecules pack chirally or non-chirally. Spector et al. reported the first spectroscopic evidence that the number of bilayers in the LNT wall can be evaluated from the intensity of peaks in the CD spectra.^{61,257,270} Two distinct peaks were observed in the CD spectrum of the nanotubes of **1**(8,9): a peak at 195 nm assignable to chiral packing of the diacetylene groups within single bilayers and a peak at 202–205 nm attributable to chiral ordering of the head-groups between adjacent bilayers. The thickness of the nanotube wall gradually changes as a function of lipid concentration in methanol/water mixtures. The peak at 205 nm is appreciable in the 4 mg/mL sample, whereas the peak appears only as a small shoulder at lower concentrations (Figure 30). Spector

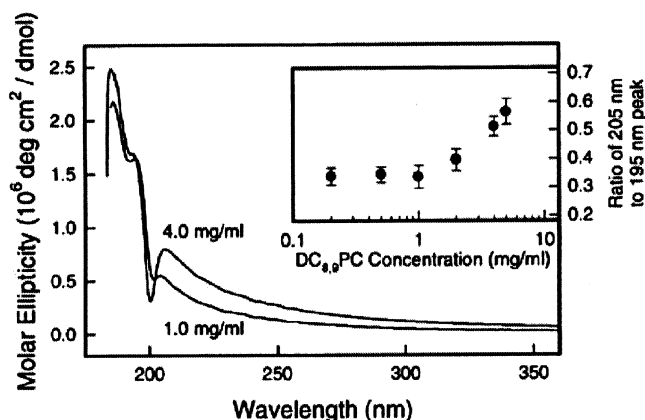


Figure 30. Concentration dependence of the CD spectra of 1(8,9) nanotubes in methanol/water (7:3) at 25 °C. The inset shows the ratio of the spectral intensities at 205 and 195 nm. (Reproduced with permission from ref 270. Copyright 1996 the National Academy of Sciences.)

et al. claim that once the crossover concentration can be evaluated, nanotubes with two-bilayer walls can be prepared exclusively.⁶¹ Nanotubes prepared in methanol/water solutions have predominantly single-bilayer walls at low concentrations and two- to four-bilayer walls at high lipid concentrations.

6. Synthesis of Hybrid Tubular Structures

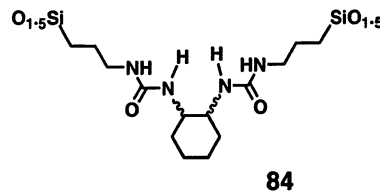
6.1. Classification of Template-Directed Syntheses

Organic tubular nanostructures with well-defined morphologies can serve as templates for mineral nucleation and deposition of metal oxide precursors (Figure 3c–e). Template-directed synthesis of tubular organic–inorganic hybrids involves three principal methods, the choice of which depends on which parts of the template surfaces are involved in the synthesis (Figure 31). Supramolecular rod or fiber morphologies produce metal or metal oxide nanotubes with a single layer with a hollow inside that is complementary to the outer surface of the rod or fiber (Figure 31a).^{271–273} This process, whereby the outer surfaces of the

organic template act as a mold, can be called *exo*-templating (for example, see, Figure 3c and h).

Supramolecular tubular shapes can also provide a hollow cylindrical environment to serve as a confined reaction field whose dimensions range from several to tens of nanometers (Figure 31b). This nanospace with a high axial ratio favors the production of confined one-dimensional organization of appropriate nanostructures with dimensions in the single-nanometer range (Figure 3e). This templating process can be called *endo*-templating. Using only the inner space of the supramolecular nanotube as a templating field is generally difficult unless inorganic substances deposited on or coating the outer surfaces can be removed in some way. The deposition or coating of inorganic substances occurs concurrently at both the inner and the outer surfaces (Figure 3d). This template process is associated with the morphological conversion of the tubular morphology of an organic template into double-layered tubular replicas.

In addition to *exo*- and *endo*-templating, there are also examples of self-templating methods that yield organic–inorganic tubular hybrid structures. Hollow tubes were first fabricated by hydrolyzing silylated organic molecules bearing a urea group (**84**).²⁷⁴ The hydrolysis of enantiomerically pure (*R,R*)-**84** or (*S,S*)-**84** gave hybrid silicas with hollow tubular morphologies, whereas the corresponding racemic mixture, *rac*-**84**, yielded a hybrid with a ball-like structure. Thus, self-assembly through intermolecular hydrogen bonding resulted in supramolecular architectures.



A variety of experimental procedures for template-directed synthesis have been reported, including (1) self-assembly of lipids in an aqueous dispersion in the presence of a metal complex solution and subsequent addition of a metal plating solution for reduction,^{50,275} (2) addition of metal nanoparticles, synthetic polymers, or proteins in aqueous dispersions of LNT aggregates,^{276–278} (3) crystallization of metal complex solutions in the presence of nanotube aggregates,^{279,280} (4) addition of dried LNTs with a vacant hollow cylinder into an aqueous solution containing metal nanoparticles,^{54,281} (5) mixing of centrifuged LNTs in an aqueous dispersion with a dialyzed fluid containing metal nanoparticles,²⁸² and (6) coassembly of metal oxide precursors and nanotube-forming lipids in aqueous or organic solutions.^{39,283,284}

6.2. *exo*-Templating (Chart 4)

Mixtures of galactocerebrosides such as α -hydroxy fatty acid galactocerebroside **85** (HFA-Cer) and non-hydroxy fatty acid galactocerebroside **86** (NFA-Cer) form a range of nanostructures including lamellar disks, multilamellar nanotubes, and viscoelastic gels of fibrous unilamellar nanotubes, depending on the

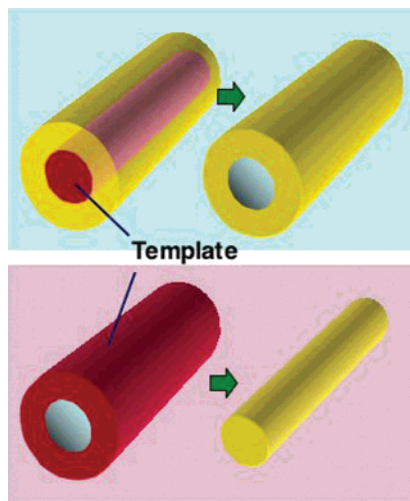
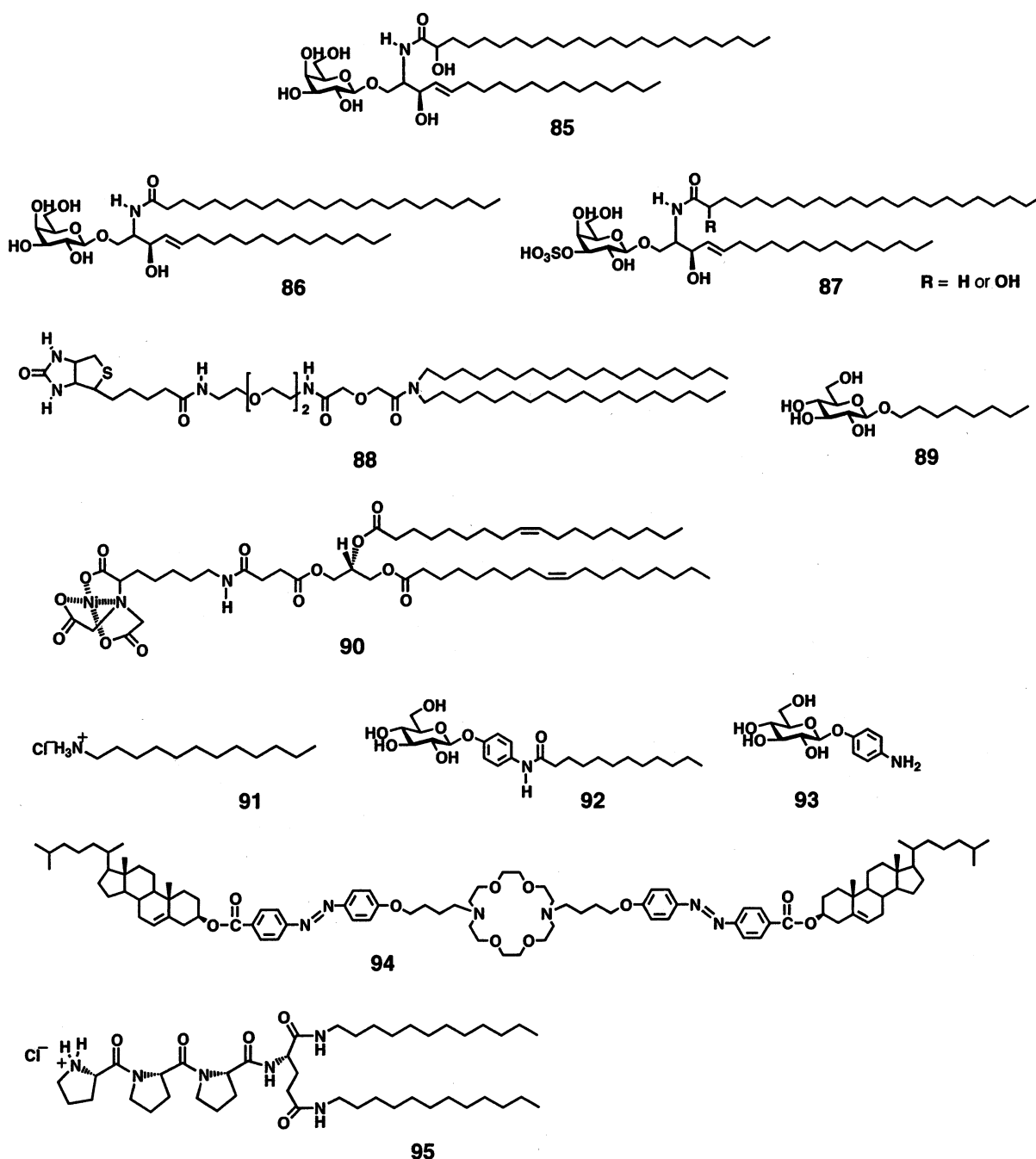


Figure 31. Schematic illustration of (top) *exo*- and (bottom) *endo*-templating. The red parts indicate a template for further synthetic process.

Chart 4



lipid composition. Doping of low levels of anionic sulfated galactocerebroside **87** (S-Cer) into the neutral lipid nanostructures of **85** and **86** permits the induction of nucleation of magnetic and nonmagnetic iron oxide.⁵⁰

Electroless deposition of copper¹¹ or permalloy²⁸⁵ can be used to metallize the LNTs of **1(8,9)**; chemical precipitation of metal carbonates also mineralizes the nanotubes.⁵¹ Nanotubes of **1(8,9)** were successfully coated with a mineral phase composed of iron oxyhydroxide by hydrolysis of ferric chloride.²⁷⁹ Electroless Pd metallization of LNTs composed of negatively charged diacetylenic phospholipid 1,2-bis(tricosanoate)-sn-glycero-3-phosphohydroxyethanol [**82(2)**] in the presence of tetraamine palladium (II) chloride has been reported.²⁸⁰ Patil et al. reported the higher-order synthesis of micropipes of a magnesium

phylo(organo)silicate clay containing a covalently linked ethylenediaminopropyl moiety using self-assembled nanotubes of **1(8,9)** as templates.²⁸⁶ This report was the first to address control of the deposition of organically functionalized layered materials. A nanometer-thick, continuous coating of organoclay was applied by immersing the lipid nanotubes into an ethanol/water solution containing *N*-(2-aminoethyl)-3-aminopropyltrimethoxysilane and magnesium chloride.

Helical protein arrays on the outer surfaces of LNTs provide valuable information in studies of protein structure and protein–lipid interactions by electron microscopy and crystallography. For example, a functionalized lipid nanotube fully covered with biotin has been shown to induce the spontaneous formation of ordered streptavidin arrays.²⁷⁶ A

biotinylated, dioctadecylamine lipid molecule containing an ethylene oxide spacer (**88**) self-assembles in the presence of *n*-octyl- β -D-glucopyranoside (**89**) into unilamellar nanotube structures²⁸⁷ with a constant outer diameter of 27 nm and an inner diameter of about 16 nm (Table 1). Detailed TEM and X-ray analysis revealed that a single layer of streptavidin covers the **88** nanotubes (Figure 32). The obtained

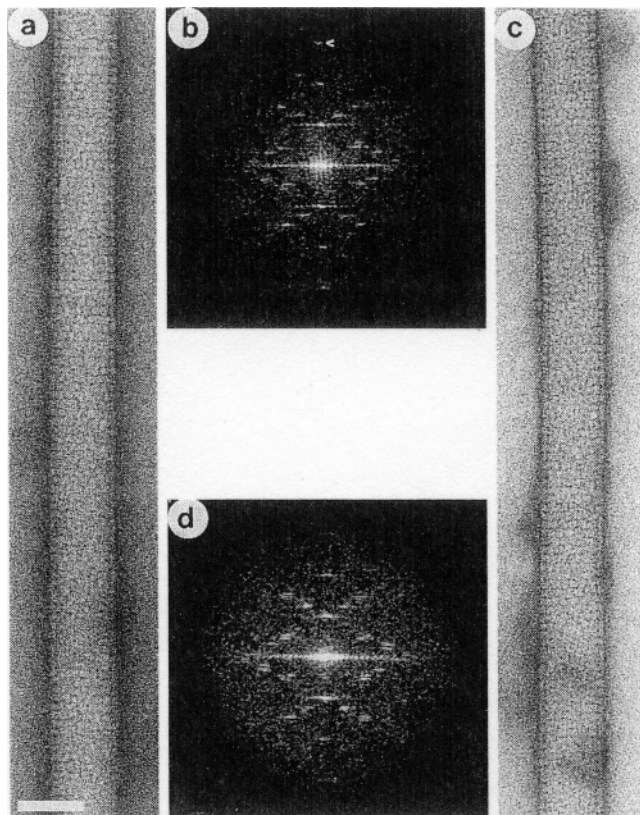


Figure 32. (a and c) Images and (b and d) Fourier transforms of helical crystals of streptavidin formed on lipid nanotubes containing **88**. (a and c) Stain striations extend along the tubules. Protein densities are particularly visible at tube edges, corresponding to streptavidin molecules viewed edge-on. Scale bar: 40 nm. (b and d) Distribution of Fourier transform amplitudes from the tubes shown in parts (a and c), corresponding to about 1700 streptavidin molecules. The finest spacing between layer lines indicates a helical repeat of 47 nm. Visible diffraction peaks extend up to 1.7 nm (arrowhead in part (b)). (Reproduced with permission from ref 276. Copyright 1997 VCH.)

tubular crystals of streptavidin differ in nature from tubular crystals of other proteins.²⁸⁸ The resolution for the crystalline order extended up to about 1.5 nm. This new methodology has two notable advantages. In protein crystals with helical symmetry, the repeat motif can be viewed in many different orientations along the helix, and therefore, the three-dimensional structure can be calculated from a single image by Fourier-Bessel reconstruction methods.²⁸⁹ In addition, the helical crystals of proteins can be transferred onto electron microscopy grids more easily than two-dimensional protein crystals can.

This elegant work has been developed into a general approach for helical crystallization of proteins.²⁷⁷ A mixture of glycolipids, galactosylceramide **37** (GalCer), and 10% 1,2-dioleoyl-*sn*-glycero-3-(N-(6-

carboxy-6-iminodiacetic acid)-hexyl-succinamide) nickel salt (**90**) produces mainly tubular structures up to several micrometers long. They are unilamellar and have a fairly uniform diameter (~27 nm). In a similar way to the procedure by Ringler et al.,²⁷⁶ LNTs with a biotinylated lipid allow crystallization of streptavidin. The generality of this method may permit the crystallization of a wide variety of proteins on LNTs.²⁹⁰ The resultant helical arrays can be subjected to helical analysis to derive structural information at moderate (~2 nm) resolution. This method provides an exciting alternative to existing lipid layer crystallization techniques.^{291–293}

LNTs can also serve as templates for the alternate adsorption of oppositely charged polymers and nanoparticles. By observing where and how these charges adsorb on the nanotubes, one can infer information about the charge pattern in the nanotubes. The charge distribution on LNTs of **1(8,11)** mixed with 2% of the negatively charged lipid **82(2)** is manifested in the layer-by-layer assembly of nanoparticles and polyions.^{278,294} A series of treatment of the **1(8,11)** LNTs with polyethyleneimine (PEI⁺), sodium poly(styrenesulfonate) (PSS⁻), PEI⁺, and 45 nm silica nanoparticles resulted in the formation of nanoparticle caps at the ends of the nanotubes and along the edges of the helices of nanoparticles that wind around the interior surface of the nanotube walls (Figure 33). Interestingly, this finding indicates that the charged lipid is concentrated along helical defect lines that are not otherwise visible.

Similarly, the helical edges of a helical ribbon made from **1(8,9)** can serve as chemically patterned organic surfaces for the spatial organization of arrays of gold nanoparticles.²⁷⁵ Interestingly, *in situ* reduction of HAuCl₄ can decorate the lipid nanotubes with discrete gold particles; when gold particles are synthesized by reduction of Au^{III} to Au⁰ on preformed nanotubes of **1(8,9)**, arrays of gold “dots” follow the underlying helical ribbon edges. In contrast, no underlying helical features were observed in previous syntheses involving the mineralization of **1(8,9)** nanotubes with nickel,¹¹ copper,¹¹ alumina,⁵¹ or silica.⁵²

A variety of mesoporous materials consisting of silicate and aluminosilicate, such as MCM41^{295,296} and FSM16,^{297,298} are known to afford integrated forms of a unit hollow structure. A new method was developed to prepare single silica nanotubes with a discrete morphology, as well as bundles of silica nanotubes, by using the sol-gel reaction with both tetraethoxysilane (TEOS) as a silica precursor and an organic template based on laurylamine hydrochloride (LAHC) **91** (Figure 34).^{299–301} This formation process, referred to as a “surfactant-assisted templating mechanism”, obviously contrasts to a sol-gel transcription method using organogel templates, which have been extensively studied by Shinkai’s research group (Figure 35). In 1998, Shinkai’s group reported the first successful utilization of organogels as templates.²⁷¹ A wide variety of organogelators, for example, **66** and **92–94**, generate entanglements or three-dimensional networks of nanometer-sized fibrils.^{302–304} This type of nontubular feature can lead to a rod-to-hollow morphological conversion by the

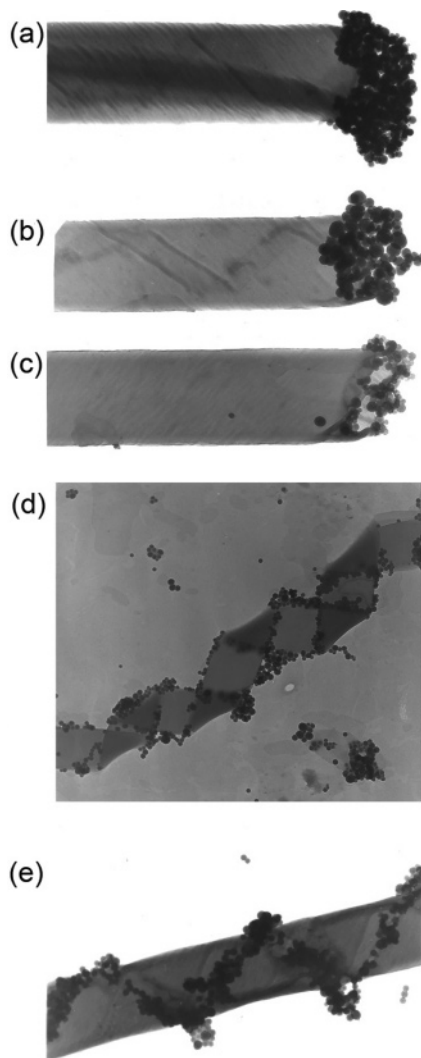


Figure 33. Nanoparticle caps at the ends of the nanotubes of **1**(8,11): (a) after $\text{PSS}^-/\text{PEI}^+$ /45 nm SiO_2^-) treatment, nanotube diameter 1 μm ; (b) after $\text{PSS}^-/\text{PEI}^+$ /(75 nm SiO_2^-) treatment, nanotube diameter 0.75 μm . (c) Unfinished cap after $\text{PSS}^-/\text{PEI}^+$ /45 nm SiO_2^-) treatment, nanotube diameter 0.75 μm . (d) Nanoparticle helices inside the nanotubes of **1**(8,11) + 2% **69**(8,9) after $\text{PEI}^+/\text{PSS}^-/\text{PEI}^+$ /45 nm SiO_2^-) treatment, nanotube diameter 1 μm , magnification 5000. (e) Part of the nanotube at magnification 50 000. (Reproduced with permission from ref 278. Copyright 2000 American Chemical Society.)

sol–gel transcription method.^{305–307} The formation of discrete inorganic nanostructures such as fibers, nanotubes, and spheres using separate organic templates including polymers, surfactants, organogels, carbon nanotubes, organic crystals, and biomaterials has been reviewed.^{39,308} Morphological transcription from an organic nanotube into inorganic double-layered or rolled paper-like structures has also been performed using the aza-18-crown-6-functionalized gelator **64**.³⁰⁹ Interestingly, the organogels prepared from diaza analogue **94** consist exclusively of tubular structures. In the presence of cationic charges, sol–gel transcription of organogels consisting of tubular structures resulted in the formation of rolled paper-like silica.

Note that neither the surfactant-mediated method nor the organogel-template method can reproduce an exact copy through currently known sol–gel pro-

cesses. Typically, rod-shaped molecular assemblies can produce tubular morphologies of metal oxide.²⁷² Similarly, the morphology of a helical fiber, nanotube, or double-helical rope could turn out to be helical,³⁰⁷ double-layered,²⁰⁷ or double-helical nanotubes,³¹⁰ respectively. An elegant method for close reproduction of a nanotube shape has been recently developed by using the molecular assembly of synthetic peptidic lipid **95** with a single-bilayer wall as a template (Figure 36a).^{83,283,311,312} A relatively small population of positive charges and a very mildly catalytic site on the organic nanotube are crucial for the formation of silica nanotubes with smooth and ultrathin (~8 nm) silica walls (Figure 36d). This unique process using the mild catalytic function of the terminal headgroup enabled us to control the wall thickness of the resultant silica nanotubes within 4 nm precision, depending on the amount of TEOS added (Figure 37).³¹³

Electrostatic interactions between biological polyelectrolytes and oppositely charged membranes provide a useful alternative strategy for higher-order self-assembled architectures exhibiting complex polymorphism. Safinya's research group described a distinct type of hierarchical self-assembly of cytoskeletal filamentous actin (F-actin) and charged membranes; the lengths ranged from nanometers to micrometers.³¹⁴ The use of a stacked three-layer membrane resulted in the formation of ribbon-like nanotube structures (average width, 250 nm; length, up to 100 μm) consisting of lipid bilayers sandwiched between two layers of actin (Figure 38). A lamellar phase with DNA chains confined between lipid sheets³¹⁵ and an inverted hexagonal phase with DNA contained within the LNTs³¹⁶ are other typical examples of DNA–membrane systems.

Templated growth of conducting polymers has been performed using the edges and seams of a LNT.³¹⁷ Template synthesis of the conducting polymer poly-pyrrole (Ppy) has also been reported in the presence of microporous polycarbonate membranes possessing a condensed nanopore assembly, superconductor surfaces ($\text{YBa}_2\text{Cu}_3\text{O}_7$),³¹⁸ and single-crystal graphite surfaces.^{319,320} The same research group tried the polymerization of pyrrole in the presence of **1**(8,9) nanotubes and found a highly selective, nonconformal growth of Ppy on the edges rather than the surface of the nanotubes (Figure 39). Surprisingly, unusually long strands 10–100 nm wide and micrometers long appeared in the presence of the nanotubes. By contrast, in the absence of the nanotubes, spherical aggregates 80–200 nm in diameter were formed.

Several researchers, including Mann and co-workers, have demonstrated the potential of controlled crystallization at inorganic–organic interfaces.³²¹ In particular, they have employed biological templates, such as compressed monolayers of amphiphiles,^{322–324} supramolecular lipid or protein cages,^{325–330} bacterial microstructures,^{331–334} and DNA,^{335–338} for the templating or nucleation of inorganic materials. Each biological template possesses an identical dimension as its own structure and acts as an ideal template for inorganic synthesis of nanomaterials. Tobacco

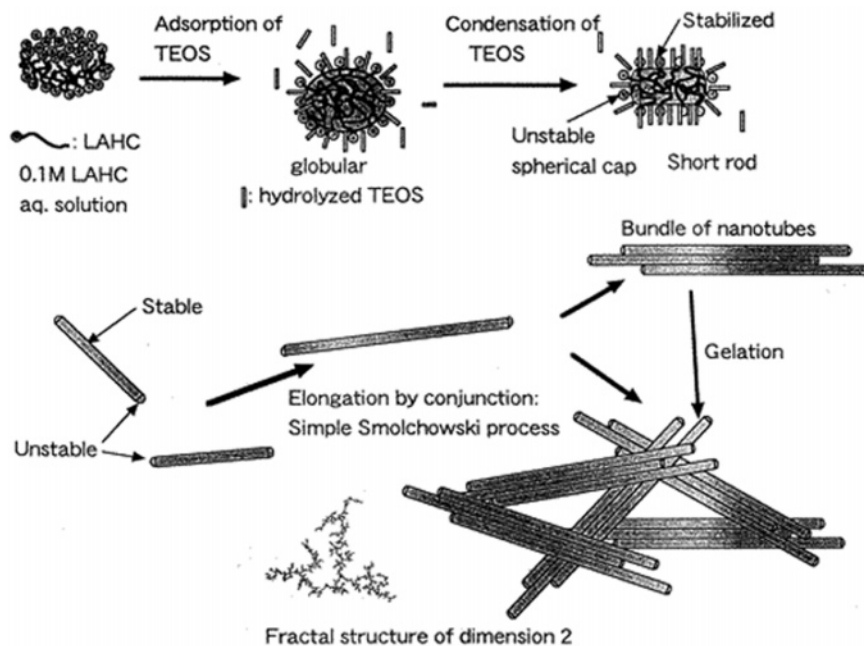


Figure 34. Formation mechanism of silica nanotubes. (Reproduced with permission from ref 300. Copyright 2000 American Chemical Society.)

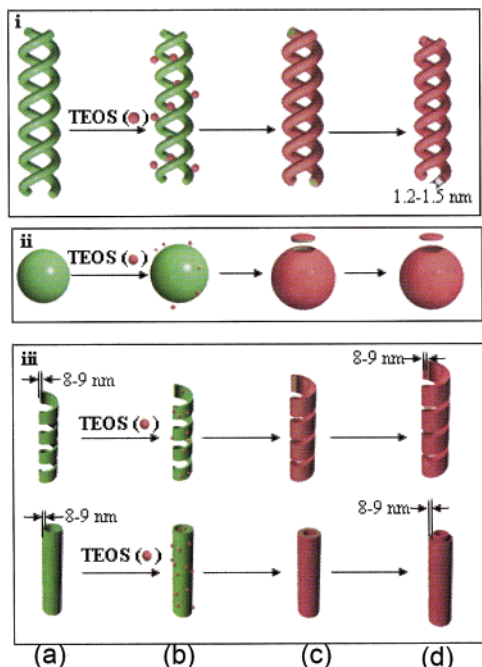


Figure 35. Schematic representation for the creation of various silica structures from the organogel state of (i) **92** + **93**, (ii) **94**, and (iii) **66** by sol–gel polymerization: (a) gelators; (b) sol–gel polymerization of TEOS and adsorption onto the gelators; (c and d) (i) double-helical structure, (ii) vesicular structure, (iii) double-walled and helical ribbon structure of the silica materials formed after calcinations. (Reproduced with permission from ref 308. Copyright 2003 John Wiley & Sons, Inc. and The Japan Chemical Forum.)

mosaic virus (TMV) is a suitable biological nanotube for a new approach to the template-directed synthesis of inorganic–organic nanotubes.³³⁹ The TMV particle comprises 2130 identical protein subunits that are arranged in a helical motif around a single strand of RNA, forming a hollow protein nanotube 18 nm wide

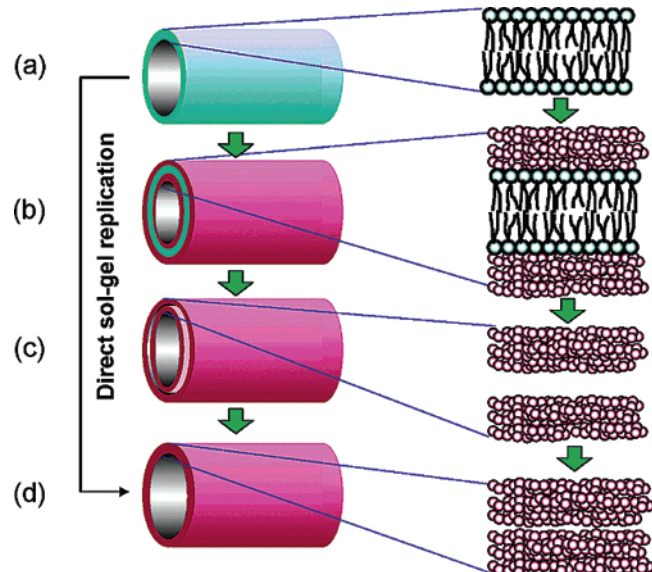


Figure 36. Possible mechanism for the direct sol–gel replication in an aqueous gel system: (a) a lipid nanotube with a single bilayers wall is formed from **95**; (b) a minimum amount of silica precursor is deposited onto the template surfaces due to electrostatic interaction; (c and d) a silica nanotube is aged to shrink the interlayer void. Thus, a nanotube architecture with wall thickness similar to that of the lipid nanotube can be exactly reproduced with pure silica. (Reproduced with permission from ref 283. Copyright 2004 American Chemical Society.)

and 300 nm long, with a 4 nm wide central channel.^{340,341} The outer surfaces of TMV were found to be effective sites for reactions such as the cocrystallization of CdS or PbS (which was accomplished by bubbling H₂S through solutions of CdCl₂ or Pb(NO₃)₂), the oxidative hydrolysis of Fe oxides, and the sol–gel condensation of SiO₂ (Figure 40). In a similar way, protein microtubules (diameter, 25 nm; length, tens of micrometers) have been used as

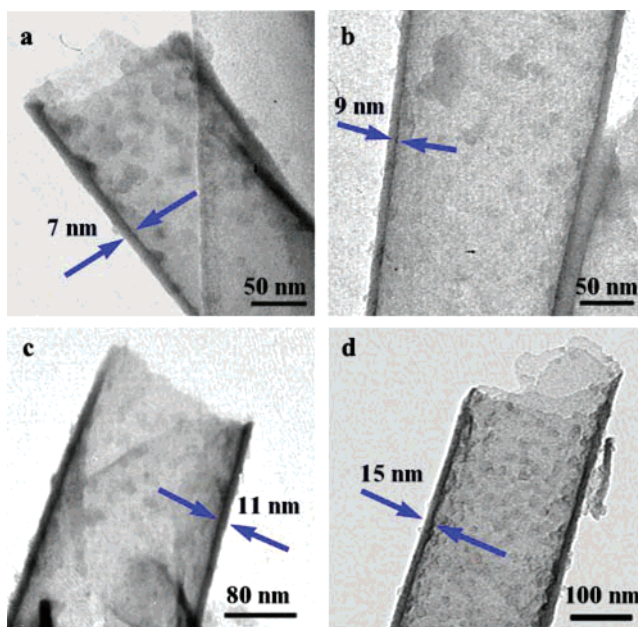


Figure 37. TEM micrographs for silica nanotubes with different wall thicknesses obtained, showing the dependence on the amount of TEOS added. (Reproduced with permission from ref 313. Copyright 2004 The Chemical Society of Japan.)

templates for the biomimetic mineralization of FeOOH. Exposure of microtubules to anaerobic aque-

ous solutions of Fe^{2+} buffered to neutral pH and subsequent aerobic oxidation resulted in the formation of iron oxide coated microtubules.³⁴²

6.3. endo-Templating

Positively charged, magnetic nanoparticles with mean diameters of 7 nm penetrate into the confined volume of hollow cylinders of **1**(8,9) nanotubes (outer diameters, ~500 nm).²⁸² The nanotubes look like uniformly black cylinders in electron micrographs. However, negatively charged particles did not enter the hollow cylinder at all. This finding strongly suggests that the electrostatic interactions between the nanotubes and particles are crucial for efficient preparation of magnetic tubules.

The core of nonionic reverse micelles with inner diameters in the single-nanometer range can provide a confined reaction field for the reaction of barium and carbonate ions, eventually producing single-crystal BaCO_3 nanowires.³⁴³ This process is limited, however, to crystals with morphologies compatible with the shape of the inner core of the micelle. The cylindrical protein self-assembly TMV mentioned above also affords a well-defined hollow cylinder 4 nm wide as an *endo*-template.³⁴⁴ Photochemical reduction of Ag(I) salts at pH 7 produced a linear array of regularly spaced Ag nanoparticles aligned within the central channel of the TMV (Figure 41).³⁴⁵

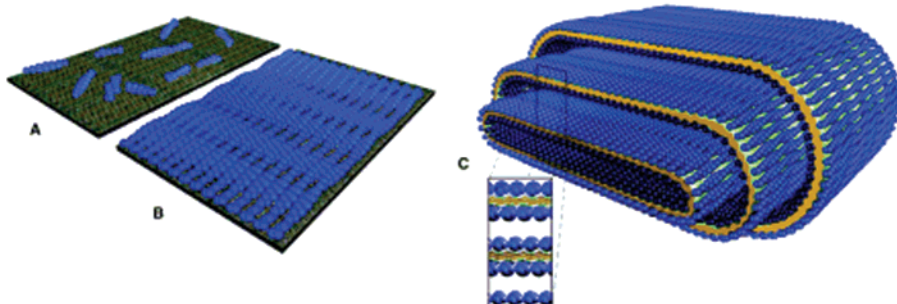


Figure 38. Summary of the hierarchical self-assembly process resulting in the formation of ribbon-like nanotubes. (A) G-actin self-assembles into short F-actin filaments. (B) Long F-actin filaments spontaneously form a 2-D crystal layer of F-actin. (C) The cationic lipid bilayers are sandwiched between two layers of F-actin, forming a three-layer membrane (inset), which folds into ribbon-like nanotubes. (Reproduced with permission from *Science* (<http://www.aaas.org>), ref 314. Copyright 2000 American Association for the Advancement of Science.)

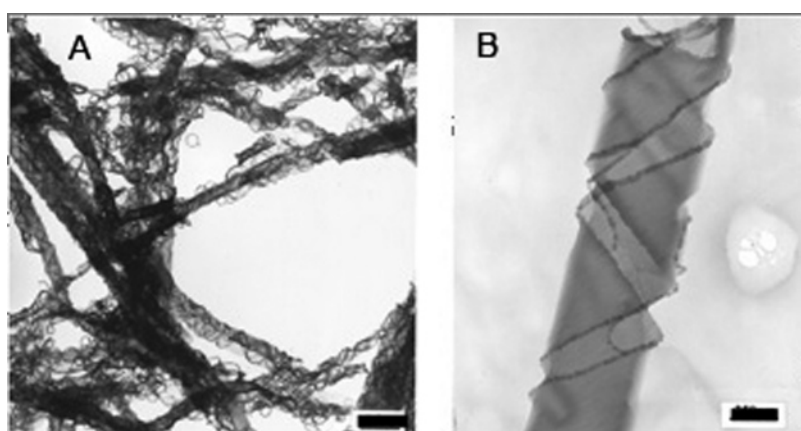


Figure 39. Polypyrrole (Ppy) strands formed on the **1**(8,9) nanotubes. The faint gray regions are the lipid nanotubes themselves, and the dark gray/black lines are the Ppy strands. (A) Overall appearance of Ppy templated on the **1**(8,9) nanotubes (scale bar = 1.5 μm). (B) Ppy templated on an open nanotube (scale bar = 250 nm). (Reproduced with permission from ref 317. Copyright 2000 American Chemical Society.)

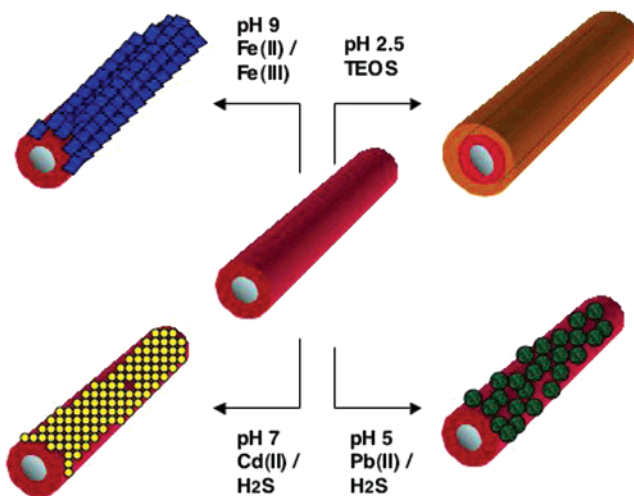


Figure 40. Scheme showing routes for the synthesis of nanotube composites using TMV templates. Clockwise from top right: sol-gel condensation (silica); coprecipitation (PbS and CdS nanocrystals); oxidative hydrolysis (iron oxide).

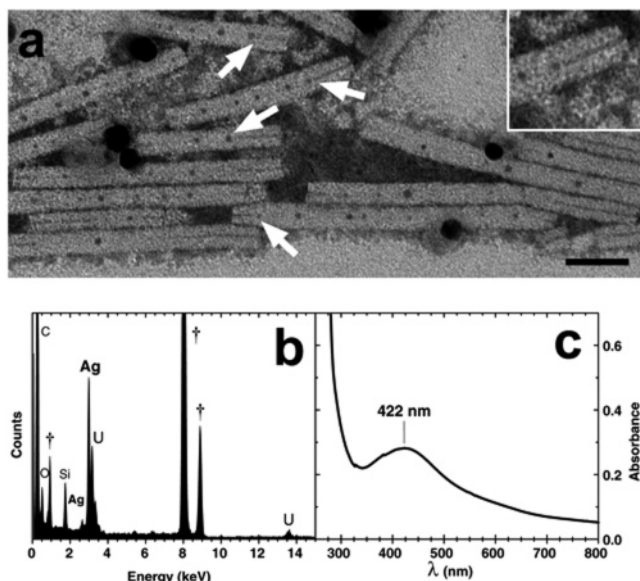


Figure 41. (a) TEM micrograph of ~ 5 nm silver nanoparticles grown inside the hollow channel of wild-type TMV. Arrows indicate nanoparticles that prevented the stain (uranyl acetate) from penetrating further in the cavity. One of these is magnified in the inset. The scale bar for the main image is 50 nm. (b) Energy-dispersive X-ray analysis spectrum showing the presence of silver and uranium (stain). \dagger indicates Cu as a supporting grid. (c) UV-visible absorption spectrum displaying a plasmon band at 422 nm, characteristic of metallic silver colloid. (Reproduced with permission from ref 345. Copyright 2003 American Chemical Society.)

However, chemical reduction of $[\text{PtCl}_6]^{2-}$ or $[\text{AuCl}_4]^-$ complexes at acidic pH resulted in the specific coating of the external surface of wild-type TMV with metallic nanoparticles less than 10 nm in size. The charges on the inner and outer surfaces depend on pH and the location of constituent amino acid residues (aspartic and glutamic acid residues and lysine and arginine residues populate the inner and outer surfaces, respectively).³⁴⁶ Reflecting this charge distribution, the TMV acted as an *exo*- or *endo*-template for the anisotropic self-assembly of spherical metallic

nanoparticles. Very recently, the central channel of TMV was found to be applicable as a template for the synthesis of nickel and cobalt nanowires.⁵³ First, TMV was activated by the selective binding of Pd(II) or Pt(II) ions and then metallized with borane-containing nickel and cobalt solutions; nickel and cobalt wires 3 nm wide with lengths of up to 600 nm grew selectively in the hollow.

Anisotropic Au-LNT nanohybrids have recently been fabricated under mild conditions. Interestingly, gold nanocrystals 3–10 nm wide were fully packed exclusively in the hollow cylinder of glycolipid nanotubes to produce one-dimensional organization (Figure 42).^{54,281} *N*-(11-*cis*-Octadecenoyl)- β -D-glucopyra-

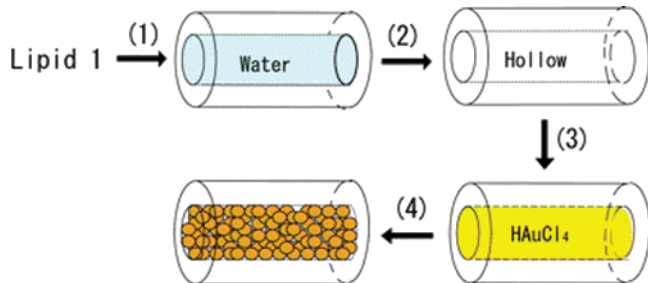


Figure 42. Schematic diagram for the fabrication of a glucose-derived LNT hollow cylinder, filled with Au nanocrystals, which self-assembled from 32. (Reproduced with permission from ref 281. Copyright 2004 The Royal Society of Chemistry.)

nosylamine (32) can self-assemble in water to produce monodispersed and well-defined LNTs with an 80 nm wide interior channel in approximately 100% yields.¹⁴⁹ Another method that, irrespective of the absence of charged surfaces on the LNT, has resulted in successful filling of nanoparticles is the use of lyophilized LNTs possessing a vacant internal channel. HAuCl₄ aqueous solutions can thus penetrate easily into the hollow cylinder by capillary action. Eventually, confined photochemical reduction of Au^{III} to Au⁰ in the presence of small amounts of alcohol produced a well-defined LNT filled with Au nanocrystals (Figure 43). Furthermore, the resultant gold 1-D nanohybrid also served as a second template to fabricate a continuous gold nanowire (Figure 44).⁵⁴ These uses of the tubular assemblies as *endo*-templates will open up possibilities for preparing 1-D arrays of a wide range of inorganic dots and continuous wires.

Synergistic coassembly of silica-lipid helical coils has been achieved by acid hydrolysis and condensation of TEOS in the presence of 1(8,9).²⁸⁴ This method differs strikingly from the sol-gel transcription method developed by Shinkai et al.^{39,308} in that hydrolysis and condensation of TEOS by the acid catalyst are specifically associated and coupled with self-assembly of the lipid molecule. The resultant hybrid nanostructures consist of smooth outer and inner surfaces, indicating the absence of colloidal silica precipitation. The lattice fringes in high-resolution TEM images correspond to a lamellar hybrid nanostructure, in which the lipid bilayers are intercalated with thin sheets of amorphous silica (Figure 45). From the viewpoint of *endo*-templating, this finding is particularly noteworthy because chiral

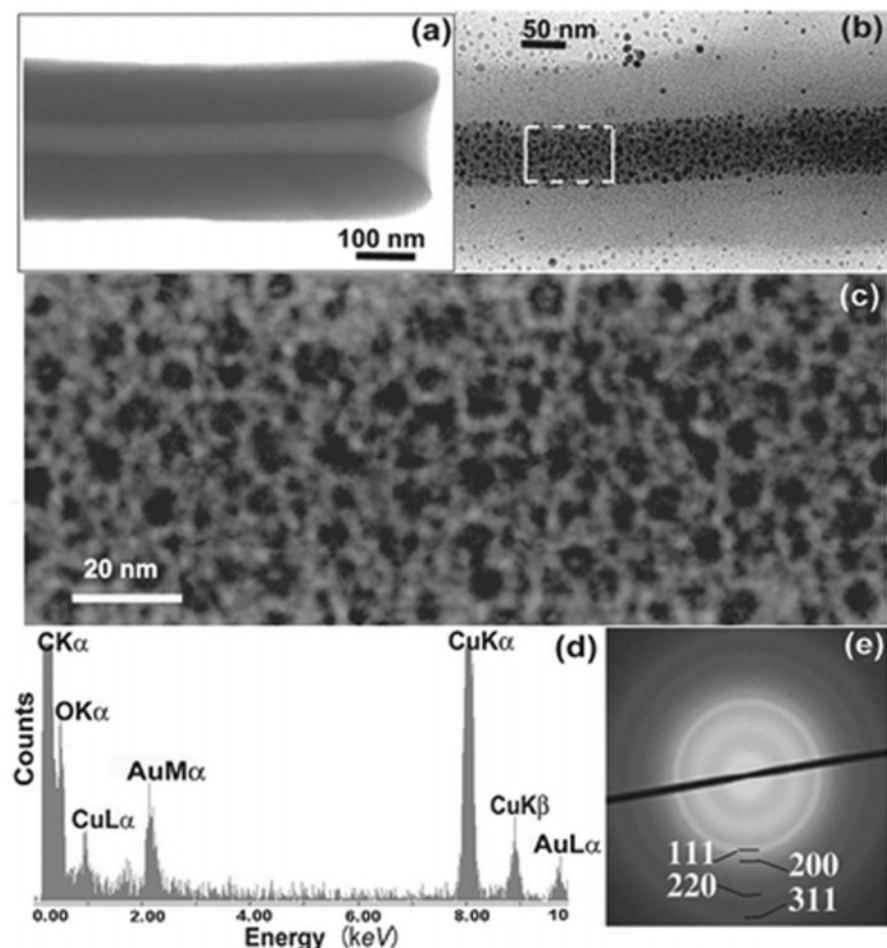


Figure 43. TEM images of (a) a lyophilized LNT from **32**, (b) a LNT filled with Au nanocrystals (low magnification), and (c) the magnified core part of image (b). (d) EDX spectrum and (e) SAED pattern for the area shown in image (b). (Reproduced with permission from ref 281. Copyright 2004 The Royal Society of Chemistry.)

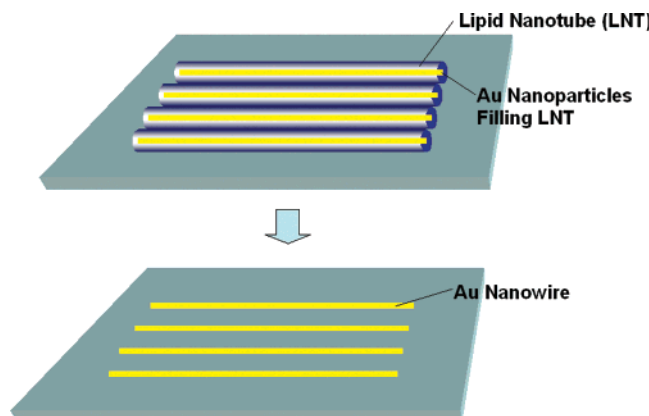


Figure 44. Schematic diagram for the fabrication of a gold nanowire using the tubular assembly as an *endo*-template. An appropriate firing process in air can remove the LNT shell, resulting in the formation of continuous gold nanowires on a substrate.

templating and *in situ* silica synthesis took place even between lipid bilayers.

7. Applications and Properties

7.1. Technological Applications

Most the studies on the applications of LNTs have used diacetylenic lipid **1(8,9)**. In an early review,

Schnur described two examples of potential applications of **1(8,9)** nanotubes.¹² The first was a field-emitting cathode based on nickel-coated nanotubes, which demonstrated vacuum field emission of current $I > 10$ mA at electric fields of 60–150 kVcm⁻¹.³⁴⁷ The second concerned controlled-release applications, in which a paint that included LNTs containing anti-fouling reagents was used to reduce marine fouling;^{348,349} test rods coated with the nanotube-containing paint showed little fouling in off-shore testing in Hawaii after 6 months of exposure.

The hollowness of nanotubes also suggests potential medical^{350,351} and industrial encapsulation applications,^{12,352,353} as well as filtration and purification applications.³⁵⁴ The LNTs formed from **1(8,9)** can be aerosolized in respirable aerodynamic sizes using a standard air-jet nebulizer and are capable of encapsulating water-soluble drugs.³⁵⁰ LNTs are also promising vehicles for delivery of drugs to respiratory tract tissues.³⁵⁵

LNTs have been coated with permalloy and employed in composites to produce high-dielectric, low-loss materials by aligning the nanotubes with a magnetic field.^{11,356} A similar technique was also utilized to produce composites with important ferromagnetic properties.²⁸⁵ A method for producing kilogram quantities of metal microcylinders with a simplified lipid pretreatment procedure has recently

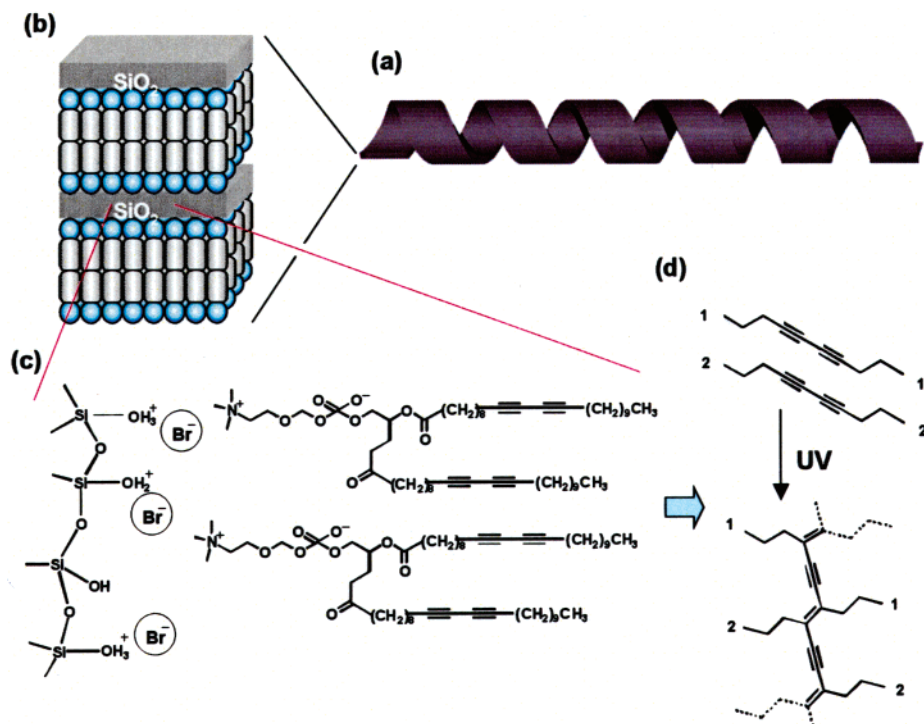


Figure 45. Schematic representation showing a silica–lipid lamellar nanostructure and diacetylenic polymerization: (a) helical silica–lipid composite with coiled multilamellar architecture; (b) 3 nm thick sheet of silica interspersed with lipid bilayers, 5.6 nm in width; (c) hypothetical section across the interface showing interactions between the lipid headgroup, Br^- counterions, and the protonated silica surface; (d) formation of ene-yne linkages.

been reported.³⁵⁷ The obtained composites were used to form parallel plate capacitors, and the conductivity of the bulk materials was then compared with the derived conductivity of a composite showing electromagnetic percolation. The specific density proved to be proportional to the critical volume fraction characteristic of percolating systems.

A foot-square composite dielectric panel was fabricated from LNTs: the LNTs were metallized electrolessly with an average aspect ratio of approximately 12 with copper or nickel–copper, and mixed with vinyl to form the panels.³⁵⁸ As the loading was increased, the metal nanotube composites displayed an onset of electrical percolation with an accompanying sharp increase in real and imaginary permittivities.

7.2. Mechanical Properties

The thermal, dynamic, mechanical, and dielectric properties of polymer matrixes containing copper-coated LNTs made of **1(8,9)** at three concentrations have been examined.³⁵⁹ The presence of the nanotubes had no significant effect on the glass-transition temperature of the polymer matrixes. This finding indicates that the nanotube–polymer interactions may not be strong enough to restrict the mobility of polymer chains near the filler surface. Although the three polymer matrixes have different surface and interfacial tensions, the values for the real part of the permittivity are comparable at each nanotube concentration.

Unlike carbon nanotubes,⁹ synthetic LNTs consisting of self-assembling amphiphilic molecules can provide characteristic hydrophilic internal and ex-

ternal surfaces. Therefore, they have the unique potential to act not only as cytomimetic tubules but also as hollow nanospaces for chemical reactions. However, little is currently known about their mechanical properties. Although biological tubulin-based microtubules^{360,361} or carbon nanotubes³⁶² have been extensively studied, the mechanical properties of a particular single LNT, however, have not been investigated. The Young's modulus for a single LNT self-assembled from glycolipid (cardanyl- β -D-glucopyranoside) **25**¹⁴⁴ has been for the first time found to be $E = \sim 720$ MPa.³⁶³ This value indicates much smaller elasticity than that observed for a carbon nanotube ($E = \sim 10^6$ MPa) and is roughly in line with the value for naturally occurring microtubules ($E = \sim 1000$ MPa)³⁶¹ with outer and inner diameters of the same order. The moderate stiffness of the single glycolipid nanotubes allowed the development of a microinjection method³⁶³ in which individual discrete nanotubes were extruded from ultrafine glass capillaries (internal diameters, ~ 500 nm) onto a substrate and freely aligned or arranged (Figure 46). This micromanipulation of single LNTs in a crystalline phase of the hydrophobic chain clearly differs from the electroinjection technique^{364–371} involving fluidic lipid bilayer systems detailed below.

LNTs have diameters that are greater than the diameters of single-wall carbon nanotubes (1 nm to a few tens of nanometers) but smaller than the diameters of the finest glass capillaries (approximately 500 nm). Therefore, the LNTs can cover a tube-diameter distribution that is unavailable from any other materials. LNTs with inner diameters of

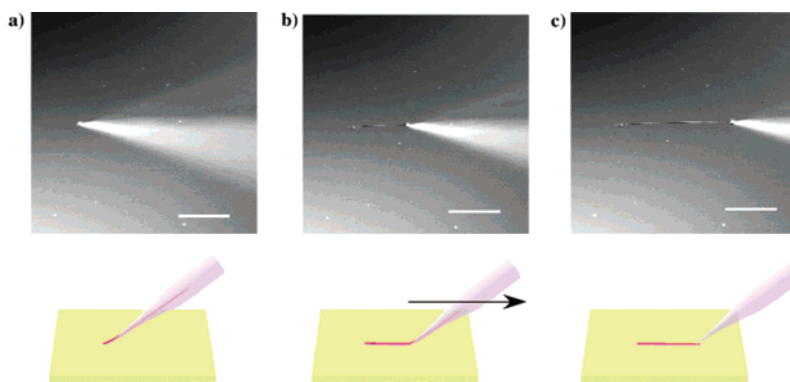


Figure 46. Confocal laser scanning micrographs of a fine line drawn with single lipid nanotubes of **25** by microextrusion, and its explanatory schematics. The white triangles in the images correspond to the tip of the needle: (a) The needle end touches a glass slide, and because a positive pressure is applied against backward flow, even before injection, a very small amount of solution drops onto the glass. As a consequence, while water quickly evaporates, the lipid nanotubes become attached. (b) By slowly moving the needle linearly, lipid nanotubes are extruded one after another. (c) When the injection is stopped, the line ends. (Reproduced with permission from ref 363. Copyright 2003 Wiley-VCH.)

10 nm are smaller by a factor of 10^{-4} in diameter and a factor of 10^{-8} in volume than the common microchannels currently used in DNA or electrophoresis chips (inner diameter, $\sim 100 \mu\text{m}$), assuming the same length for both. However, miniaturization of conventional microchannels into the nanometer region will be accompanied by many difficulties because it is hard not only to produce the nanochannels by using conventional microfabrication techniques but also to manipulate the flow of fluid inside the channel. Fluid devices with inner channel diameters approaching several tens of nanometers are capable of accommodating a single large protein or a single small virus. Ito et al. fabricated a nanochannel device made of resist resin, with each channel having a 50–100 nm inner diameter. They deposited approximately ten discrete linear arrays of LNTs of **25** on a glass substrate by microinjection, and these arrays act as templates for UV lithography of photosensitive resin (Figure 47).³⁷² The same research group also succeeded in filling the glass microchannels with a concentrated aqueous dispersion of the LNTs from **25** and, thus, were able to align a mass of LNT bundles along the long axis of the channel. The density attained was 3000 times that obtained with the employed microchannel (150 μm wide).

7.3. Nanotube–Vesicle Networks

LNTs can function as nanoscale channels and can be used as templates for nanoscale conduit patterns connecting liposome containers. Tirrel's research group introduced a method for laying out LNT networks and a photochemical polymerization process for stabilizing the resultant patterns *in situ*.³⁷³ Each nanotube was prepared by pulling it from a micropipet-held feeder vesicle,³⁷⁴ consisting of a mixture of 66 mol % stearoyl–oleoyl phosphatidylcholine **96**, 33 mol % cholesterol, and 1 mol % *N*-(6-(biotinyloyl)amino)hexanoyl-1,2-dihexadecanoyl-*sn*-glycero-3-phosphoethanolamine, triethylammonium salt, by mechanical retraction of the vesicle. They were able to control the inner diameters of the

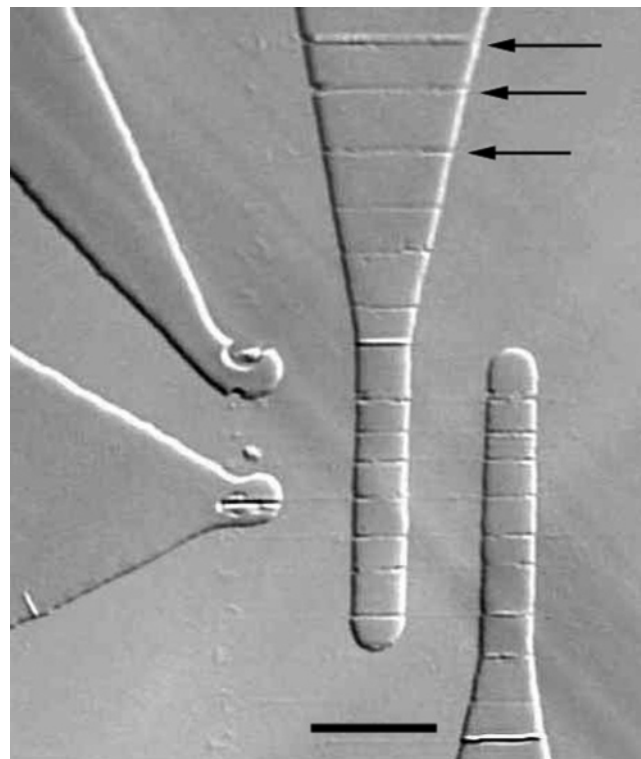
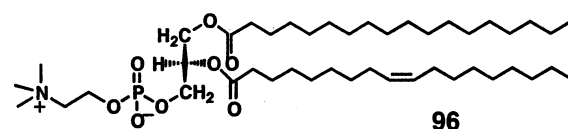


Figure 47. Optical micrograph of a nanochannel device. Hollow channels 50–100 nm wide (noted by arrows) remain in the UV-polymerized resin (scale bar = 10 μm).

nano tubes precisely in the range from 20 to 200 nm merely by setting the suction pressure in the micropipet.



Orwar and co-workers, who followed the micromanipulation protocols for LNT networks by Tirrel et al.,^{373,374} recently developed an electroinjection technique that permits the formation of LNTs and networks between liposome reservoirs.^{364,366} They

eventually constructed complex two-dimensional microscopic networks of fluid-state phospholipid bilayer vesicles interconnected by LNTs. This technique should lead to model system devices for studying confined biochemical reactions,^{364,375,376} intracellular transport phenomena,¹⁸³ and chemical computations.³⁷⁷ Furthermore, they can control the connectivity, the container size, the nanotube length, and the angle between the nanotube extensions.³⁶⁶ A typical procedure for the nanotube–vesicle network is shown in Figure 48.³⁶⁵ The resultant nanotubes have

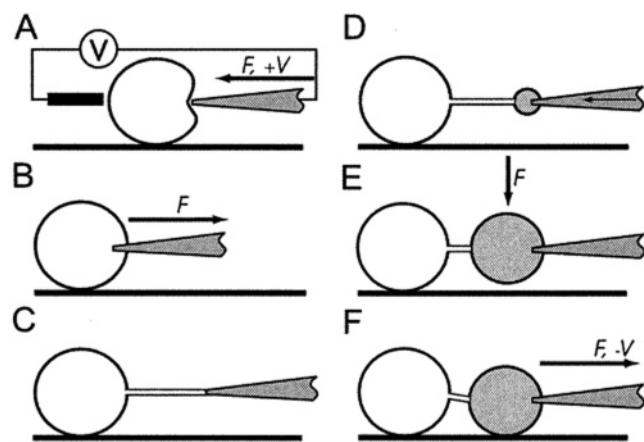


Figure 48. Schematic sequence showing the formation of a nanotube-connected daughter vesicle from a unilamellar mother vesicle. (A) The membrane of a giant vesicle is penetrated through a combination of mechanical force (F) applied from the micropipet and anodic electric pulses ($+V$) from a low-voltage pulse generator (V). As a counter electrode, a $5\text{ }\mu\text{m}$ carbon fiber was used. (B and C) A nanotube is created by pulling the micropipet away from the mother vesicle. (D) A daughter vesicle is created at the end of the nanotube by injecting buffer solution into the nanotube orifice. (E) A daughter vesicle is positioned on the cover slip surface by applying a small axial force (F) by translating the micropipet. (F) The micropipet is withdrawn from the daughter vesicle. LNTs adhering to the pipet tip after removal from the daughter vesicle were detached by applying one or several cathodic electric pulses ($-V$). (Reproduced with permission from ref 365. Copyright 2001 American Chemical Society.)

100–300 nm diameters. A recently developed nanotube–vesicle network is giving high geometrical complexity, up to fully connected networks with genus = 3 topology (Figure 49).³⁶⁸

A platform to build nanofluidic devices operating with single molecules and nanoparticles has been developed.^{367,370} These nanofluidic devices, which are considered to be more advanced than microfluid devices, have attractive applications for chip-based chemical analysis,³⁷⁸ drug screening,³⁷⁹ computations,³⁸⁰ and chemical kinetics.³⁸¹ One can view these systems as simplistic single-tube analogues to the endoplasmic reticulum–Golgi networks.¹⁸³ Orwar's research group has also developed a large-scale integration of nanotube–vesicle networks in nanofluidic applications.^{369,371,382} Appropriately designed nanofluidic systems used in this manner can provide a useful platform for studying single-molecule dynamics,³⁸³ enzyme-catalyzed reactions,³⁸⁴ single-file diffusion,³⁸⁵ and single-molecule sequencing and syn-

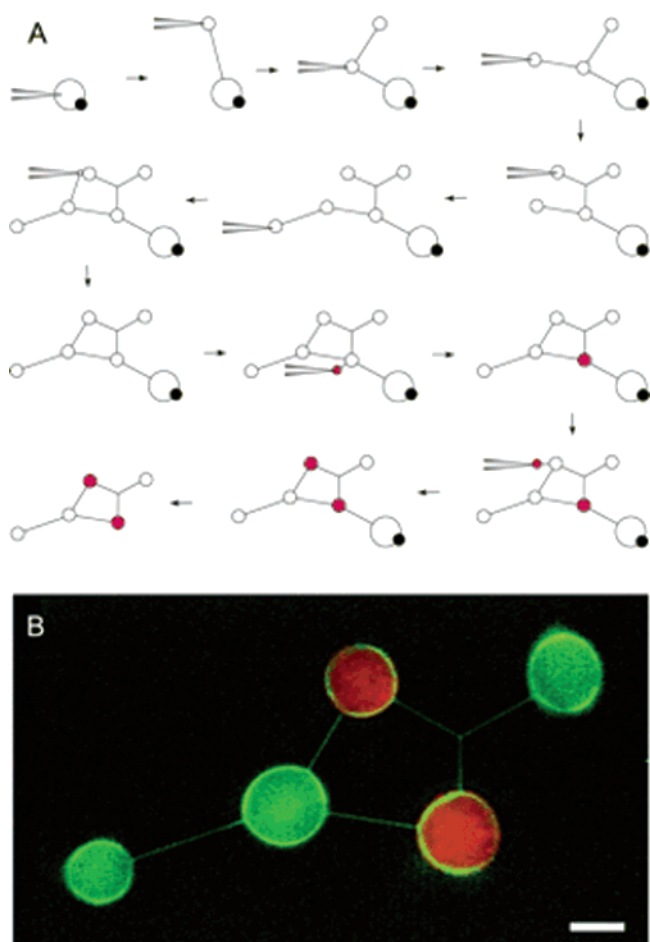
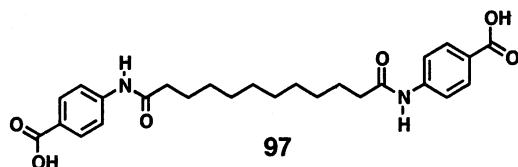


Figure 49. Differentiation of networks. (A) Schematic showing the procedure of creating a differentiated network having closed loops and branching nanotubes. Differentiation of the chemical composition of individual liposomes in the network was obtained by nanotube-mediated fusion of satellite vesicles containing red fluorescent 30 nm latex beads. (B) A fluorescence micrograph of the actual structure is shown. The membrane of the lipid nanotube–vesicle network is stained with DiO (3,3'-diiodoadecylxocarbocyanine perchlorate) (0.5 mol %). The colors were detected by using separate channels and were overlaid using ADOBE software (scale bar = $5\text{ }\mu\text{m}$). (Reproduced with permission from ref 368. Copyright 2002 the National Academy of Sciences.)

thesis, as well as for gaining a better understanding of materials transport and reactions in biological systems.^{183,386}

Gangliosides are biologically interesting molecules that play a physicochemical role in the formation of tubular structures such as axons or dendrites in neurons. Recently, a ganglioside was observed to induce neuron-like nanotubes to connect cell-size liposomes formed from dioleoylphosphatidylcholine.³⁸⁷ This result suggests that the gangliosides play a crucial role in the formation and stabilization of unique tubular structures in neurons. On the other hand, instead of the micromanipulation technique mentioned above, tuning the pH of the solutions containing molecular aggregates caused switching of the self-assembled morphology from spherical vesicles to tubular morphology.³⁸⁸ After microspheres were formed from synthetic benzoic diacid diamide **97** in pH 8 solution, lowering the pH to 7 resulted in the

formation of a nanotube bridge connecting the microspheres.



7.4. Properties of Water Confined in a Hollow Cylinder

In wet nanomaterials, understanding the physical properties of the water confined in nanospaces is critical because the confined water plays a fundamental role in controlling the performance of high-functional nanomaterials, such as solid-state electrodes, separators in fuel cells, selective gas permeation membranes, membrane catalysts, microfluidics devices, biosensors, and biomaterials. Inside nanospaces that are tens of nanometers in width, the effects of wall surfaces and microscopic dynamics become critical, and eventually the properties of the confined water deviate significantly from those of the bulk water. Several molecular dynamics calculations were performed for confined water inside cylindrical nanospaces. These calculations model various hollow cylindrical nanostructures, including single-walled carbon nanotubes,^{389,390} a cyclic peptide nanotube,^{391–394} polar cylindrical pores with diameters of up to 4 nm,³⁹⁵ and a porous glass with a 4 nm diameter.³⁹⁶ Depending on the surface properties and the inner diameters, the water molecules were found to show different structural and transport behavior inside the cylindrical nanospace.

Water in a confined geometry is, thus, of great interest in connection with both molecular dynamics simulation of confined water and the nanochannel devices described in sections 7.2 and 7.3. The lyophilization method²⁸¹ permits the introduction of a fluorescent probe molecule, 8-anilinonaphthalene-1-sulfonate (ANS), exclusively into the water confined in the cyclic, hollow cylinder of nanotubes of glycolipids **25**. Both time-resolved fluorescent and attenuated total reflection (ATR) IR measurements revealed new features of water molecules confined in the hollow.³⁹⁷ A dynamic Stokes shift with a 1.26 ns correlation time was observed, indicating that the reorganization motion of the confined water is extremely hindered (Figure 50). The correlation time is approximately 3 orders of magnitude larger than that in bulk water at room temperature. This reorganization time corresponds to that for water confined in sodium bis(2-ethylhexyl) sulfosuccinate (AOT) reversed micelles with diameters of a few nanometers³⁹⁸ and also for propanol solution at deep supercooled temperatures.³⁹⁹ ATR-IR measurements indicated that the water inside the LNT hollow cylinder had features similar to those observed at low temperature (<273 K),⁴⁰⁰ which suggests the formation of glassy water.

8. Concluding Remarks

Once the molecular structures of monomers that self-assemble into tubular morphologies are ratio-

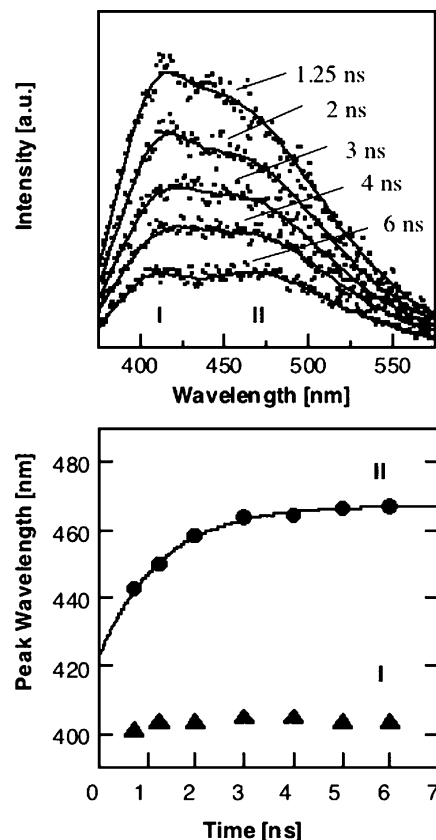


Figure 50. (top) Time-resolved spectra of ANS in confined water in the renewable resource-based **27** LNT. The spectra were obtained at (a) 1.25, (b) 2.0, (c) 3.0, (d) 4.0, and (e) 6.0 ns after the excitation. The solid lines are fitted by the sum of two log-normal functions. The shorter wavelength component is denoted as I, relative to the longer one II. (bottom) Changes in the peak wavelengths of components I and II in the nanosecond time scale. A single-exponential function was fitted to the time course of the peak position of component II and is given by the solid line.

nally designed and synthesized, they spontaneously produce fascinating nanotube structures with well-defined hollow inner cylinders. This assembly process takes place in a bottom-up fashion with minimum energy and maximum accuracy. The advantages of molecular self-assembly are most apparent in the fabrication of high-axial-ratio nanostructures with diameters of one to several tens of nanometers. In this respect, when considering the regulation of the dimension of nanostructures, LNTs should be suitable targeting objects. Thus, the outer and inner diameters and the membrane thicknesses of LNTs have been controllable under optimized preparation conditions and by means of exquisite molecular design on the basis of the experimental results of structure-morphology relationship. Careful modification and optimization of the chemical structure of potential molecules, such as phosphatidylcholine and glycolipid derivatives, enable us to obtain LNTs in gram or kilogram quantities. LNTs can also act as tiny templates for the fabrication of useful inorganic nanotubes and one-dimensional organic-inorganic or organic-metal nanocomposites. Supra-inorganic nanomaterials with a variety of compositions and three-dimensional structures will thus emerge in a similar way to supramolecular structures.

Discrete, homogeneous cylindrical hollows with 10–1000 nm inner diameters will have beneficial uses in the emerging fields of bio-nanotechnology and related nanotechnologies. With the goal of designing gene carriers, submicron channels for capillary electrophoresis, and continuous nanoreactors by using supramolecular nanotube architectures, a few studies based on advanced analytical chemistry are just starting. Work on nanotube-vesicle networks linked with each other, for which carbon nanotubes are not applicable, represents a new research trend in this field. For the purpose of bio-nanotechnology applications, the mechanical and thermal stabilization of LNTs must be enhanced by, for example, the used of polymer amphiphiles, polymerization, or cross-linking of constituent monomer lipids. Various theories have proven helpful for rationalizing the optimum molecular structure for self-assembled nanotubes and regulating their dimensions. However, at present there are no comprehensive theoretical models. Although there are still unresolved issues in research on LNTs, the accumulation of knowledge regarding LNTs and their supramolecular hybrid derivatives will certainly open up novel research disciplines as well contribute to the traditional disciplines of physics, biology, and analytical chemistry.

Several excellent reviews and books regarding related organic nanotubes and molecular self-assemblies are available. For example, Ghadiri et al. fully reviewed organic nanotubes in terms of one-dimensional stacking of cyclic molecular building blocks, including peptide and cyclodextrin nanotubes.³⁰ Fuhrhop and Koenig have written an excellent book dealing with membranes and molecular assemblies on the basis of “synkinesis” (the synthesis of noncovalent molecular assemblies) and “synkinons” (the corresponding monomers).¹⁸⁷ In addition, chiral self-assembled structures, which are closely related to lipid nanotubes, from biomolecules and synthetic analogues have been reviewed by Feiters and Nolte,¹²³ and Spector et al.¹²⁴ Very recently, excellent reviews focusing on bolaamphiphiles¹³⁸ and supramolecular assemblies in aqueous dispersions¹³⁷ were published.

9. Acknowledgment

The authors thank their colleagues Dr. Masaki Kogiso, Dr. Masumi Asakawa, Dr. Masaru Aoyagi, Dr. Rika Iwaura, Dr. Bo Yang, Dr. Naohiro Kameta, Dr. Norihiko Minoura, Dr. Hirotaka Uzawa, and Dr. Qingmin Ji for their continuous support at NARC, AIST, during the course of this work on supramolecular nanotube architectures. Dr. George John, Dr. Jong Hwa Jung, Dr. Shoko Kamiya, Dr. Nikolay V. Goutev, and Dr. Hiroharu Yui (CREST-JST) are acknowledged for collaboration on the synthesis and analysis of self-assembled tubular and fiber structures. Drs. Kiyoshi Yase (AIST), Takeshi Hanada (Osaka University), Yuji Okada (NIMC), Yoshiki Shimizu (AIST), and Kaname Yoshida (AIST) are gratefully acknowledged for carrying out TEM measurements. Prof. Tsuguo Sawada, Prof. Kohzo Ito, Dr. Hiroshi Furusawa, and Mr. Akihiro Fukagawa (University of Tokyo) are also acknowledged for fruitful

collaboration on novel physicochemical properties of LNTs. Prof. Seiji Shinkai (Kyushu University), Prof. Sumio Iijima, and Dr. Morio Yumura (AIST) are thanked for collaboration on novel nanotube exploitation and kind encouragement. The Japan Science and Technology Agency (JST) is acknowledged for financial support of the CREST project.

10. References

- (1) Curatolo, W. *Biochim. Biophys. Acta* **1987**, *906*, 111.
- (2) Curatolo, W. *Biochim. Biophys. Acta* **1987**, *906*, 137.
- (3) Israelachvili, J. N. *Intermolecular and Surface Forces*; Academic Press: New York, 1985.
- (4) Kunitake, T.; Okahata, Y. *J. Am. Chem. Soc.* **1980**, *102*, 549.
- (5) Kunitake, T.; Okahata, Y.; Shimomura, M.; Yasunami, S.; Takarabe, K. *J. Am. Chem. Soc.* **1981**, *103*, 5401.
- (6) Kunitake, T. *Angew. Chem., Int. Ed. Engl.* **1992**, *31*, 709.
- (7) Whitesides, G. M.; Mathias, J. P. *Science* **1991**, *254*, 1312.
- (8) Chandross, E. A.; Miller, R. D. *Chem. Rev.* **1999**, *99*, 1641.
- (9) Iijima, S. *Nature* **1991**, *354*, 56.
- (10) Iijima, S.; Ichihashi, T. *Nature* **1993**, *363*, 603.
- (11) Schnur, J. M.; Price, R.; Schoen, P.; Yager, P.; Calvert, J. M.; Georger, J.; Singh, A. *Thin Solid Films* **1987**, *152*, 181.
- (12) Schnur, J. M. *Science* **1993**, *262*, 1669.
- (13) Yager, P.; Schoen, P. E. *Mol. Cryst. Liq. Cryst.* **1984**, *106*, 371.
- (14) Yager, P.; Schoen, P. E.; Davies, C.; Price, R.; Singh, A. *Biophys. J.* **1985**, *48*, 899.
- (15) Schoen, P. E.; Yager, P. *J. Polym. Sci., Polym. Phys. Ed.* **1985**, *23*, 2203.
- (16) Schoen, P. E.; Yager, P.; Priest, R. G. *NATO Sci. Ser., Ser. E* **1985**, *102*, 223.
- (17) Yamada, K.; Ihara, H.; Ide, T.; Fukumoto, T.; Hirayama, C. *Chem. Lett.* **1984**, 1713.
- (18) Nakashima, N.; Asakuma, S.; Kim, J.-M.; Kunitake, T. *Chem. Lett.* **1984**, 1709.
- (19) Nakashima, N.; Asakuma, S.; Kunitake, T. *J. Am. Chem. Soc.* **1985**, *107*, 509.
- (20) Antonietti, M.; Forster, S. *Adv. Mater.* **2003**, *15*, 1323.
- (21) Lazzari, M.; Lopez-Quintela, M. *Adv. Mater.* **2003**, *15*, 1583.
- (22) Yu, K.; Eisenberg, A. *Macromolecules* **1998**, *31*, 3509.
- (23) Shen, H.; Eisenberg, A. *Macromolecules* **2000**, *33*, 2561.
- (24) Jenekhe, S. A.; Chen, X. L. *Science* **1999**, *283*, 372.
- (25) Raez, J.; Barjavanu, R.; Massey, J. A.; Winnik, M. A.; Manners, I. *Angew. Chem., Int. Ed.* **2000**, *39*, 3862.
- (26) Raez, J.; Manners, I.; Winnik, M. A. *J. Am. Chem. Soc.* **2002**, *124*, 10381.
- (27) Li, Z.-C.; Liang, Y.-Z.; Li, F.-M. *Chem. Commun.* **1999**, 1557.
- (28) Harada, A.; Li, J.; Kamachi, M. *Nature* **1993**, *364*, 516.
- (29) Ghadiri, M. R.; Granja, J. R.; Milligan, R. A.; McRee, D. E.; Khazanovich, N. *Nature* **1993**, *366*, 324.
- (30) Bong, D. T.; Clark, T. D.; Granja, J. R.; Ghadiri, M. R. *Angew. Chem., Int. Ed.* **2001**, *40*, 988.
- (31) Harada, A.; Kamachi, M. *J. Am. Chem. Soc.* **1994**, *116*, 3192.
- (32) Ghadiri, M. R.; Granja, J. R.; Buehler, L. K. *Nature* **1994**, *369*, 301.
- (33) Ghadiri, M. R. *Adv. Mater.* **1995**, *7*, 675.
- (34) Ghadiri, M. R.; Kobayashi, K.; Granja, J. R.; Chadha, R. K.; McRee, D. E. *Angew. Chem., Int. Ed. Engl.* **1995**, *34*, 93.
- (35) Hartgerink, J. D.; Granja, J. R.; Milligan, R. A.; Ghadiri, M. R. *J. Am. Chem. Soc.* **1996**, *118*, 43.
- (36) Remskar, M.; Skraba, Z.; Stadelmann, P.; Levy, F. *Adv. Mater.* **2000**, *12*, 814.
- (37) Remskar, M.; Mrzel, A.; Skraba, Z.; Jesih, A.; Ceh, M.; Demsar, J.; Stadelmann, P.; Levy, F.; Mihailovic, D. *Science* **2001**, *292*, 479.
- (38) Middleton, G. V.; Church, M. J.; Coniglio, M.; Hardie, L. A. *Encyclopedia of Sediments and Sedimentary Rocks; Encyclopedia of Earth Science Series*; Kluwer Academic Publishers Group: 2003.
- (39) Bommel, K. J. C. v.; Friggeri, A.; Shinkai, S. *Angew. Chem., Int. Ed.* **2003**, *42*, 980.
- (40) Fowler, C. E.; Khushalani, D.; Lebeau, B.; Mann, S. *Adv. Mater.* **2001**, *13*, 649.
- (41) Lu, Y.; Fan, H.; Stump, A.; Ward, T. L.; Rieker, T.; Brinker, C. J. *Nature* **1999**, *398*, 223.
- (42) Kim, S. S.; Zhang, W.; Pinnavaia, T. J. *Science* **1998**, *282*, 1302.
- (43) Lin, H.-P.; Mou, C.-Y. *Science* **1996**, *273*, 765.
- (44) Lin, H.-P.; Cheng, S.; Mou, C.-Y. *Chem. Mater.* **1998**, *10*, 581.
- (45) Kleitz, F.; Marlow, F.; Stucky, G. D.; Schuth, F. *Chem. Mater.* **2001**, *13*, 3587.
- (46) Lin, H.-P.; Mou, C.-Y.; Liu, S.-B. *Adv. Mater.* **2000**, *12*, 103.
- (47) Fowler, C. E.; Khushalani, D.; Mann, S. *Chem. Commun.* **2001**, 2028.

- (48) Schacht, S.; Huo, Q.; Voigt-Martin, I. G.; Stucky, G. D.; Schueth, F. *Science* **1996**, *273*, 768.
- (49) Oliver, S.; Kuperman, A.; Coombs, N.; Ozin, G. A. *Can. J. Chem.* **1999**, *77*, 2001.
- (50) Archibald, D. D.; Mann, S. *Nature* **1993**, *364*, 430.
- (51) Chappell, J. S.; Yager, P. *J. Mater. Sci. Lett.* **1992**, *11*, 633.
- (52) Baral, S.; Schoen, P. *Chem. Mater.* **1993**, *5*, 145.
- (53) Knez, M.; Bittner, A. M.; Boes, F.; Wege, C.; Jeske, H.; Maiss, E.; Kern, K. *Nano Lett.* **2003**, *3*, 1079.
- (54) Yang, B.; Kamiya, S.; Shimizu, Y.; Koshizaki, N.; Shimizu, T. *Chem. Mater.* **2004**, *16*, 2826.
- (55) Ji, Q.; Kamiya, S.; Jung, J.-H.; Shimizu, T. *J. Mater. Chem.* **2005**, *15*, 743.
- (56) Sakai, H.; Baba, R.; Hashimoto, K.; Fujishima, A. *J. Phys. Chem.* **1995**, *99*, 11896.
- (57) Lindner, E.; Cosofret, V. V.; Ulfer, S.; Buck, R. P. *J. Chem. Soc., Faraday Trans.* **1993**, *89*, 361.
- (58) Li, W. Z.; Xie, S. S.; Qian, L. X.; Chang, B. H.; Zou, B. S.; Zhou, W. Y.; Zhao, R. A.; Wang, G. *Science* **1996**, *274*, 1701.
- (59) Trau, M.; Yao, N.; Kim, E.; Xia, Y.; Whitesides, G. M.; Aksay, I. A. *Nature* **1997**, *390*, 674.
- (60) Fendler, J. H. *Chem. Mater.* **1996**, *8*, 1616.
- (61) Spector, M. S.; Selinger, J. V.; Singh, A.; Rodriguez, J. M.; Price, R. R.; Schnur, J. M. *Langmuir* **1998**, *14*, 3493 and references therein.
- (62) Gelbart, W. M.; Ben-Shaul, A.; Roux, D. *Micelles, Membranes, Microemulsions, and Monolayers*; Springer-Verlag: New York, 1994.
- (63) Safran, S. A. *Statistical Thermodynamics of Surfaces, Interfaces, and Membranes*; Addison-Wesley: Reading, MA, 1994.
- (64) Lipowsky, R.; Sackmann, E. *Structure and Dynamics of Membranes*; Elsevier Science: New York, 1995.
- (65) de Gennes, P. G.; Prost, J. *The Physics of Liquid Crystals*; Oxford University Press: Oxford, 1993.
- (66) Dahl, I.; Lagerwall, S. T. *Ferroelectrics* **1984**, *58*, 215.
- (67) Helfrich, W.; Prost, J. *Phys. Rev. A* **1988**, *38*, 3065.
- (68) Nelson, P.; Powers, T. *Phys. Rev. Lett.* **1992**, *69*, 3409.
- (69) Nelson, P.; Powers, T. *J. Phys. II* **1993**, *3*, 1535.
- (70) Ou-Yang, Z.; Liu, J. *Phys. Rev. Lett.* **1990**, *65*, 1679.
- (71) Ou-Yang, Z.; Liu, J. *Phys. Rev. A* **1991**, *43*, 6826.
- (72) Chung, D. S.; Benedek, G. B.; Konikoff, F. M.; Donovan, J. M. *Proc. Natl. Acad. Sci. U.S.A.* **1993**, *90*, 11341.
- (73) Selinger, J. V.; MacKintosh, F. C.; Schnur, J. M. *Phys. Rev. E* **1996**, *53*, 3804.
- (74) Schnur, J. M.; Ratna, B. R.; Selinger, J. V.; Singh, A.; Jyothi, G.; Easwaran, K. R. K. *Science* **1994**, *264*, 945.
- (75) Komura, S.; Ou-Yang, Z. *Phys. Rev. Lett.* **1998**, *81*, 473.
- (76) Nandi, N.; Bagchi, B. *J. Am. Chem. Soc.* **1996**, *118*, 11208.
- (77) Smith, G. S.; Sirota, E. B.; Safinya, C. R.; Clark, N. A. *Phys. Rev. Lett.* **1988**, *60*, 813.
- (78) Chappel, J. S.; Yager, P. *Chem. Phys. Lipids* **1991**, *58*, 253.
- (79) Thomas, B. N.; Safinya, C. R.; Plano, R. J.; Clark, N. A. *Science* **1995**, *267*, 1635.
- (80) Thomas, B. N.; Lindemann, C. M.; Clark, N. A. *Phys. Rev. E* **1999**, *59*, 3040.
- (81) Fuhrhop, J. H.; Spiroski, D.; Boettcher, C. *J. Am. Chem. Soc.* **1993**, *115*, 1600.
- (82) Masuda, M.; Shimizu, T. *Langmuir* **2004**, *20*, 5969.
- (83) Shimizu, T.; Hato, M. *Biochim. Biophys. Acta* **1993**, *1147*, 50.
- (84) Stewart, S.; Liu, G. *Angew. Chem., Int. Ed.* **2000**, *39*, 340.
- (85) Li, Z.; Liu, G. *Langmuir* **2003**, *19*, 10480.
- (86) Huang, H.; Remsen, E. E.; Kowalewski, T.; Wooley, K. L. *J. Am. Chem. Soc.* **1999**, *121*, 3805.
- (87) Kim, Y.; Mayer, M. F.; Zimmerman, S. C. *Angew. Chem., Int. Ed.* **2003**, *42*, 1121.
- (88) Martin, C. R. *Science* **1994**, *266*, 1961.
- (89) Steinhart, M.; Wehrspohn, R. B.; Goesele, U.; Wendorff, J. H. *Angew. Chem., Int. Ed.* **2004**, *43*, 1334.
- (90) Obare, O. S.; Jana, N. R.; Murphy, C. J. *Nano Lett.* **2001**, *1*, 601.
- (91) Bognitzki, M.; Hou, H.; Ishaque, M.; Frese, T.; Hellwig, M.; Schwarte, C.; Schaper, A.; Wendorff, J. H.; Greiner, A. *Adv. Mater.* **2000**, *12*, 637.
- (92) Porrata, P.; Goun, E.; Matsui, H. *Chem. Mater.* **2002**, *14*, 4378.
- (93) Steinhart, M.; Wendorff, J. H.; Greiner, A.; Wehrspohn, R. B.; Nielsch, K.; Schilling, J.; Choi, J.; Goesele, U. *Science* **2002**, *296*, 1997.
- (94) Liang, Z.; Susha, A. S.; Yu, A.; Caruso, F. *Adv. Mater.* **2003**, *15*, 1849.
- (95) Brumlik, C. J.; Martin, C. R. *J. Am. Chem. Soc.* **1991**, *113*, 3174.
- (96) Steinhart, M.; Jia, Z.; Schaper, A. K.; Wehrspohn, R. B.; Goesele, U.; Wendorff, J. H. *Adv. Mater.* **2003**, *15*, 706.
- (97) Menon, V. P.; Martin, C. R. *Anal. Chem.* **1995**, *67*, 1920.
- (98) Demoustier-Champagne, S.; Duchet, J.; Legras, R. *Synth. Met.* **1999**, *101*, 20.
- (99) Kim, K.; Jin, J.-I. *Nano Lett.* **2001**, *1*, 631.
- (100) Hou, H.; Jun, Z.; Reuning, A.; Schaper, A.; Wendorff, J. H.; Greiner, A. *Macromolecules* **2002**, *35*, 2429.
- (101) Zhang, Z.; Wei, Z.; Wan, M. *Macromolecules* **2002**, *35*, 5937.
- (102) Wei, Z.; Zhang, L.; Yu, M.; Yang, Y.; Wan, M. *Adv. Mater.* **2003**, *15*, 1382.
- (103) Georger, J. H.; Singh, A.; Price, R. R.; Schnur, J. M.; Yager, P.; Schoen, P. E. *J. Am. Chem. Soc.* **1987**, *109*, 6169.
- (104) Davies, M. A.; Ratna, B. R.; Rudolph, A. S. *Langmuir* **1994**, *10*, 2872.
- (105) Singh, A.; Chow, G. M.; Chang, E. L.; Markowitz, M. A. *CHEMTECH* **1995**, 38.
- (106) Johnston, D. S.; Sangera, S.; Pons, M.; Chapman, D. *Biochim. Biophys. Acta* **1980**, *602*, 57.
- (107) O'Brien, D. F.; Whitesides, T. H.; Klingbiel, R. T. *J. Polym. Sci., Polym. Lett. Ed.* **1981**, *19*, 95.
- (108) Hupfer, B.; Ringsdorf, H.; Schupp, H. *Makromol. Chem.* **1981**, *182*, 247.
- (109) Kusumi, A.; Singh, M.; Tirrell, D. A.; Oehme, G.; Singh, A.; Samuel, N. K. P.; Hyde, J. S.; Regen, S. L. *J. Am. Chem. Soc.* **1983**, *105*, 2975.
- (110) Hub, H. H.; Hupfer, B.; Koch, H.; Ringsdorf, H. *Angew. Chem., Int. Ed. Engl.* **1980**, *19*, 938.
- (111) Burke, T. G.; Rudolph, A. S.; Price, R. R.; Sheridan, J. P.; Dalziel, A. W.; Singh, A.; Schoen, P. E. *Chem. Phys. Lipids* **1988**, *48*, 215.
- (112) Yager, P.; Price, R. R.; Schnur, J. M.; Schoen, P. E.; Singh, A.; Rhodes, D. G. *Chem. Phys. Lipids* **1988**, *46*, 171.
- (113) Schnur, D. M.; Yuh, Y. H.; Dalton, D. R. *J. Org. Chem.* **1989**, *54*, 3779.
- (114) Rudolph, A. S.; Burke, T. G. *Biochim. Biophys. Acta* **1987**, *902*, 349.
- (115) Rudolph, A. S.; Calvert, J. M.; Schoen, P. E.; Schnur, J. M. *Adv. Exp. Med. Biol.* **1988**, *238*, 305.
- (116) Rudolph, A. S.; Calvert, J. M.; Ayers, M. E.; Schnur, J. M. *J. Am. Chem. Soc.* **1989**, *111*, 8516.
- (117) Rudolph, A. S.; Ratna, B. R.; Kahn, B. *Nature* **1991**, *352*, 52.
- (118) Rudolph, A. S.; Testoff, M. A.; Shashidhar, R. *Biochim. Biophys. Acta* **1992**, *1127*, 186.
- (119) Schoen, P. E.; Price, R. R.; Schnur, J. M.; Gulik, A.; Gulik-Krzywicki, T. *Chem. Phys. Lipids* **1993**, *65*, 179.
- (120) Singh, A.; Markowitz, M. A. *New J. Chem.* **1994**, *18*, 377.
- (121) Schnur, J. M.; Shashidhar, R. *Adv. Mater.* **1994**, *6*, 971.
- (122) Fuhrhop, J. H.; Helfrich, W. *Chem. Rev.* **1993**, *93*, 1565.
- (123) Feiters, M. C.; Nolte, R. J. M. In *Advances in Supramolecular Chemistry*; Gokel, G. W., Ed.; JAI Press Inc.: Stamford, CT, 2000; Vol. 6.
- (124) Spector, M. S.; Selinger, J. V.; Schnur, J. M. In *Topics in Stereochemistry, Volume 24, Materials-Chirality*; Green, M. M., Nolte, R. J. M., Meijer, E. W., Eds.; Wiley: 2003; pp 281–372.
- (125) Thomas, B. N.; Corcoran, R. C.; Cotant, C. L.; Lindemann, C. M.; Kirsch, J. E.; Persichini, P. *J. Am. Chem. Soc.* **1998**, *120*, 12178.
- (126) Seifert, U.; Shillcock, J.; Nelson, P. *Phys. Rev. Lett.* **1996**, *77*, 5237.
- (127) Spector, M. S.; Easwaran, K. R. K.; Selinger, J. V.; Singh, A.; Schnur, J. M. *Polym. Prepr. (Am. Chem. Soc., Div. Polym. Chem.)* **1996**, *37*, 482.
- (128) Spector, M. S.; Selinger, J. V.; Schnur, J. M. *J. Am. Chem. Soc.* **1997**, *119*, 8533.
- (129) Nounesis, G.; Ratna, B. R.; Shin, S.; Flugel, R. S.; Sprunt, S. N.; Singh, A.; Lister, J. D.; Shashidhar, R.; Kumar, S. *Phys. Rev. Lett.* **1996**, *76*, 3650.
- (130) Fuhrhop, J.-H.; Schnieder, P.; Boekema, E.; Helfrich, W. *J. Am. Chem. Soc.* **1988**, *110*, 2861.
- (131) Boettcher, C.; Schade, B.; Fuhrhop, J.-H. *Langmuir* **2001**, *17*, 873.
- (132) Fuhrhop, J.-H.; Blumtritt, P.; Lehmann, C.; Luger, P. *J. Am. Chem. Soc.* **1991**, *113*, 7437.
- (133) Frankel, D. A.; O'Brien, D. F. *J. Am. Chem. Soc.* **1991**, *113*, 7436.
- (134) Frankel, D. A.; O'Brien, D. F. *Macromol. Symp.* **1994**, *77*, 141.
- (135) Ladika, M.; Fisk, T. E.; Wu, W. W.; Jons, S. D. *J. Am. Chem. Soc.* **1994**, *116*, 12093.
- (136) Frankel, D. A.; O'Brien, D. F. *J. Am. Chem. Soc.* **1994**, *116*, 10057.
- (137) Estroff, L. A.; Hamilton, A. D. *Chem. Rev.* **2004**, *104*, 1201.
- (138) Fuhrhop, J.-H.; Wang, T. *Chem. Rev.* **2004**, *104*, 2901.
- (139) Shimizu, T.; Masuda, M. *J. Am. Chem. Soc.* **1997**, *119*, 2812.
- (140) Nakazawa, I.; Masuda, M.; Okada, Y.; Hanada, T.; Yase, K.; Asai, M.; Shimizu, T. *Langmuir* **1999**, *15*, 4757.
- (141) Masuda, M.; Shimizu, T. *Carbohydr. Res.* **2000**, *326*, 56.
- (142) Shimizu, T. *Macromol. Rapid Commun.* **2002**, *23*, 311.
- (143) Smitz, E.; Engmerts, J. B. F. N.; Kellogg, R. M.; Doren, H. A. V. *Liq. Cryst.* **1997**, *23*, 481.
- (144) John, G.; Masuda, M.; Okada, Y.; Yase, K.; Shimizu, T. *Adv. Mater.* **2001**, *13*, 715.
- (145) Kozubek, A.; Tyman, J. H. P. *Chem. Rev.* **1999**, *99*, 1.
- (146) John, G.; Jung, J. H.; Masuda, M.; Shimizu, T. *Langmuir* **2004**, *20*, 2060.
- (147) John, G.; Jung, J. H.; Minamikawa, H.; Yoshida, K.; Shimizu, T. *Chem.—Eur. J.* **2002**, *8*, 5494.
- (148) Jung, J. H.; John, G.; Yoshida, K.; Shimizu, T. *J. Am. Chem. Soc.* **2002**, *124*, 10674.

- (149) Kamiya, S.; Minamikawa, H.; Jung, J. H.; Yang, B.; Masuda, M.; Shimizu, T. *Langmuir* **2005**, *21*, 743.
- (150) Mishima, K.; Ogihara, T.; Tomita, M.; Satoh, K. *Chem. Phys. Lipids* **1992**, *62*, 87.
- (151) Archibald, D. D.; Yager, P. *Biochemistry* **1992**, *31*, 9045.
- (152) Goldstein, A. S.; Lukyanov, A. N.; Carlson, P. A.; Yager, P.; Gelb, M. H. *Chem. Phys. Lipids* **1997**, *88*, 21.
- (153) Kulkarni, V. S.; Anderson, W. H.; Brown, R. E. *Biophys. J.* **1995**, *69*, 1976.
- (154) Kulkarni, V. S.; Boggs, J. M.; Brown, R. E. *Biophys. J.* **1999**, *77*, 319.
- (155) Mutz, M.; Servuss, R.-M.; Helfrich, W. *J. Phys. Paris* **1990**, *51*, 2557.
- (156) Curatolo, W.; Neuringer, L. *J. J. Biol. Chem.* **1986**, *261*, 17177.
- (157) Maggio, B.; Albert, J.; Yu, R. K. *Biochim. Biophys. Acta* **1988**, *945*, 145.
- (158) Yunis, E. J.; Lee, R. E. *Science* **1970**, *169*, 64.
- (159) Giulieri, F.; Krafft, M.-P.; Riess, J. G. *Angew. Chem., Int. Ed. Engl.* **1994**, *33*, 1514.
- (160) Giulieri, F.; Guillod, F.; Greiner, J.; Krafft, M.-P. *Chem.-Eur. J.* **1996**, *2*, 1335.
- (161) Imae, T.; Krafft, M.-P.; Giulieri, F.; Matsumoto, T.; Tada, T. *Prog. Colloid Polym. Sci.* **1997**, *106*, 52.
- (162) Terech, P.; Volino, F.; Ramasseul, R. *J. Phys.* **1985**, *46*, 895.
- (163) Terech, P. *Prog. Colloid Polym. Sci.* **1990**, *82*, 263.
- (164) Wade, R. H.; Terech, P.; Hewat, E. A.; Ramasseul, R.; Volino, F. *J. Colloid Interface Sci.* **1986**, *114*, 442.
- (165) Imae, T.; Funayama, K.; Krafft, M. P.; Giulieri, F.; Tada, T.; Matsumoto, T. *J. Colloid Interface Sci.* **1999**, *212*, 330.
- (166) Shimizu, T.; Kogiso, M.; Masuda, M. *Nature* **1996**, *383*, 487.
- (167) Kogiso, M.; Ohnishi, S.; Yase, K.; Masuda, M.; Shimizu, T. *Langmuir* **1998**, *14*, 4978.
- (168) Shimizu, T.; Ohnishi, S.; Kogiso, M. *Angew. Chem., Int. Ed.* **1998**, *37*, 3260.
- (169) Kogiso, M.; Shimizu, T. Unpublished results.
- (170) Kogiso, M.; Okada, Y.; Hanada, T.; Yase, K.; Shimizu, T. *Biochim. Biophys. Acta* **2000**, *1475*, 346.
- (171) Kogiso, M.; Yoshida, K.; Yase, K.; Shimizu, T. *Chem. Commun.* **2002**, *2002*, 2492.
- (172) Kogiso, M.; Okada, Y.; Yase, K.; Shimizu, T. *J. Colloid Interface Sci.* **2004**, *273*, 394.
- (173) Lu, K.; Jacob, J.; Thiagarajan, P.; Conticello, V. P.; Lynn, D. G. *J. Am. Chem. Soc.* **2003**, *125*, 6391.
- (174) Vauthery, S.; Santos, S.; Gong, H.; Watson, N.; Zhang, S. *Proc. Natl. Acad. Sci. U.S.A.* **2002**, *99*, 5355.
- (175) Aggeli, A.; Bell, M.; Boden, N.; Keen, J. N.; Knowles, P. F.; McLeish, T. C. B.; Pitkeathly, M.; Radford, S. E. *Nature* **1997**, *386*, 259.
- (176) Aggeli, A.; Nyrkova, I. A.; Bell, M.; Harding, R.; Carrick, L.; McLeish, T. C. B.; Semenov, A. N.; Boden, N. *Proc. Natl. Acad. Sci. U.S.A.* **2001**, *98*, 11857.
- (177) Marini, D. M.; Hwang, W.; Lauffenburger, D. A.; Zhang, S.; Kamm, R. D. *Nano Lett.* **2002**, *2*, 295.
- (178) Fishwick, C. W. G.; Beevers, A. J.; Carrick, L. M.; Whitehouse, C. D.; Aggeli, A.; Boden, N. *Nano Lett.* **2003**, *3*, 1475.
- (179) Rothman, J. E.; Wieland, F. T. *Science* **1996**, *272*, 227.
- (180) Furuya, T.; Kiyota, T.; Lee, S.; Inoue, T.; Sugihara, G.; Logvinova, A.; Goldsmith, P.; Ellerby, H. M. *Biophys. J.* **2003**, *84*, 1950.
- (181) Weidman, P.; Roth, R.; Heuser, J. *Cell* **1993**, *5*, 123.
- (182) Urrutia, R.; Henley, J. R.; Cook, T.; McNiven, M. A. *Proc. Natl. Acad. Sci. U.S.A.* **1997**, *94*, 377.
- (183) Sciaky, N.; Presley, J.; Smith, C.; Zaal, K. J. M.; Cole, N.; Moreira, J. E.; Terasaki, M.; Siggia, E.; Lippincott-Schwartz, J. *J. Cell. Biol.* **1997**, *139*, 1137.
- (184) Presley, J. F.; Smith, C.; Hirschberg, K.; Miller, C.; Cole, N. B.; Zaal, K. J. M.; Lippincott-Schwartz, J. *Mol. Biol. Cell* **1998**, *16*, 1617.
- (185) Lee, S.; Furuya, T.; Kiyota, T.; Takami, N.; Murata, K.; Niidome, Y.; Bredesen, D. E.; Ellerby, H. M.; Sugihara, G. *J. Biol. Chem.* **2001**, *276*, 41224.
- (186) Fuhrhop, J.-H.; Fritsch, D. *Acc. Chem. Res.* **1986**, *19*, 130.
- (187) Fuhrhop, J.-H.; Koenig, J. *Membranes and Molecular Assemblies: The Synergetic Approach*; The Royal Society of Chemistry: Cambridge, 1994.
- (188) Fuhrhop, J.-H.; Tank, H. *Chem. Phys. Lipids* **1987**, *43*, 193.
- (189) Sirieix, J.; Viguerie, N. L.-d.; Riviere, M.; Lattes, A. *New J. Chem.* **2000**, *24*, 1043.
- (190) Prata, C.; Mora, N.; Polidori, A.; Lacombe, J.-M.; Pucci, B. *Carbohydr. Res.* **1999**, *321*, 15.
- (191) Claussen, R. C.; Rabatic, B. M.; Stupp, S. I. *J. Am. Chem. Soc.* **2003**, *125*, 12680.
- (192) Guilbot, J.; Benguegnu, T.; Legros, N.; Plusquellec, D. *Langmuir* **2001**, *17*, 613.
- (193) Schneider, J.; Messerschmidt, C.; Schulz, A.; Gnade, M.; Schade, B.; Luger, P.; Bombicz, P.; Hubert, V.; Fuhrhop, J. H. *Langmuir* **2000**, *16*, 8575.
- (194) Song, J.; Cheng, Q.; Kopta, S.; Stevens, R. C. *J. Am. Chem. Soc.* **2001**, *123*, 3205.
- (195) Jaeger, D. A.; Li, G.; Subotkowski, W.; Carron, K. T. *Langmuir* **1997**, *13*, 5563.
- (196) Fuhrhop, J. H.; David, H. H.; Mathieu, J.; Liman, U.; Winter, H. J.; Boekema, E. J. *Am. Chem. Soc.* **1986**, *108*, 1785.
- (197) Fuhrhop, J.-H.; Mathieu, J. *Chem. Commun.* **1983**, 144.
- (198) Liang, K.; Hui, Y. *J. Am. Chem. Soc.* **1992**, *114*, 6588.
- (199) Masuda, M.; Shimizu, T. *Chem. Commun.* **2001**, *2001*, 2442.
- (200) Szafran, M.; Dega-Szafran, Z.; Katrusiak, A.; Buczak, G.; Glowacki, T.; Sitkowski, J.; Stefaniak, L. *J. Org. Chem.* **1998**, *63*, 2898.
- (201) Aigouy, P. T.; Costeseque, P.; Sempere, R.; Senac, T. *Acta Crystallogr.* **1995**, *B51*, 55.
- (202) Donovan, J. M.; Carey, M. C. *Gastroenterol. Clin.* **1991**, *20*, 47.
- (203) Konikoff, F. M. *J. Clin. Invest.* **1992**, *90*, 1155.
- (204) Zastavker, Y. V.; Asherie, N.; Lomakin, A.; Pande, J.; Donovan, J. M.; Schnur, J. M.; Benedek, G. B. *Proc. Natl. Acad. Sci. U.S.A.* **1999**, *96*, 7883.
- (205) Terech, P.; Geyer, A. D.; Struth, B.; Talmon, Y. *Adv. Mater.* **2002**, *14*, 495.
- (206) Jung, J. H.; Ono, Y.; Shinkai, S. *Langmuir* **2000**, *16*, 1643.
- (207) Jung, J. H.; Kobayashi, H.; Masuda, M.; Shimizu, T.; Shinkai, S. *J. Am. Chem. Soc.* **2001**, *123*, 8785.
- (208) Jung, J. H.; Lee, S.-H.; Yoo, J. S.; Yoshida, K.; Shimizu, T.; Shinkai, S. *Chem.-Eur. J.* **2003**, *9*, 5307.
- (209) Yamaguchi, T.; Ishii, N.; Tashiro, K.; Aida, T. *J. Am. Chem. Soc.* **2003**, *125*, 13934.
- (210) Hill, J. P.; Jin, W.; Kosaka, A.; Fukushima, T.; Ichihara, H.; Shimomura, T.; Ito, K.; Hashizume, T.; Ishii, N.; Aida, T. *Science* **2004**, *304*, 1481.
- (211) Oda, R.; Huc, I.; Candau, S. *J. Chem. Commun.* **1997**, 2105.
- (212) Oda, R.; Huc, I.; Homo, J.-C.; Heinrich, B.; Schmutz, M.; Candau, S. *Langmuir* **1999**, *15*, 2384.
- (213) Oda, R.; Huc, I.; Candau, S. *J. Angew. Chem., Int. Ed. Engl.* **1998**, *37*, 2689.
- (214) Oda, R.; Huc, I.; Schmutz, M.; Candau, S. J.; Mackintosh, F. C. *Nature* **1999**, *399*, 566.
- (215) Miyawaki, K.; Goto, R.; Shibakami, M. *Chem. Lett.* **2003**, *32*, 1170.
- (216) Wang, G.; Hollingsworth, R. I. *Langmuir* **1999**, *15*, 6135.
- (217) Wang, X.; Shen, Y.; Pan, Y.; Liang, Y. *Langmuir* **2001**, *17*, 3162.
- (218) Wettstein-Knowles, P. *J. Ultrastruct. Res.* **1974**, *46*, 483.
- (219) Fuhrhop, J.-H.; Bedurke, T.; Hahn, A.; Grund, S.; Gatzmann, J.; Riederer, M. *Angew. Chem., Int. Ed. Engl.* **1994**, *33*, 350.
- (220) Guenthardt, M. S. *Bull. Cos. Bot. Suisse* **1985**, *95*, 5.
- (221) Jenekhe, S. A.; Chen, X. L. *Science* **1998**, *279*, 1903.
- (222) Massey, J.; Power, K. N.; Manners, I.; Winnik, M. A. *J. Am. Chem. Soc.* **1998**, *120*, 9533.
- (223) Raez, J.; Tomba, J. P.; Manners, I.; Winnik, M. A. *J. Am. Chem. Soc.* **2003**, *125*, 9546.
- (224) Cameron, N. S.; Corbierre, M. K.; Eisenberg, A. *Can. J. Chem.* **1999**, *77*, 1311.
- (225) Zhang, L.; Eisenberg, A. *Polym. Adv. Technol.* **1998**, *9*, 677.
- (226) de Gennes, P. G. *Solid State Physics*; Academic Press: 1978.
- (227) Zhang, L.; Eisenberg, A. *J. Am. Chem. Soc.* **1996**, *118*, 3168.
- (228) Cornelissen, J. J. L. M.; Fischer, M.; Sommerdijk, N. A. J. M.; Nolte, R. J. M. *Science* **1998**, *280*, 1427.
- (229) Tajima, K.; Aida, T. *Chem. Commun.* **2000**, 2399.
- (230) Ringsdorf, H.; Schlarb, B.; Venzmer, J. *Angew. Chem., Int. Ed. Engl.* **1988**, *27*, 113.
- (231) Mueller, A.; O'Brien, D. F. *Chem. Rev.* **2002**, *102*, 727.
- (232) Liu, G.; Yan, X.; Li, Z.; Zhou, J.; Duncan, S. *J. Am. Chem. Soc.* **2003**, *125*, 14039.
- (233) Natta, G.; Farina, M.; Donati, M. *Makromol. Chem.* **1961**, *43*, 251.
- (234) Wegner, G. *Makromol. Chem.* **1972**, *154*, 35.
- (235) Matsumoto, A.; Nagahama, S.; Odani, T. *J. Am. Chem. Soc.* **2000**, *122*, 9109.
- (236) Tieke, B. *J. Polym. Sci., Polym. Chem.* **1984**, 2895.
- (237) Tieke, B. *Colloid Polym. Sci.* **1985**, *263*, 965.
- (238) Rubner, M. F. *Macromolecules* **1986**, *19*, 2114.
- (239) Lopez, E.; O'Brien, D. F.; Whitesides, T. H. *J. Am. Chem. Soc.* **1982**, *104*, 305.
- (240) Tsuchida, E.; Hasegawa, E.; Kimura, N.; Hatashita, M.; Makino, C. *Macromolecules* **1992**, *25*, 207.
- (241) Lamparski, H.; O'Brien, D. F. *Macromolecules* **1995**, *28*, 1786.
- (242) Sirsiri, W.; Sisson, T. M.; O'Brien, D. F.; McGrath, K. M.; Han, Y.; Gruner, S. M. *J. Am. Chem. Soc.* **1997**, *119*, 4866.
- (243) Hoag, B. P.; Gin, D. L. *Macromolecules* **2000**, *33*, 8549.
- (244) Masuda, M.; Jonkheijm, P.; Sijbesma, R. P.; Meijer, E. W. J. *Am. Chem. Soc.* **2003**, *125*, 15935.
- (245) Masuda, M.; Hanada, T.; Yase, K.; Shimizu, T. *Macromolecules* **1998**, *31*, 9403.
- (246) Masuda, M.; Hanada, T.; Okada, Y.; Yase, K.; Shimizu, T. *Macromolecules* **2000**, *33*, 9233.
- (247) Reichel, F.; Roelofsen, A. M.; Geurts, H. P. M.; van der Gaast, S. J.; Feiters, M. C.; Boons, G.-J. *J. Org. Chem.* **2000**, *65*, 3357.
- (248) Leaver, J.; Alonso, A.; Durrani, A. A.; Chapman, D. *Biochim. Biophys. Acta* **1983**, *732*, 210.
- (249) Svenson, S.; Messersmith, P. B. *Langmuir* **1999**, *15*, 4464.

- (250) Ihara, H.; Takafuji, M.; Hirayama, C.; O'Brien, D. F. *Langmuir* **1992**, *8*, 1548.
- (251) Ihara, H.; Takafuji, M.; Sakurai, T. In *Encyclopedia of Nanoscience and Nanotechnology*; American Science Publishers: California, 2004; Vol. 9.
- (252) Rhodes, D. G.; Singh, A. *Chem. Phys. Lipids* **1991**, *59*, 215.
- (253) Singh, A.; Schoen, P. E.; Schnur, J. M. *J. Chem. Soc., Chem. Commun.* **1988**, 1222.
- (254) Bassler, H.; Enkelmann, V.; Sixl, H. *Advances in Polymer Science*; Springer-Verlag: Berlin, 1984.
- (255) Zhu, C. F.; Lee, I.; Li, J. W.; Wang, C.; Cao, X. Y.; Xu, H.; Zhang, R. B. *J. Mater. Res.* **1999**, *14*, 1084.
- (256) Zhu, C. F.; Xu, Q. M.; Zhou, C. Q.; Yin, S. X.; Shang, G. Y.; Wang, C.; Liu, C. Q.; Zhang, R. B. *Surf. Interface Anal.* **2001**, *32*, 278.
- (257) Spector, M. S.; Price, R. R.; Schnur, J. M. *Adv. Mater.* **1999**, *11*, 337.
- (258) Selinger, J. V.; Schnur, J. M. *Phys. Rev. Lett.* **1993**, *71*, 4091.
- (259) Markowitz, M.; Singh, A. *Langmuir* **1991**, *7*, 16.
- (260) Markowitz, M. A.; Schnur, J. M.; Singh, A. In *Synthetic Microstructures in Biological Research*; Plenum: New York, 1992.
- (261) Markowitz, M. A.; Schnur, J. M.; Singh, A. *Chem. Phys. Lipids* **1992**, *62*, 193.
- (262) Singh, A.; Gaber, B. P. In *Applied Polymeric Materials*; Gebelein, C. G., Carragher, C. E., Forster, V. R., Eds.; Plenum: New York, 1988.
- (263) Spector, M. S.; Singh, A.; Messersmith, P. B.; Schnur, J. M. *Nano Lett.* **2001**, *1*, 375.
- (264) Singh, A.; Wong, E. M.; Schnur, J. M. *Langmuir* **2003**, *19*, 1888.
- (265) Thomas, B. N.; Lindemann, C. M.; Corcoran, R. C.; Cotant, C. L.; Kirshch, J. E.; Persichini, P. *J. Am. Chem. Soc.* **2002**, *124*, 1227.
- (266) Singh, A.; Burke, T. G.; Calvert, J. M.; Georger, J. H.; Herendeen, B.; Price, R. R.; Schoen, P. E.; Yager, P. *Chem. Phys. Lipids* **1988**, *47*, 135.
- (267) Ratna, B. R.; Baral-Tosh, S.; Kahn, B.; Schnur, J. M.; Rudolph, A. S. *Chem. Phys. Lipids* **1992**, *63*, 47.
- (268) Caffrey, M.; Hogan, J.; Rudolph, A. S. *Biochemistry* **1991**, *30*, 2134.
- (269) Yang, B.; Kamiya, S.; Yui, H.; Masuda, M.; Shimizu, T. *Chem. Lett.* **2003**, *32*, 1146.
- (270) Spector, M. S.; Easwaran, K. R. K.; Jyothi, G.; Selinger, J. V.; Singh, A.; Schnur, J. M. *Proc. Natl. Acad. Sci. U.S.A.* **1996**, *93*, 12943.
- (271) Ono, Y.; Nakashima, K.; Sano, M.; Kanekiyo, Y.; Inoue, K.; Hojo, J.; Shinkai, S. *Chem. Commun.* **1998**, 1477.
- (272) Jung, J. H.; Shinkai, S.; Shimizu, T. *Nano Lett.* **2002**, *2*, 17.
- (273) Nakagawa, M.; Ishii, D.; Aoki, K.; Seki, T.; Iyoda, T. *Adv. Mater.* **2005**, *17*, 200.
- (274) Moreau, J. J. E.; Vellutini, L.; Man, M. W. C.; Bied, C.; Bantignies, J.-L.; Dieudonne, P.; Sauvajol, J.-L. *J. Am. Chem. Soc.* **2001**, *123*, 7957.
- (275) Burkett, S. L.; Mann, S. *Chem. Commun.* **1996**, 1996, 321.
- (276) Ringler, P.; Mueller, W.; Ringsdorf, H.; Brisson, A. *Chem.-Eur. J.* **1997**, *3*, 620.
- (277) Wilson-Kubalek, E. M.; Brown, R. E.; Celia, H.; Milligan, R. A. *Proc. Natl. Acad. Sci. U.S.A.* **1998**, *95*, 8040.
- (278) Lvov, Y. M.; Price, R. R.; Selinger, J. V.; Singh, A.; Spector, M. S.; Schnur, J. M. *Langmuir* **2000**, *16*, 5932.
- (279) Letellier, D.; Cabuil, V. *Prog. Colloid Polym. Sci.* **2001**, *118*, 248.
- (280) Markowitz, M.; Baral, S.; Brandow, S.; Singh, A. *Thin Solid Films* **1993**, *224*, 242.
- (281) Yang, B.; Kamiya, S.; Yoshida, K.; Shimizu, T. *Chem. Commun.* **2004**, 500.
- (282) Letellier, D.; Sandre, O.; Menager, C.; Cabuil, V.; Lavergne, M. *Mater. Sci. Eng.* **1997**, *5*, 153.
- (283) Ji, Q.; Iwaura, R.; Kogiso, M.; Jung, J. H.; Yoshida, K.; Shimizu, T. *Chem. Mater.* **2004**, *16*, 250.
- (284) Seddon, A. M.; Patel, H. M.; Burkett, S. L.; Mann, S. *Angew. Chem., Int. Ed.* **2002**, *41*, 2988.
- (285) Krebs, J. J.; Rubinstein, R.; Lubitz, P.; Harford, M. Z.; Baral, S.; Shashidhar, R.; Ho, Y. S.; Chow, G. M.; Qadri, S. *J. Appl. Phys.* **1991**, *70*, 6404.
- (286) Patil, A. J.; Muthusamy, E.; Seddon, A. M.; Mann, S. *Adv. Mater.* **2003**, *15*, 1816.
- (287) Lepault, J.; Pottus, F.; Martin, N. *Biochim. Biophys. Acta* **1985**, *820*, 315.
- (288) Baker, T. S.; Caspar, D. L. D.; Murakami, W. T. *Nature* **1983**, *303*, 446.
- (289) DeRosier, D. J.; Moore, P. B. *J. Mol. Biol.* **1970**, *52*, 355.
- (290) Melia, T. J.; Sowa, M. E.; Schutze, L.; Wensel, T. G. *J. Struct. Biol.* **1999**, *128*, 119.
- (291) Uzgiris, E. E.; Kornberg, R. D. *Nature* **1983**, *301*, 125.
- (292) Kubalek, E. W.; Kornberg, R. D.; Darst, S. A. *Ultramicroscopy* **1991**, *35*, 295.
- (293) Avila-Sakar, A. J.; Chiu, W. *Biophys. J.* **1996**, *70*, 57.
- (294) Lvov, Y. M.; Price, R. R. *Colloids Surf., B: Biointerfaces* **2002**, *23*, 251.
- (295) Kresge, C. T.; Leonowicz, M. E.; Roth, W. J.; Vartuli, J. C.; Beck, J. S. *Nature* **1992**, *359*, 710.
- (296) Beck, J. S.; Vartuli, J. C.; Roth, W. J.; Leonozic, M. E.; Kresge, C. T.; Schmitt, K. D.; Chu, C. T.-W.; Olson, D. H.; Sheppar, E. W.; McCullen, S. B.; Higgins, J. B.; Schlenker, J. L. *J. Am. Chem. Soc.* **1992**, *114*, 10834.
- (297) Inagaki, S.; Fukushima, Y.; Kuroda, K. *J. Chem. Soc., Chem. Commun.* **1993**, *1993*, 680.
- (298) Inagaki, S.; Koawai, A.; Suzuki, N.; Fukushima, Y.; Kuroda, K. *Bull. Chem. Soc. Jpn.* **1996**, *69*, 1449.
- (299) Adachi, M.; Harada, T.; Harada, M. *Langmuir* **1999**, *15*, 7097.
- (300) Adachi, M.; Harada, T.; Harada, M. *Langmuir* **2000**, *16*, 2376.
- (301) Harada, M.; Adachi, M. *Adv. Mater.* **2000**, *12*, 839.
- (302) Terech, P.; Weiss, R. G. *Chem. Rev.* **1997**, *97*, 3133.
- (303) Hanabusa, K.; Tanaka, R.; Suzuki, M.; Kimura, M.; Shirai, H. *Adv. Mater.* **1997**, *9*, 1095.
- (304) Hanabusa, K.; Hiratsuka, K.; Kimura, M.; Shirai, H. *Chem. Mater.* **1999**, *11*, 649.
- (305) Shinkai, S.; Murata, K. *J. Mater. Chem.* **1998**, *8*, 485.
- (306) Kobayashi, S.; Hanabusa, K.; Hamasaki, N.; Kimura, M.; Shirai, H. *Chem. Mater.* **2000**, *12*, 1523.
- (307) Kobayashi, S.; Hamasaki, N.; Suzuki, M.; Kimura, M.; Shirai, H.; Hanabusa, K. *J. Am. Chem. Soc.* **2002**, *124*, 6550.
- (308) Jung, J. H.; Shinkai, S.; Shimizu, T. *Chem. Rec.* **2003**, *3*, 212.
- (309) Jung, J. H.; Ono, Y.; Shinkai, S. *J. Chem. Soc., Perkin Trans. 1999*, *2*, 1289.
- (310) Jung, J. H.; Yoshida, K.; Shimizu, T. *Langmuir* **2002**, *18*, 8724.
- (311) Shimizu, T.; Hato, M. *Thin Solid Films* **1989**, *180*, 179.
- (312) Shimizu, T.; Mori, M.; Minamikawa, H.; Hato, M. *Chem. Lett.* **1989**, *8*, 1341.
- (313) Ji, Q.; Iwaura, R.; Shimizu, T. *Chem. Lett.* **2004**, *33*, 504.
- (314) Wong, G. C. L.; Tang, J. X.; Lin, A.; Li, Y.; Janmey, P. A.; Safinya, C. R. *Science* **2000**, *288*, 2035.
- (315) Raedler, J. O.; Koltover, I.; Salditt, T.; Safinya, C. R. *Science* **1997**, *275*, 810.
- (316) Koltover, I.; Salditt, T.; Raedler, J. O.; Safinya, C. R. *Science* **1998**, *281*, 78.
- (317) Goren, M.; Qi, Z.; Lennox, R. B. *Chem. Mater.* **2000**, *12*, 1222.
- (318) Lo, R.-K.; Ritchie, J. E.; Zhou, J.-P.; Zhao, J.; McDevitts, J. T. *J. Am. Chem. Soc.* **1996**, *118*, 11295.
- (319) Cai, X. W.; Gao, J. S.; Xie, Z. X.; Xie, Y.; Tian, Z. Q.; Mao, B. W. *Langmuir* **1998**, *14*, 2508.
- (320) Noll, J. D.; Nicholson, M. A.; Patten, P. G. V.; Chung, C.-W.; Myrick, M. L. *J. Electrochem. Soc.* **1998**, *145*, 3320.
- (321) Hall, N. *Chem. Commun.* **2004**, *2004*, 1.
- (322) Mann, S.; Heywood, B. R.; Rajam, S.; Birchall, J. D. *Nature* **1988**, *334*, 692.
- (323) Zhao, X. K.; Yang, J.; McCormick, L. D.; Fender, J. H. *J. Phys. Chem.* **1992**, *96*, 9933.
- (324) Gavish, M.; P-Biro, R.; Lahav, M.; Leiserowitz, L. *Science* **1990**, *250*, 973.
- (325) Meldrum, F. C.; Wade, V. J.; Nimmo, D. L.; Heywood, B. R.; Mann, S. *Nature* **1991**, *349*, 684.
- (326) Meldrum, F. C.; Heywood, B. R.; Mann, S. *Science* **1992**, *257*, 522.
- (327) Mann, S.; Hannington, J. P.; Williams, R. J. P. *Nature* **1986**, *324*, 565.
- (328) Mendelson, N. H. *Science* **1992**, *258*, 1633.
- (329) Wong, K. K. W.; Douglas, T.; Gider, S.; Awschalom, D. D.; Mann, S. *Chem. Mater.* **1998**, *10*, 279.
- (330) Wong, K. K. W.; Mann, S. *Adv. Mater.* **1996**, *8*, 928.
- (331) Douglas, T.; Young, M. *Nature* **1998**, *393*, 152.
- (332) Pazirandeh, M.; Baral, S.; Campbell, J. R. *Biomimetics* **1992**, *41*.
- (333) Shenton, W.; Pum, D.; Sleytr, U. B.; Mann, S. *Nature* **1997**, *389*, 585.
- (334) Davis, S. A.; Burkett, S. L.; Mendelson, N. H.; Mann, S. *Nature* **1997**, *385*, 420.
- (335) Braun, E.; Eichen, Y.; Sivan, U.; Ben-Yoseph, G. *Nature* **1998**, *391*, 775.
- (336) Mirkin, C. A.; Letsinger, R. L.; Mucic, R. C.; Storhoff, J. J. *Nature* **1996**, *382*, 607.
- (337) Alivisatos, A. P.; Johnsson, K. P.; Peng, X.; Wilson, T. E.; Loweth, C. J.; Bruchez, M. P., Jr.; Schultz, P. G. *Nature* **1996**, *382*, 609.
- (338) Coffer, J. L.; Bigham, S. R.; Li, X.; Pinizzotto, R. F.; Rho, Y. G.; Pirtle, R. M.; Pirtle, I. L. *Appl. Phys. Lett.* **1996**, *69*, 3851.
- (339) Shenton, W.; Douglas, T.; Young, M.; Stubbs, G.; Mann, S. *Adv. Mater.* **1999**, *11*, 253.
- (340) Stubbs, G. In *Biological Macromolecules and Assemblies*; McPherson, A.; Jurnak, F., Eds.; Wiley: New York, 1984; Vol. 1.
- (341) Stubbs, G. *Semin. Virol.* **1990**, *1*, 405.
- (342) Boal, A. K.; Headley, T. J.; Tissot, R. G.; Bunker, B. C. *Adv. Funct. Mater.* **2004**, *14*, 19.
- (343) Qi, L.; Ma, J.; Cheng, H.; Zhao, Z. *J. Phys. Chem. B* **1997**, *101*, 3460.
- (344) Knez, M.; Sumser, M.; Bittner, A. M.; Wege, C.; Jeske, H.; Kooi, S.; Burgnard, M.; Kern, K. *J. Electroanal. Chem.* **2002**, *522*, 70.
- (345) Dujardin, E.; Peet, C.; Stubbs, G.; Culver, J. N.; Mann, S. *Nano Lett.* **2003**, *3*, 413.
- (346) Lu, B.; Stubbs, G.; Culver, J. N. *Virology* **1996**, *225*, 11.

- (347) Chow, G. M.; Stockton, W. B.; Price, R.; Baral, S.; Ting, A. C.; Ratna, B. R.; Shoen, P. E.; Schnur, J. M.; Bergeron, G. L.; Czarnaski, M. A.; Hickman, J. J.; Kirkpatrick, D. A. *Mater. Sci. Eng.* **1992**, *A158*, 1.
- (348) Price, R.; Patchan, M. *J. Microencapsulation* **1991**, *8*, 301.
- (349) Price, R.; Patchan, J.; Clare, A.; Rittschof, D.; Bonaventura, J. *Biofouling* **1992**, *6*, 207.
- (350) Johnson, D. L.; Polikandritou-Lambros, M.; Martone, T. B. *Drug Delivery* **1996**, *3*, 9.
- (351) Lasic, D. D. *Liposomes in Gene Delivery*; CRC Press: Boca Raton, FL, 1997.
- (352) Archibald, D. D.; Mann, S. *Chem. Phys. Lipids* **1994**, *69*, 51.
- (353) Baum, R. *Chem. Eng. News* **1993**, *19*.
- (354) Schnur, J. M.; Pice, R.; Rudolph, A. S. *J. Controlled Release* **1994**, *28*, 3.
- (355) Johnson, D. L.; Esmen, N. A.; Carlson, K. D.; Pearce, T. A.; Thomas, B. N. *J. Aerosol Sci.* **2000**, *31*, 181.
- (356) Stockton, W.; Lodge, J.; Rachform, F.; Orman, M.; Falco, F.; Schoen, P. *J. Appl. Phys.* **1991**, *70*, 4679.
- (357) Zabetakis, D. *J. Mater. Res.* **2000**, *15*, 2368.
- (358) Browning, S. L.; Lodge, J.; Price, R. R.; Schelleng, J.; Schoen, P. E.; Zabetakis, D. *J. Appl. Phys.* **1998**, *84*, 6109.
- (359) Chiou, B.-S.; Lankfor, A. R.; Schoen, P. E. *J. Appl. Polym. Sci.* **2003**, *88*, 3218.
- (360) Gittes, F.; Mickey, B.; Nettleton, J.; Howard, J. *J. Cell. Biol.* **1993**, *120*, 923.
- (361) Felgner, H.; Frank, R.; Schliwa, M. *J. Cell. Sci.* **1996**, *109*, 509.
- (362) Treacy, M. M.; Ebbesen, T. W.; Gibson, J. M. *Nature* **1996**, *381*, 678.
- (363) Frusawa, H.; Fukagawa, A.; Ikeda, Y.; Araki, J.; Ito, K.; John, G.; Shimizu, T. *Angew. Chem., Int. Ed.* **2003**, *42*, 72.
- (364) Karlsson, M.; Nolkrantz, K.; Davidson, M. J.; Stroemberg, A.; Ryttsen, F.; Akerman, B.; Orwar, O. *Anal. Chem.* **2000**, *72*, 5857.
- (365) Karlsson, M.; Sott, K.; Cans, A.-S.; Karlsson, A.; Karlsson, R.; Orwar, O. *Langmuir* **2001**, *17*, 6754.
- (366) Karlsson, A.; Karlsson, R.; Karlsson, M.; Cans, A.-S.; Stroemberg, A.; Ryttsen, F.; Orwar, O. *Nature* **2001**, *409*, 150.
- (367) Karlsson, R.; Karlsson, M.; Karlsson, A.; Cans, A.-S.; Bergenholz, J.; Akerman, B.; Ewing, A. G.; Voinova, M.; Orwar, O. *Langmuir* **2002**, *18*, 4186.
- (368) Karlsson, M.; Sott, K.; Davidson, M.; Cans, A.-S.; Linderhom, P.; Chiu, D.; Orwar, O. *Proc. Natl. Acad. Sci. U.S.A.* **2002**, *99*, 11573.
- (369) Karlsson, R.; Karlsson, A.; Orwar, O. *J. Am. Chem. Soc.* **2003**, *125*, 8442.
- (370) Karlsson, A.; Karlsson, M.; Karlsson, R.; Sott, K.; Lundqvist, A.; Tokarz, M.; Orwar, O. *Anal. Chem.* **2003**, *75*, 2529.
- (371) Sott, K.; Karlsson, M.; Pihl, J.; Hurtig, J.; Lobovkina, T.; Orwar, O. *Langmuir* **2003**, *19*, 3904.
- (372) Frusawa, H.; Fukagawa, A.; Ikeda, Y.; Ito, K.; John, G.; Shimizu, T. Unpublished result, 2004.
- (373) Evans, E.; Bowman, H.; Leung, A.; Needham, D.; Tirrel, D. *Science* **1996**, *273*, 933.
- (374) Waugh, R. E.; Hochmuth, R. M. *Biophys. J.* **1987**, *1987*, 391.
- (375) Bucher, P.; Fischer, A.; Luise, P. L.; Oberholzer, T.; Walde, P. *Langmuir* **1998**, *14*, 2712.
- (376) Donner, D.; Boettcher, C.; Messerschmidt, C.; Siggel, U.; Führhop, J.-H. *Langmuir* **1999**, *15*, 5029.
- (377) Laplante, J.-P.; Pemberton, M.; Hjelmfelt, A.; Ross, J. *J. Phys. Chem.* **1999**, *99*, 10063.
- (378) Culbertson, C. T.; Jacobson, S. C.; Ramsey, J. M. *Anal. Chem.* **2000**, *72*, 5814.
- (379) Dove, A. *Nat. Biotechnol.* **1999**, *17*, 859.
- (380) Chiu, D. T.; Pezzoli, E.; Wu, H.; Stroock, A. D.; Whitesides, G. M. *Proc. Natl. Acad. Sci. U.S.A.* **2001**, *98*, 2961.
- (381) Service, R. F. *Science* **1994**, *265*, 316.
- (382) Davidson, M.; Karlsson, M.; Sinclair, J.; Sott, K.; Orwar, O. *J. Am. Chem. Soc.* **2003**, *125*, 374.
- (383) LeDuc, P.; Haber, C.; Bao, G.; Wirtz, D. *Nature* **1999**, *399*, 564.
- (384) Lu, H. P.; Xun, L.; Xie, X. S. *Science* **1998**, *282*, 1877.
- (385) Wei, Q.-H.; Bechinger, C.; Leiderer, P. *Science* **2000**, *287*, 625.
- (386) Ishii, Y.; Yanagida, T. *Single Mol.* **2000**, *1*, 5.
- (387) Akiyoshi, K.; Itaya, A.; Nomura, S. M.; Ono, N.; Yoshikawa, K. *FEBS Lett.* **2003**, *534*, 33.
- (388) Matsui, H.; Holtman, C. *Nano Lett.* **2002**, *2*, 887.
- (389) Hummer, G.; Rasaiah, J. C.; Noworyta, J. P. *Nature* **2001**, *414*, 188.
- (390) Kalra, A.; Garde, S.; Hummer, G. *Proc. Natl. Acad. Sci. U.S.A.* **2003**, *100*, 10175.
- (391) Roux, B. *Acc. Chem. Res.* **2002**, *35*, 366.
- (392) Engels, M.; Bashford, D.; Ghadiri, M. R. *J. Am. Chem. Soc.* **1995**, *117*, 9151.
- (393) Asthagiri, D.; Bashford, D. *Biophys. J.* **2002**, *82*, 1176.
- (394) Tarek, M.; Maigret, B.; Chipot, C. *Biophys. J.* **2003**, *85*, 2287.
- (395) Hartnig, C.; Witschel, W.; Spohr, E. *J. Phys. Chem. B* **1998**, *102*, 1241.
- (396) Hartig, C.; Witschel, W.; Spohr, E.; Gallo, P.; Ricci, M. A.; Rovere, M. *J. Mol. Liq.* **2000**, *85*, 127.
- (397) Yui, H.; Guo, Y.; Koyama, K.; Sawada, D.; Sawada, T.; John, G.; Yang, B.; Masuda, M.; Shimizu, T. *Langmuir* **2005**, *21*, 721.
- (398) Zhang, J.; Bright, F. V. *J. Phys. Chem.* **1991**, *95*, 7900.
- (399) Chakrabarti, S. K.; Ware, W. R. *J. Chem. Phys.* **1971**, *55*, 5494.
- (400) Basses, M.-P.; Robinson, G. W. *J. Phys. Chem.* **1987**, *91*, 5818.

CR030072J

